Muscle phenotype of the myostatin mutant *Compact* mice and myostatin/IGF-I transcript levels in pathological human hearts

Ph.D. Thesis

Júlia Aliz Baán

Department of Biochemistry
Doctoral School of Multidisciplinary Medicine
Faculty of Medicine
University of Szeged

Supervisor: Luca Mendler, MD, Ph.D.

Szeged

2015

1. List of papers related to the subject of thesis

I. Baán JA, Kocsis T, Keller-Pintér A, Müller G, Zádor E, Dux L, Mendler L (2013) The Compact mutation of myostatin causes a glycolytic shift in the phenotype of fast skeletal muscles. J Histochem Cytochem. 61:889-900.
IF: 2.403

II. Baán JA[#], Varga VZ[#], Leszek P, Kusmierczyk M, Baranyai T, Dux L, Ferdinandy P, Braun T, Mendler L (2015) Myostatin and IGF-I signaling in end-stage human heart failure:a qRT-PCR study. Journal of Translational Medicine. 13(1):1-9. DOI: 10.1186/s12967-014-0365-0
IF:3.99
[#] The authors contributed equally to this work.

Table of contents

2. Abbreviations

A	adenine
ActRI	activin receptor type I
ActRIIA	activin receptor type IIA
ActRIIB	activin receptor type IIB
ActRIIB/IGF-IR	receptor ratio (ratio of ActRIIB and IGF-IR)
Ala	alanine
ARP	acidic ribosomal protein
Asn	asparagine
ATPase	adenosine triphosphatase
$BEH^{c/c}$	*Compact* Berlin High Line mouse line
bHLH	basic helix-loop-helix
BMP	bone morphogenetic protein
C	cytosine
cDNA	complementary desoxyribonucleic acid
Cmpt	*Compact*
CONT	human healthy controls
DAB	diaminobenzidine
DEP	diethyl pyrocarbonate
DCM	dilated cardiomyopathy
DNA	desoxyribonucleic acid
dNTP	desoxynucleotide triphosphate
DTT	dithiotreitol
DUHi	Dummerstorf high inbred (mouse line)
EDL	extensor digitorum longus (muscle)
FLRG	follistatin-like related gene
G	guanine
GASP1	growth and differentiation factor associated serum protein
GAPDH	glycerinaldehide-3-phosphate dehydrogenase
Gastro	gastrocnemius (muscle)
GDF-8	growth/differentiation factor 8 (=Mstn)
Glu	glutamic acid
Gly	glycine
HE	hematoxylin-eosin
Hprt and HPRT	hypoxantine guanine phosphorybosyl transferase
ICM	ischemic cardiomyopathy
IGF-I	insulin-like growth factor I
IGF-IR	IGF-I receptor
IGF-I signaling index	multiplied value of IGF-I x IGF-IR transcript levels
Ile	isoleucine
LAP	latency-associated peptide
Leu	leucine
LTBP3	covalent binding to latent TGF-beta binding protein
LV	left ventricle of human heart

Lys	lysine
m.	musculus
MAPK	mitogen activated protein kinase
MHC	myosin heavy chain
min	minutes
miR-208	microRNA-208
MMLV-RT	Moloney Murine Leukemia Virus Reverse Transcriptase
MRF	myogenic regulatory factor (family)
Mstn signaling index	multiplied value of Mstn x ActRIIB transcript levels
Mstn/IGF-I	growth factor ratio (ratio of Mstn and IGF-I signaling)
Mstn/IGF-I signaling index	(Mstn x ActRIIB)/(IGF-I x IGF-IR) transcript levels
mRNA	messenger RNA
Mstn	myostatin
mtDNA	mitochondrial DNA
MyoD	myogenic differentiation 1 (transcription factor)
myf5	myogenic factor protein 5 (transcription factor)
NYHA	New York Heart Association
PBS	phosphate buffered saline
Phe	phenylalanine
PI3K	phosphoinositide 3-kinase
PKB	protein kinase B/Akt
PTEN	phosphatase and tensin homolog
RV	right ventricle of human heart
qRT-PCR	quantitative reverse transcriptase polymerase chain reaction
Quadr	quadriceps (muscle)
RNA	ribonucleic acid
rpm	revolutions per minute
S	interventricular septum of human heart
SDH	succinate dehydrogenase
Ser	serine
Smad	Caenorhabditis elegans protein SMA (=small body size) Mothers Against Decapentaplegic (MAD): homologous to *Drosophila* protein
SOL	soleus (muscle)
SolD	Solution D
T	thymine
TA	tibialis anterior (muscle)
TBE	Tris/boric acid/EDTA (ethylene diamine tetraacetate)
TGF-β	transforming growth factor β
Tris	tris-hydroximethyl-aminomethane

3. Summary

Myostatin (Mstn) is an important negative regulator of skeletal muscle growth. However, it plays also a crucial role in governing cardiomyocyte growth, heart metabolism and contraction. Our aim was to describe different aspects of Mstn signaling in skeletal muscle and heart tissue. To this end, two different model systems have been used in our experiments: (1) the Mstn mutant *Compact (Cmpt)* mice and (2) healthy and pathological human hearts.

The hypermuscular *Cmpt* mice carry a 12-bp natural mutation in the Mstn propeptide, with additional modifier genes being responsible for the phenotype. Muscle cellularity of the fast tibialis anterior (TA) and extensor digitorum longus (EDL) as well as the mixed-type soleus (SOL) muscles of *Cmpt* and BALB/c mice was examined by immunohistochemical staining of the myosin heavy chain (MHC) proteins. In addition, transcript levels of MHC isoforms were quantified by qRT-PCR.

On the other hand, gene expression of Mstn and IGF-I, the two major but mostly counteracting regulators of heart tissue have been investigated in different regions (septum, left and right ventricles) of healthy or dilated (DCM) and ischemic cardiomyopathic (ICM) patient hearts. A comprehensive qRT-PCR analysis was carried out by measuring the expression of Mstn, its receptor Activin receptor IIB (ActRIIB), IGF-I, IGF-I receptor (IGF-I receptor), as well as microRNA-208, the negative post-transcriptional regulator of Mstn.

According to our results all investigated muscles of *Cmpt* mice were significantly larger compared to wild type characterized by fiber hyperplasia of different grade. Fiber hypertrophy was not present in TA, however, EDL muscles showed specific IIB fiber hypertrophy while the (I and IIA) fibers of SOL muscles were generally hypertrophied. Both the fast TA and EDL muscles of *Cmpt* mice contained significantly more glycolytic IIB fibers accompanied by decreased number of IIX and IIA fibers, however, this was not the case for the SOL muscles. In summary, *Cmpt* mouse, inspite of its complex genetic background, shows similarities (at least in fast muscles) to Mstn knockout mice in terms of muscle cellularity and glycolytic muscle phenotype, suggesting that the lack of Mstn is responsible for these morphological changes. However, based on the more pronounced hyperplasia in *Cmpt* fast muscles as well as the different cellularity and oxidative phenotype of *Cmpt* SOL, additional studies are needed to elucidate the molecular mechanisms of Mstn inactivity and the possible role of modifier genes in *Cmpt* mice.

In our human heart study, we have found that in healthy control hearts the ratio of Mstn/IGF-I signaling was significantly higher in the left ventricle/septum than in the right ventricle. Moreover, Mstn transcript levels were significantly upregulated in all heart regions of DCM but not ICM patients. However, the ratio of Mstn/IGF-I signaling remained increased in the left ventricle/septum compared to the right ventricle of DCM patients (similar to healthy hearts). In contrast, in ICM hearts significant transcript changes were detected mainly in IGF-I signaling. In paralell with these results microRNA-208 showed mild upregulation in the left ventricle of both DCM and ICM hearts. This is the first demonstration of a spatial asymmetry in the expression pattern of Mstn/IGF-I in healthy hearts, which is likely to play a role in the different growth regulation of left vs. right ventricle. Moreover, we identified Mstn as a massively up-regulated gene in DCM but not in ICM as part of potential compensatory mechanisms in the failing heart.

4. Introduction

4.1. Significance of myostatin

Since its identification in 1997 (McPherron et al. 1997), growth differentiation factor 8 (GDF8), also called myostatin (Mstn) has been considered as a novel and unique endogenous negative regulator of skeletal muscle growth and maintenance. Mstn is a member of the TGF-β (transforming growth factor β) superfamily, mainly expressed in skeletal muscle, with less, but still significant expression in the heart (Sharma et al. 1999) and adipose tissues (McPherron and Lee 2002). Enhanced production of Mstn inhibits skeletal muscle growth and decreases muscle mass (e.g. in cachexia, muscle dystrophy or aging) while Mstn mutations cause hypermuscular phenotype in several different species. Furthermore, Mstn plays a crucial role in the regulation of cardiomyocyte growth as well as in the maintenance of oxidative metabolism and contractility of the heart (Biesemann et al. 2014). In heart failure patients myocardium produces and secretes Mstn protein into the circulation thereby inhibiting skeletal muscle growth leading to cachexia (Heineke et al. 2010). Mstn secreted by skeletal muscles might also have an impact on the heart and adipose tissues. How adipose tissues are regulated by Mstn is still debated, however Mstn deficiency inhibits adipogenesis and improves insulin sensitivity (McPherron and Lee 2002; Guo et al. 2009). Its mechanism of action has not been clarified in its full complexity so far, although it might be a promising therapeutical target molecule in both metabolic and muscle diseases.

4.2. Molecular signaling mechanisms of myostatin

Mstn is synthetized as a precursor protein from its respective gene and the biologically active form develop in further steps. First, promyostatin is produced from pre-promyostatin by the cleavage of the signal peptide from the N-terminal end in endoplasmic reticulum (Fig. 1). Promyostatin is either modified intracellularly or secreted to the extracellular matrix (Anderson et al. 2008). As a next step, mature Mstn and LAP (latency associated protein) propeptide are produced through cleavage of promyostatin by furin proteases (Lee 2004). Then mature Mstn forms a dimer through disulfide bridges, with the propeptides binding non-covalently to the N-terminal end of Mstn.

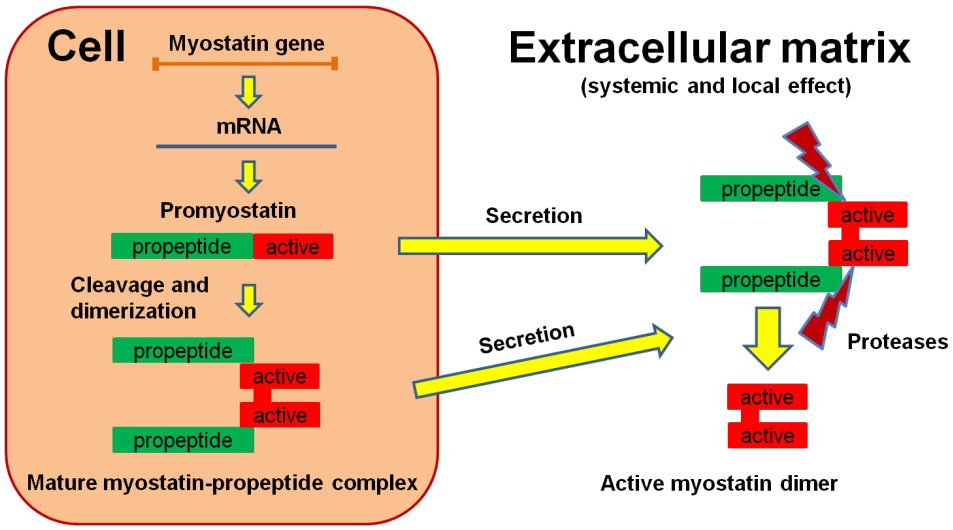

Figure 1. Synthesis and secretion of myostatin.

After secretion or elimination from extracellular matrix, the Mstn-propeptide complex enters circulation where Mstn dimer is activated by other proteases ((paired dibasic amino acid-cleaving enzyme (PACE) or matrix metalloproteases (bone morphogenetic protein (BMP)-1/tolloid)) (Otto and Patel 2010), by cutting off the propeptide from the complex (Rodgers and Garikipati 2008). Upon reaching target cells, Mstn binds to activin type IIB receptor (ActRIIB), which dimerizes with and phosphorylates type I receptor (ActRI) (Elkina et al. 2011) (Fig. 2). Mstn acts through different intracellular pathways with Smads representing the classical way to transduce Mstn effects (Lee 2004). After receptor activation, Smad2 and Smad3 become phosphorylated forming a heterodimer, which in turn enters the nucleus and binds to regulatory gene regions. Smad2/smad3 complex represses expression of myogenic transcription factors (myoD, myf5, myogenin) (Massague 1998; Kollias and McDermott 2008), thereby inhibiting myoblast proliferation and differentitation (Langley et al. 2002). Mstn expression is regulated by an endogenous negative feedback mechanism through inhibition of Smad2/3 complex by Smad7 (Chen et al 1996; Forbes et al. 2006). Mstn has also been reported to regulate the expression of myogenic factors by an alternative mechanism involving mitogen activated protein kinase (MAPK) pathway (Philip et al. 2005).

Insulin-like growth factor I (IGF-I) was also shown to play a crucial role in the regulation of muscle mass, but in contrast to Mstn, IGF-I supports skeletal and heart muscle growth (Serneri et al. 1999). Numerous studies have demonstrated that Mstn and IGF-I counteract each other through different mechanisms. IGF-I as a positive regulator of muscle

mass, activates mTOR pathway through the central molecular switch Akt (protein-kinase B), which in turn enhances protein synthesis, while inhibits protein degradation by depressing FoxO activity and the transcripition of E3 ubiquitine ligases (MURF-1, atrogin-1) (Elkina et al. 2011). Mstn have been shown to influence IGF-I pathway through inhibition of Akt and underlying factors (FoxO, MuRF1, Atrogin) but also might activate PTEN (phosphatase and tensin homolog) which in turn inhibits PI3K/Akt pathway (Ji et al. 2008). As a consequence, Mstn induces protein degradation while inhibits myoblast proliferation and differentiation; on the contrary, IGF-I facilitates protein synthesis and cellular proliferation and differentiation in a dynamically regulated manner (Fig. 2) (Elkina et al. 2011).

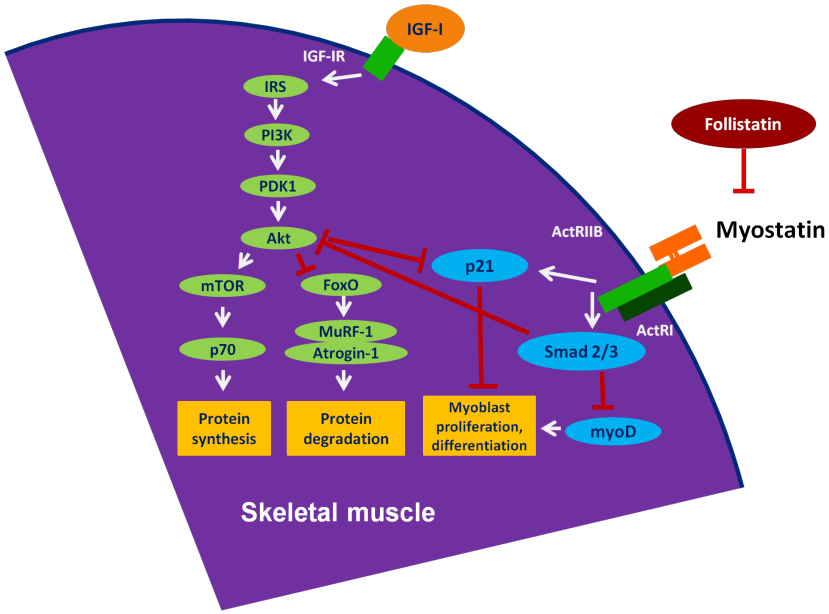

Figure 2. Interplay of myostatin and IGF-I signaling pathways in skeletal muscle. ActRIIB/I: activin receptor IIB/I, IGF-I: insulin-like growth factor I, IGF-IR: IGF-I receptor, IRS: insulin receptor substrate, PDK1: phosphoinositide-dependent kinase-1, Akt: protein kinase B, mTOR: mammalian target of rapamycin, p70: hypothetical protein, FoxO: forkhead box protein, sub-group O, MURF-1: muscle RING-finger protein-1, Atrogin-1: E3 ubiquitin ligase, p21: tumor suppressor protein, Smad 2/3: Sma-MAD (Mothers against Decapentaplegic) protein, myoD: myogenic differentitation protein 1.

Extracellular molecules play also an important role in modulating Mstn's effect. Follistatin, a positive regulator of muscle growth, binds directly to Mstn thereby inhibiting its activity (Fig. 2) (Lee and McPherron 2001). On the other hand, growth and differentitation factor associated serum protein (GASP-1) can cleave Mstn propeptide (Hill et al. 2003) while covalent binding to latent TGF-beta binding protein 3 (LTBP3) leads to the inactivation of Mstn (Anderson et al. 2008). In summary, once Mstn is inhibited, independent of the underlying mechanism Mstn defect results in a hypermuscular phenotype.

4.3. Skeletal muscle development and adult muscle phenotype

Skeletal muscle development is controlled by a complex regulatory network of several different factors. MyoD, myogenin, myf5 and MRF4 (myf6) all belong to the basic helix-loop-helix (bHLH) myogenic regulator factor (MRF) family and are crucial regulators of myogenic determination and differentiation. Through their sequential action, mesodermal somitic precursor cells form myoblasts which then proliferate (resulting in muscle growth by increasing cell number = hyperplasia), and fuse with each other to give rise to multinucleated myotubes (Chargé and Rudnicki 2004). Myotubes start growing (resulting in muscle growth by increasing cell size = hypertrophy) as long as mature post-mitotic muscle fibers are fully developed characterized by expression of typical muscle specific proteins such as myosin and actin, creatine kinase, calcium regulatory proteins and others (Schiaffino and Reggiani 2011). Altogether, structural and functional proteoms define muscle fiber phenotype. According to the ATPase activity of myosin heavy chains (MHC), slow type MHC I and fast type MHC II are distinguished giving rise to type I and type II fibers, respectively. Within type II fibers, oxidative MHCIIA, oxidative-glycolytic MHCIIX and glycolytic MHCIIB isoforms are identified, representing the dominating isoforms in type IIA, IIX and IIB fibers, respectively. Moreover, hybrid fibers containing two or more closely related MHC isoforms (I/IIA, IIA/IIX, IIX/IIB) are also present in muscles (Bloemberg and Quadrilatero 2012) which reflect the high capacity of muscle tissue to adapt to different physiological or pathological requirements defined as muscle plasticity. Oxidative or glycolytic metabolic characteristics of muscle fibers always corresponds to MHC isoforms, i. e. to the speed of muscle contraction. Regulation of fiber types is only partly understood, but Mstn might be one of the candidates which play an important role in this process (Bloemberg and Quadrilatero 2012).

4.4. Myostatin mutations in skeletal muscle

4.4.1. Artificial myostatin mutations

Mstn knock out (KO) mouse line has been created in order to analyze Mstn effects on skeletal muscle (McPherron et al. 1997). According to this very first report Mstn KO mice show hypermuscular phenotype caused by combined effects of muscle hyperplasia and hypertrophy, however, the ratio of hyperplasia to hypertrophy differed between the investigated muscles (Fig. 3). Moreover, a massive glycolytic shift characterized by increased

number of glycolytic IIB fibers has been detected in Mstn deficient mice pointing to the important role of Mstn in glycolytic versus oxidative fiber type determination (Carlson et al. 1999; Girgenrath et al. 2005; Hennebry et al. 2009; Wang et al. 2012).

Figure 3. The hypermuscular phenotype of myostatin knock out mice compared to control line (McPherron et al. 1997).

4.4.2. Natural myostatin mutations

Similar to Mstn KO mice, several different organisms such as Piedmontese and Belgian Blue cattles (Kambadur et al. 1997; McPherron and Lee 1997; Grobet et al. 1997), dog (Mosher et al. 2007), pig (Stinckens et al. 2008), Texel sheep (Johnson et al. 2005; Clop et al. 2006) and human (Schuelke et al. 2004) have been reported to carry naturally occuring mutations of Mstn (Fig. 4). Most of them result in an inactive protein caused by either an early STOP codon or a frameshift mutation in the bioactive domain of Mstn (McPherron and Lee 1997; Mosher et al. 2007; Boman et al. 2009). Intriguingly, a missplicing of the Mstn pre-mRNA was responsible for hypermuscularity observed in a human infant (Schuelke et al. 2004) (Fig. 4). In summary, each mutation resulted in a hypermuscular phenotype characterized by different ratios of hyperplasia to hypertrophy.

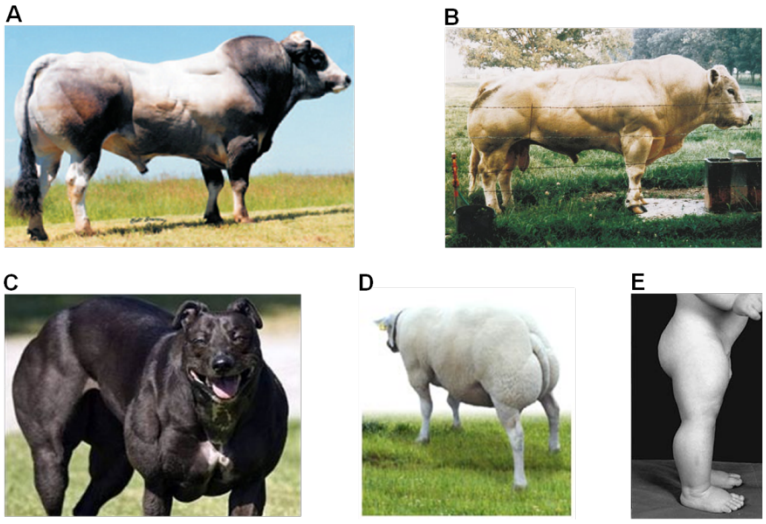

Figure 4. Natural myostatin mutant organisms. Piedmontese (A) (Rodgers and Garikipati 2008) and Belgian-blue cattles (B) (McPherron and Lee 2007), bully whippet (C) (www.dogforum.net), Texel sheep (D) (www.signalinggateway.org) and a 7-month-old human infant (E) (Schuelke et al. 2004).

4.4.3. The *Compact* mutation of the myostatin gene

In contrast to aforementioned mutations, another mechanism of Mstn inactivation induces the hypermuscular phenotype of the *Compact (Cmpt)* mice. The genetic background of the founder BEHi (**Be**rlin **H**igh **i**nbred) line is not well defined since it was derived from an out-bred line founded from mice which were bought from pet shops more than 40 years ago (Bünger et al. 2001). The mouse line was initially selected on protein mass (Weniger et al. 1974), further on high body weight/low fat content (Valle Zarate et al. 1994) and finally on body weight (Bünger et al. 2004). The '*Cmpt'* line in Berlin was derived from the first mice seen in early generations of the BEH line showing this phenotype. The new *Cmpt* line was selected on a muscularity score by visual inspection (Szabó et al. 1998; Varga et al. 2003, 2005). Animals of the Berlin *Cmpt* line were used as founders for the Hungarian *Cmpt* line, and there was no further exchange of genetic material between the laboratories in Berlin and Hungary. The Hungarian subpopulation of the *Cmpt* mice was inbred and kept by Géza Müller until 2010 in the Institute for Animal Biology, Agricultural Animal Center (Gödöllő, Hungary), and in EGIS Pharmaceuticals (Budapest, Hungary). Analysis of the Hungarian inbred subpopulation of the *Cmpt* line identified Mstn as the major gene containing a 12-bp non-frameshift deletion in the propeptide which resulted in removal of five amino acids (Leu [224], Gly [225], Ile [226], Glu [227], Ile [228]) while producing a new amino acid (Phe) instead (Fig. 5). Intriguingly, although the biologically active part of the molecule was

unaffected (Varga et al. 1997), a massive hypermuscular phenotype has been developed in *Cmpt* mice the mechanism of which has not been clarified so far. Nevertheless, additional modifier genes seem to be essentially involved in determining the full expressivity of the hypermuscular *Cmpt* phenotype (Fig. 5); however these genes have not been identified yet (Szabó et al. 1998; Varga et al. 2003, 2005). To date, only few studies provided phenotypical or molecular analysis of the *Cmpt* mice (Bünger et al. 2004; Rehfeldt et al. 2005; Amthor et al. 2007, 2009), although this line represents, in contrast to Mstn KO, a complex and mainly unknown mechanism of Mstn-dependent hypermuscularity.

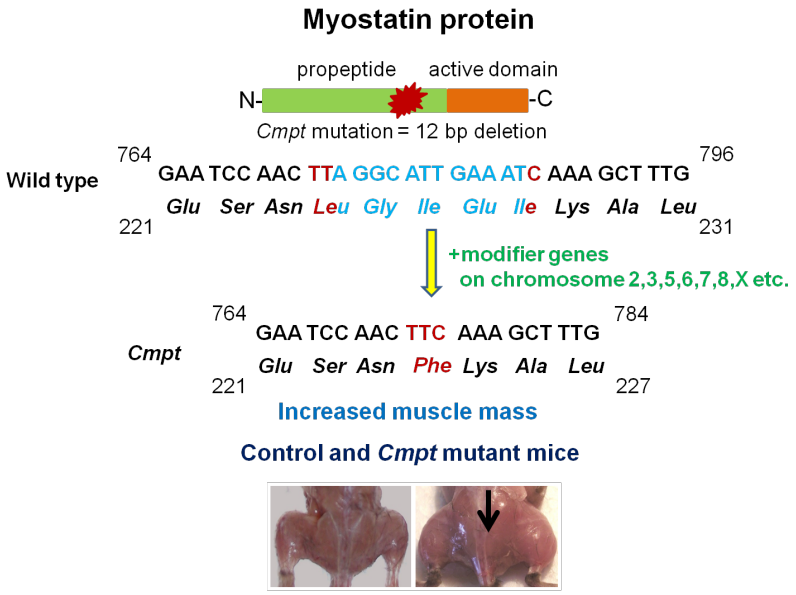

Figure 5. Natural mutation in the propeptide region of myostatin causes a hypermuscular phenotype in *Cmpt* mice. Mstn: myostatin, G: guanine, A: adenine, T: thymine, C: cytosine, Glu: glutamate, Ser: serine, Asn: asparagine; Leu: leucine, Gly: glycine, Ile: isoleucine, Lys: lysine, Ala: alanine, Phe: phenylalanine.

4.5. Overexpression of myostatin and its consequences in skeletal muscle

Enhanced production of Mstn leads to decreased muscle mass not only in Mstn transgenic mice, but also in cachectic patients, muscle dystrophies or aging (Rodgers and Garikipati 2008). Therefore, selective inhibition of Mstn may have outstanding clinical relevance by improving regeneration and growth in diverse skeletal muscle disorders and muscle wasting syndroms (Bogdanovich et al. 2002). Recently, clinical trials have been initiated in human patients that rely on inhibition of Mstn. Although several approaches have been proposed to inhibit Mstn signaling the full complexity of Mstn pathway has not been disclosed so far.

4.6. Role of myostatin in the heart under physiological and pathological conditions

Mstn, the growth inhibitor of skeletal muscle (McPherron et al. 1997) plays a significant role in myocardial physiology and pathophysiology as well. Sharma and his colleagues were the first to demonstrate that Mstn was expressed in fetal and adult heart (localized to Purkinje fibers and cardiomyocytes) suggesting that Mstn has an impact on cardiac development and growth. They also showed that Mstn expression was upregulated in post-infarct heart tissue (Sharma et al. 1999). Transgenic overexpression of Akt in hypertrophied hearts or mechanical stress in volume-overload heart failure both induced dramatic upregulation of Mstn (Cook et al. 2002; Shyu et al. 2006). Intriguingly, increased Mstn protein levels were reported by George et al. in heart biopsies of patients suffering from severe congestive heart failure (CHF) (George et al. 2010). These data implied an important role of Mstn in heart tissue and induced a significant new direction of Mstn research. However, by creating and analyzing various Mstn mutants several discrepant conclusions have been arised in the past few years. Germ-line inactivation of Mstn yielded conflicting results, describing no effect on cardiac hypertrophy or function (Morissette et al. 2006; Cohn et al. 2007) or reduced ejection fraction and eccentric hypertrophy (Rodgers et al. 2009; Jackson et al. 2012). Similarly, lineage-specific deletion of Mstn in cardiac progenitor cells revealed no differences in cardiac size and function in young mice (Heineke et al. 2010) whereas constitutive overexpression of Mstn in the heart (Heineke et al. 2010) and, in the heart and skeletal muscle (Reisz-Porszasz et al. 2003; Artaza et al. 2007) reduced cardiac mass and cardiomyocyte proliferation without effects on cardiac systolic function.

To date, only one study has addressed the consequences of acute Mstn inhibition in the adult heart as well as the role of Mstn in the regulation of metabolic changes and its impact on cardiac hypertrophy and heart failure. Biesemann et al (2014) have recently reported that conditional cardiac-specific inactivation of Mstn in the adult murine heart leads to enhanced glycolysis, increased glycogen storage, and cardiac hypertrophy, resulting in heart failure and increased lethality. Thus, Mstn has been identified as an important regulator of myocardial metabolism and growth, which suppresses AMP-activated kinase (AMPK) activity in cardiomyocytes to prevent acquisition of a fetal (glycolytic) metabolic pattern, thereby stabilizing the oxidative metabolic status of adult cardiomyocytes and restricting cardiac hypertrophy. To this end, Mstn upregulation in heart failure patients seems to be a

compensatory reaction to exert cardioprotective effects, however long-term activation of Mstn signaling in the heart might induce adverse side effects i. e. fibrosis as well (Artaza et al. 2008; Biesemann et al. 2015).

4.7. Interplay between myostatin and IGF-I in the heart

Mstn has been identified as a key regulator of heart function but its interaction with IGF-I has not been clarified in its full complexity. IGF-I was shown to play a pivotal role in cardiovascular physiology and aging (Ungvari and Csiszar 2012, Bailey-Downs et al. 2012, Toth et al. 2014). In concert with insulin itself, IGF-I proved to be a positive regulator of cardiac growth and contractility under both physiological and pathological conditions (Serneri et al. 1999, 2001; Palmieri et al. 2002; Barton et al. 2005; Pucci et al. 2009; Arcopinto et al. 2013; Madonna et al. 2014). Previous in vitro studies described a tight interplay between Mstn and IGF-I (Shyu et al. 2005; Morrisette et al. 2006, 2009; Yang et al. 2007). Blocking the IGF-I/PI3K/Akt pathway in skeletal muscle-specific C2C12 cells rendered them to undergo apoptosis in response to Mstn. On the other hand, Mstn expression in C2C12 cells was paradoxically induced by IGF-I treatment through PI3K/Akt pathway suggesting a possible feedback regulation between IGF-I and Mstn (Yang et al. 2007). Indeed, cyclic mechanical stretch enhanced Mstn expression (both mRNA and protein) in cultured rat neonatal cardiomyocytes which was mediated by IGF-I (Shyu et al. 2005). Gaussin and Deprè (2005) suggested that Mstn might be a cardiac chalone of IGF-I, since cardiac growth induced by IGF-I was feed-backed by the overexpression of the negative growth regulator Mstn. According to the hypothesis, chalones are secreted by specific tissues and provide a negative feedback mechanism to control the size of tissue that produces it (Bullough and Laurence 1960; Gaussin and Deprè 2005).

MicroRNAs (miRs) are small noncoding RNAs that negatively regulate cardiac gene expression under both physiological and pathological conditions with a potential impact on cardiac Mstn or IGF-I expression as well. Indeed, microRNA(miR)-208, encoded by the intronic region of the MHC gene has been reported to be a negative regulator of Mstn expression and to play a crucial role in pathological cardiac hypertrophy and fibrosis (Callis et al. 2009). In line with this, miR208 was upregulated in dilated cardiomyopathy (Satoh el al.

2010) as well as in myocardial infarction (Bostjancic et al. 2010) and ischemia (Varga et al. 2014).

No studies have systematically analyzed the relevance of the possible reciprocal regulation of Mstn and IGF-I at the gene expression level in healthy or failing human hearts, nor the potential role of miR-208 under these conditions. Previous investigations focused only on Mstn protein activation that has been shown to be accelerated in hearts of dilated or ischemic cardiomyopathic patients (DCM or ICM, respectively) (George et al. 2010). Moreover, no data exist in the literature about the expression pattern of Mstn in comparison with IGF-I and their receptors in various regions (i. e. left ventricles (LV) versus right ventricles (RV)) of the human heart. Given the different functional requirements LV and RV should cope with, and the markedly different development of these regions, one could assume that the gene expression pattern of Mstn and IGF-I signaling might show remarkable spatial differences under both physiological and pathological conditions.

4.8. Systemic myostatin: crosstalk between different tissues

Although it has been known for several years that skeletal muscle produce and secrete Mstn into circulation thereby supporting its systemic action besides its local effects (Fig. 6, Breitbart et al. 2011), no data have been available about the potential secretion of Mstn from the heart or adipose tissues. Recently, heart failure patients with elevated Mstn protein levels in cardiac tissue revealed increased Mstn serum levels as well (George et al. 2010; Gruson et al. 2011). Moreover, heart specific overexpression of Mstn in transgenic mice increased circulating serum Mstn levels by three- to fourfold, causing a significant reduction in skeletal muscle weight (Heineke et al. 2010). On the contrary, heart-specific deletion of Mstn in mice prevented skeletal muscle atrophy in heart failure after aortic banding (Heineke et al. 2010). These results demonstrate that Mstn secreted from the heart under pathological conditions might have an impact on skeletal muscle growth (Fig. 6, Breitbart et al. 2011). Although the role of adipose tissues in maintaining circulatory levels of Mstn is currently unclear, Mstn seems to be essential in coordinating skeletal muscle and heart function and metabolism.

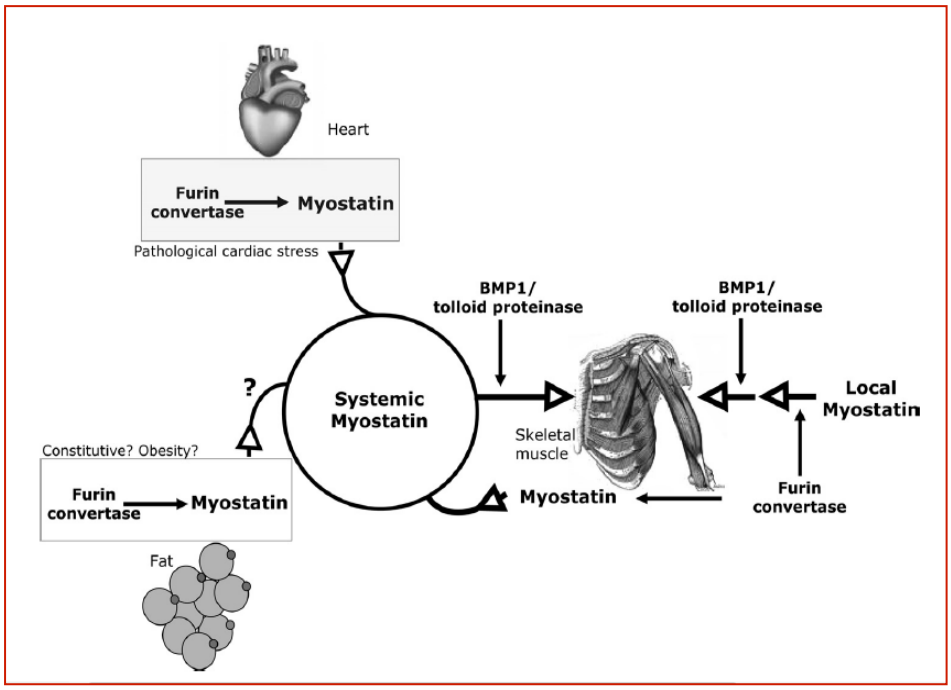

Figure 6. Crosstalk between different tissues through systemic myostatin action. Skeletal muscle and the heart (and potentially adipose tissue) secrete myostatin into circulation. Skeletal muscle growth is regulated by systemic and local myostatin, sequentially activated by the cleaveage of furin convertases and BMP-1/tolloid proteinases. During heart failure, cardiac and serum myostatin levels are increased (Breitbart et al. 2011).

5. Aims

1. To describe the muscle phenotype of the Mstn mutant *Cmpt* mice using morphological assessments in order to uncover the combined effects of the unconventional propeptide *(Cmpt)* mutation in Mstn and the unknown modifier genes in the genetic background.
2. To analyze transcript pattern of Mstn versus IGF-I with their respective receptors in different regions of healthy and pathological human hearts and to reveal their spatial regulation in healthy hearts or potential transcript alterations in dilatative (DCM) versus ischemic cardiomyopathic (ICM) patients.

6. Materials and Methods

6.1. Mouse studies: Animals and experimental design

The Mstn mutant *Cmpt* mice have been kept in the Institute of Biochemistry (Faculty of General Medicine, University of Szeged, Hungary). A suitable genetic control mouse line of *Cmpt* mice was not available at the time of our experiments given the complex and mainly unknown genetic background of the *Cmpt* mouse strain. Therefore, BALB/c mice serving as wild-type control were purchased from Biological Research Centre of Szeged, Hungary. Male, 2.5 month (10-12 week)-old male *Cmpt* (44-50,7 g) and BALB/c (24-28g) mice were used for the experiments (n=5-10). Typical hindlimb muscles (m. quadriceps (Quadr), m. tibialis anterior (TA), m. extensor digitorum longus (EDL) m. soleus (SOL) and m. gastrocnemius (Gastro)) of *Cmpt* and BALB/c strains were removed under intraperitoneal anaesthesia (3% chloral hydrate, 0.15ml/10g body weight). For comparison of body and muscle weights as well as for TA muscle fiber analysis, 4, 7, 12, 18, and 23-month-old *Cmpt* male mice were also used. All muscles were weighed and frozen in isopenthane/liquid nitrogen and kept at -80°C until further use. TA, EDL and SOL muscles of BALB/c and hypermuscular *Cmpt* mice from the right leg were used for morphological and immunohistochemical analysis while RNA isolation followed by quantitative RT-PCR was carried out from the contralateral TA counterparts.

Animal experiments were approved by the Institutional Animal Care and Use Committee at the University of Szeged in accordance with the U.S. National Institutes of Health guidelines for animal care.

6.2. Human studies: Patients and experimental design

Healthy human hearts were obtained from organ donor patients (CONT, n=5) whose hearts were explanted but due to technical reasons (CMV infection, extensive damage during harvest and size donor / recipient mismatch), not used for transplantation. The donors did not present any important previous medical history or any abnormalities in ECG and echocardiography (LV dimensions/contractility within normal ranges); these organ donors had died from head trauma, cerebral or subarachnoid hemorrhage. Explanted end-stage failing hearts were obtained from patients with advanced heart failure of non-ischaemic (DCM) (n=5) or ischaemic aethiology (ICM) (n=5). Before transplantation the clinical state of all

patients was determined according to the New York Heart Association (NYHA) classification; patients of NYHA class III–IV underwent a clinical assessment that included resting electrocardiogram, echocardiography and hemodynamic measurements. Tissue samples of the right and left ventricular free walls (RV and LV, respectively) and the inter-ventricular septum (S) were taken at the time of explantation (avoiding scarred, fibrotic, or adipose tissue, endocardium, epicardium or coronary vessels). The samples were rinsed immediately, blotted dry, frozen in liquid nitrogen and kept at − 80°C until further processing for RNA isolation and quantitative RT-PCR analysis.

All procedures were in accordance with the ethical standards of the responsible committee on human experimentation (institutional and national) and with the Helsinki Declaration of 1975. Informed consent was obtained from all patients for being included in the study according to the protocol approved by the Local Ethics Committee (IK-NP-0021-24/1426/14).

6.3. Morphological and morphometrical analysis of mouse skeletal muscles

For morphological analysis, 10μm serial cryostat sections were taken from the midbelly region of different muscles of both *Cmpt* and BALB/c mice followed by standard hematoxylin-eosin (HE) staining. Briefly, sections were fixed in -20°C acetone (for 5 min) then stained by hematoxylin for 5 min followed by 1% eosin for 1.5 min. After dehydration in isopropanol series (50-75-90-100%, 30s each) and toluol, samples were mounted with Entellan and covered with coverslips.

By taking pictures from all microscopic fields, the whole cross-sectional area (CSA) of each muscle was reconstructed using the Cell B program (Olympus DP Soft software, Version 3.2., Soft Imaging System GmbH; Münster, Germany) and fiber number was determined by counting all fibers in TA, EDL and SOL muscles with the help of Digimizer software (MedCalc Software, Mariakerke, Belgium) (Fig. 7).

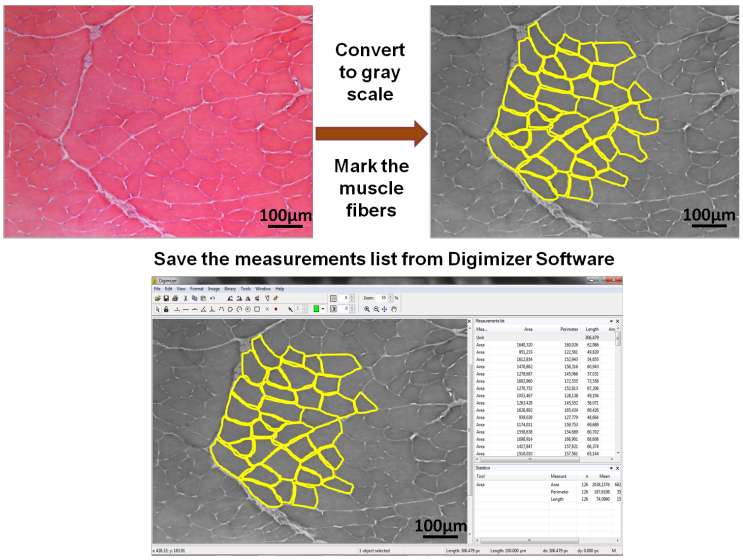

Figure 7. Steps of morphometrical analysis of skeletal muscles using Digimizer Software (MedCalc Software, Mariakerke, Belgium)**.**

6.4. Myosin heavy chain (MHC) immunohistochemistry of mouse skeletal muscles

Fiber type analysis was carried out on serial cryosections of 10µm thickness of TA, EDL and SOL muscles from both *Cmpt* and BALB/c wild type male mice. Acetone-fixed sections were first washed with PBS, blocked in 5% non-fat milk powder in PBS (for 20 min), then incubated overnight at 4°C with mouse monoclonal primary antibodies BA-D5, sc-71 and BF-F3 specific for myosin heavy chain (MHC) I (slow oxidative), MHCIIA (fast oxidative) and MHCIIB (fast glycolytic), respectively (Deutsche Sammlung von Mikroorganismen und Zellkulturen [DSMZ], Braunschweig, Germany) (Table 1).

Specificity of Ab	Name and type of Ab	Dilution
anti-MHC I	BA-D5, mouse monoclonal, purified	1:25
anti-MHCIIA	sc-71, mouse monoclonal	1:25
anti-MHCIIB	BF-F3, mouse monoclonal	1:5
peroxidase-conjugated secondary antibody	rabbit anti-mouse immunoglobulins	1:150

Table 1. Primary and secundary antibodies (Ab) used for immunohistochemistry in mouse skeletal muscles.

After incubation with the primary antibodies sections were washed in 5% non-fat milk powder in PBS for 10 min, incubated with the peroxidase-conjugated secondary antibody (rabbit anti-mouse, Dako, Denmark; Table 1) for 60 min and finally washed in PBS and Tris (20mM, pH7.5, 5 min each). Immunocomplexes were visualized by diaminobenzidine (DAB) staining (0.5mg/ml DAB, 0.006% H_2O_2 in 20 mM Tris buffer pH7.5). Nickel enhancement

(0.5mg/ml DAB, 0.15% $Ni(NH_4)_2SO_4$, 0.006% H_2O_2 in 20 mM Tris buffer pH7.5) was used for MHCIIB immunohistochemistry to improve signal intensity. DAB reaction was stopped by PBS, then sections were dehydrated and mounted with Entellan.

IIX fibers were considered as those not stained by any of the above antibodies (Fig. 8). The size and distribution of muscle fibers in SOL were determined by analyzing all (700-800) fibers in each muscle by applying Cell B and Digimizer softwares, while in EDL muscles about 50% of the fibers (600 to 1100 fibers in BALB/c and *Cmpt* mice, respectively) were measured. In TA muscles, analysis of fiber size as well as fiber type distribution was carried out by examining 2-3 representative microscopic fields (with 10x objective; Figure 8) of both superficial and deep portions. Regional results were then summarized for the whole cross sectional area of each TA muscle (500 to 1000 fibers/muscle in 4-7 microscopic fields in BALB/c and *Cmpt* mice, respectively).

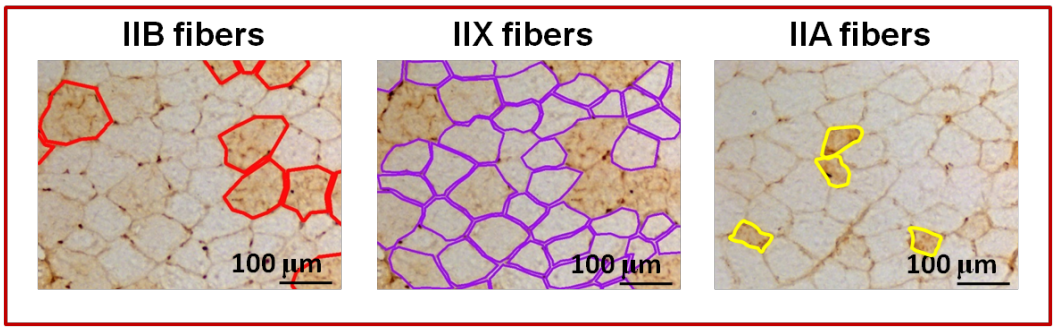

Figure 8. Representative fiber types in TA muscle (deep region). Marked fibers are representative for IIB (red), IIX (lila) and IIA (yellow) fibers, respectively.

6.5. Quantitative RT-PCR analysis of mRNA transcripts in mouse skeletal muscles and human heart samples

6.5.1. RNA isolation

Total RNA was isolated from TA muscles of *Cmpt* and BALB/c male mice (n=5) with TRI reagent (Molecular Research Center, Inc. Cincinnati, OH) or from the LV, S and RV samples of the CONT, DCM or ICM patients (n=5) with the acid guanidinium thiocyanate-phenol-chloroform (AGPC) method (Chomczynski and Sacchi 1987).

Both protocols included the following steps: homogenization, phase separation, RNA precipitation, washing and solubilization (Fig. 9). Homogenization of tissue samples were carried out in TRI reagent (1ml/50-100mg tissue) or in SolD (4M guanidine-thiocyanate, 25mM sodium citrate buffer, 0.5% N-lauroylsarcosine, 0.1M mercaptoethanol) (0.5ml/50mg

tissue) using a glass/Teflon Potter homogenizer (at 600 and 800 rpm, 2 min each). Homogenates were stored for 5 min at room temperature to support complete dissociation of nucleoprotein complexes. Insoluble materials (polysaccharides, extracellular membranes and cell debris) were then removed by centrifugation at 12000g for 10 min at 4°C. Supernatant was transferred to fresh Eppendorf tubes. According to TRI reagent protocol, 0.2ml chloroform/ 1ml Tri reagent was used for phase separation while in case of AGPC method 50µl sodium acetate (2M, pH4), 0.5ml phenol (saturated with diethyl-pyrocarbonate (DEPC)-treated water) and 0.2ml chloroform-isoamylalcohol (24:1)/ 0.5ml SolD were applied for the same reaction. Samples were incubated on ice for 15 min followed by centrifugation (10000-12000g, 15-20min, 4°C). The solution has been separated into a lower phenol-chloroform phase, an interphase and a colorless upper aqueous phase. RNA remained exclusively in the aqueous phase, whereas DNA and proteins were in the interphase and organic phase. The upper aqueous phase was carefully transferred to a new Eppendorf tube and RNA was precipitated by either isopropanol (0.5ml isopropanol/1ml TRI reagent) or 95% ethanol (1ml 95% ethanol/ 0.5ml SolD) followed by centrifugation (10000-12000g, 10-20 min, 4°C). RNA precipitate formed a gel-like or white pellet on the side and bottom of the tube. After supernatant removal RNA pellet was washed by ethanol (1ml 75% ethanol/1ml TRI reagent or 0.2-0.5ml 70% ethanol/ 0.5ml SolD) followed by centrifugation (7500-10000g, 5-10min, 4°C). Ethanol was removed carefully, while RNA was dried shortly and dissolved in RNAse-free water (DEPC-treated).

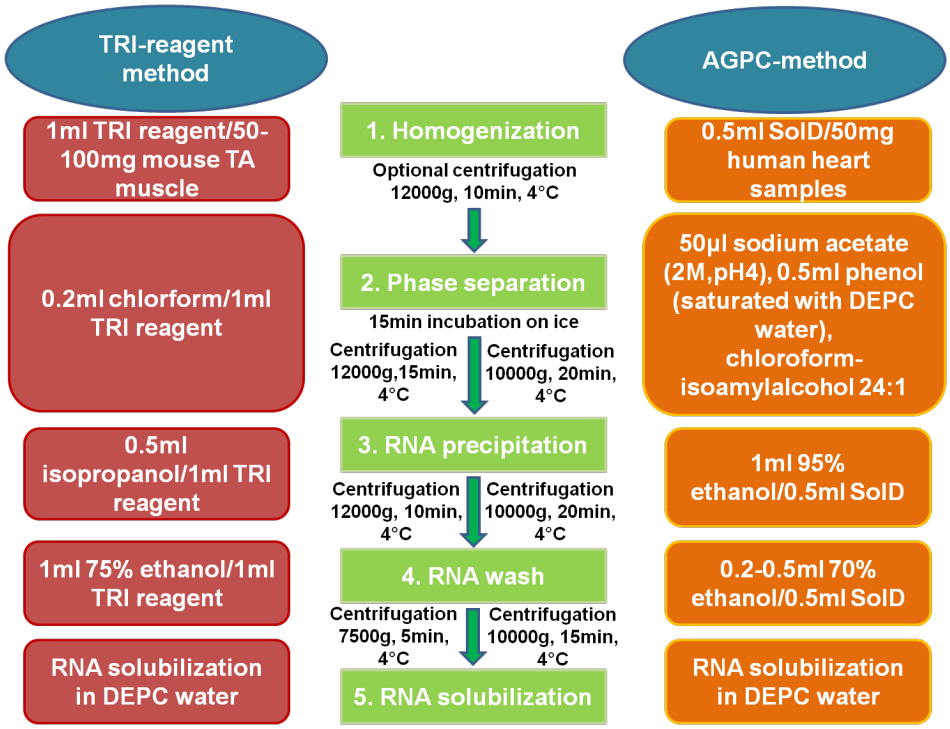

Figure 9. RNA isolation protocols: comparison of TRI reagent-method with acid-guanidinium thiocyanate-phenol-chloroform (AGPC) method (Chomczynski and Sacchi 1987).

RNA concentration and its purity were measured spectrophotometrically by NanoDrop (Thermo Scientific). Total RNA solution was essentially free of DNA and proteins and had a 260/280 ratio of 1.8-2.0. Integrity of total RNA from both TA mouse muscles and human heart samples were controlled on 1% agarose gel stained by ethidium bromide; RNA proved to be undegraded (Figure 10). RNA samples were kept at -80°C until further use.

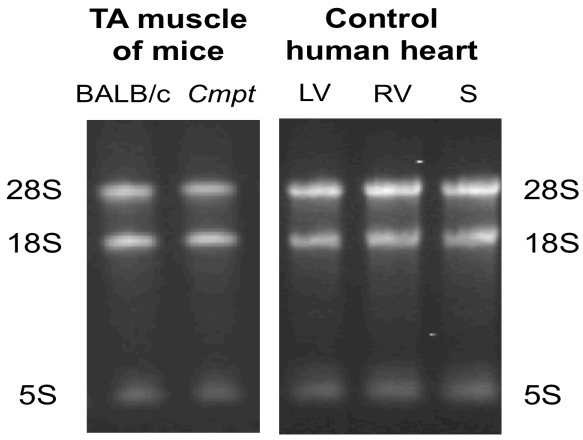

Figure 10. Representative ethidium-bromide stained gel (1% agarose) of total RNA isolated from TA (tibialis anterior) muscle of BALB/c and *Cmpt* male mice or from different human control heart regions. LV (left ventricle), RV (right ventricle), S (septum), 28S, 18S, 5S: types of ribosomal RNA.

6.5.2. Reverse transcription

Total RNA was isolated from tibialis anterior (TA) muscles of BALB/c and *Cmpt* mice and from the LV, S and RV regions of the CONT, DCM or ICM patients, followed by reverse transcription. The reaction mixture for cDNA synthesis (1µl oligo-dezoxythimidine (dT, Roche), 1µl dezoxy-nucleotide triphosphate (dNTP, Thermo Scientific), 1 or 2µg total RNA (mouse or human, respectively), DEPC water to 12.5µl) was denaturated at 65°C for 5 min followed by cooling down the samples on ice for a few minutes. 4µl 5xMoloney Murine Leukemia Virus Reverse Transcriptase (MMLV-RT) buffer (Invitrogen), 2µl 0.1M DTT (Invitrogen), 0.5µl RNase Inhibitor (20U, Fermentas) and 1µl MMLV enzyme (Invitrogen) were added to each tube to a final volume of 20µl. cDNA synthesis was carried out at 37°C for 50 min, thereafter MMLV enzyme was inactivated at 70°C for 15 min. Samples were then DNAse-treated (Fermentas) in order to avoid genomic contamination of cDNA. cDNA samples were stored at -20°C until further use.

6.5.3. qRT-PCR analysis

For the detection of transcript levels of mouse MHCI, MHCIIA, MHCIIX and MHCIIB as well as human Mstn, ActRIIB, IGF-I, and IGF-IR quantitative RT-PCR was carried out with SYBR GREEN master mix (Fermentas) on a Light Cycler 1.5 (Roche Applied Science). Since some of the genes generally used for internal normalization in qRT-PCR contain several pseudogenes (e.g. GAPDH, beta-actin) of which co-amplification may compromise their reliability as reference genes (Sun et al. 2012), hipoxanthine-guanine phosphorybosyltransferase (hprt/HPRT) has been used as a single internal control gene in our experiments. Indeed, hprt/HPRT expression did not significantly change between different mouse lines or heart regions of CONT and DCM or ICM patients. Cycle conditions were set as an initial denaturation step, followed by 45 cycles for template denaturation, annealing and extension phases (Table 2).

Steps of qPCR	Temp (°C)	Time
Initial denaturation phase	95	10min
Amplification (45 cycles)		
Denaturation phase	95	10s
Annealing phase	58	10s
Extension phase	72	10s

Table 2. qPCR amplification parameters

Specificity of the PCR products was confirmed by melting curve analysis followed by verification of amplicon length on 1.5 % agarose gels stained by ethidium bromide. Primer pairs for mouse Hprt, MHCI, MHCIIA, MHCIIX, MHCIIB as well as those for human Mstn, ActRIIB, IGF-I, IGF-IR and HPRT were designed to intron spanning exons by Primer 3 Input (version 0.40) software and tested to avoid primer dimers, unspecific amplification and self-priming formation (Table 3).

Target	Accession number	Forward primer	Reverse primer	Efficiency	Product size (bp)
MHCIIB mouse	NM_010855.2	GTGATTTCTCCTGT CACCTCTC	GGAGGACCGCAA GAACGTGCTGA	2.000	280
MHCIIX mouse	NM_030679.1	ACGGTCGAAGTTG CATCCC	CAGTAGTTCCGCC TTCGGTC	1.870	272
MHCIIA mouse	NM_001039545.2	TGCACCTTCTCGTT TGCCAG	GGCCATGTCCTCG ATCTTGT	1.832	320
MHCI mouse	NM_003689292.1	CTACAGGCCTGGG CTTACCT	TCTCCTTCTCAGA CTTCCGC	1.702	126
Hprt mouse	NM_013556.2	TCAGTCAACGGGG GACATAAA	GGGGCTGTACTG CTTAACCAG	1.719	142
Mstn human	NM_005259.2	TTCGTCTGGAAACA GCTCCT	CATTTGGGTTTTC CATCCAC	1.783	220
ActRIIB human	NM_001106.3	TGACTTTGGCTTGG CTGTTC	ATGTACTCATCCA CGGGTCC	1.834	219
IGF-I human	XM_005268835.1	ATGCTCTTCAGTTC GTGTGTG	GGGTCTTGGGCAT GTCGGTG	1.758	219
IGF-IR human	NM_000875.3	GACAACCAGAACT TGCAGCA	GATTCTTCGACGT GGTGGTG	1.714	241
HPRT human	NM_000194.2	TGCTCGAGATGTG ATGAAGG	TCCCCTGTTGACT GGTCATT	2.044	192

Table 3. Primer properties used in qRT-PCR. bp: base pair, MHC: myosin heavy chain; Mstn: myostatin, ActRIIB: activin receptor IIB, IGF-I: insulin-like growth factor I, IGF-IR: insulin-like growth factor I receptor, hprt and HPRT: hypoxanthine-guanine phosphorybosyltransferase.

6.6. Quantitative RT-PCR analysis of miRNA transcripts in human heart samples

From the above detailed total RNA isolates of human heart samples, cDNA was synthetized and quantitative real-time PCR was performed with miRCURY LNA™ Universal RT microRNA PCR kit (Exiqon, Denmark) on LightCycler®480 (Roche, Switzerland) according to the manufacturer's instructions. Briefly, total RNA was diluted to a final concentration of 5ng/µl, and mixed with Reaction buffer and Enzyme mix provided with the kit in a final volume of 10µl. Reaction mixture was incubated for 60 min at 42°C, and reverse transcriptase was heat-inactivated for 5 min at 95°C. Then, cDNA was diluted to 80x and 4µl of diluted cDNA were mixed with 6µl of the PCR Master mix and PCR primer mix supplied

by the manufacturer. The primers for both microRNA-208b and control microRNA-103a-3p were designed and prepared by using Exiqon's LNA^{TM} technology. Polymerase was activated for 10 min at 95°C, and microRNA-208b and microRNA-103a-3p were amplified and quantified (denaturation: 10 sec at 95°C; annealing/synthesis: 1 min at 60°C). The specificity of amplifications was assessed by melting curve analysis (42°C to 80°C) and by agarose gel electrophoresis (1%). At last, crossing point values (Cp) were calculated. MicroRNA-208b Cp values were normalized to the corresponding housekeeping microRNA-103a-3p Cp values. Then, all pairwise ΔCp value normalization was carried out to control ΔCp values, and expressed as mean of the three replicates of 2-ΔΔCp values (fold change).

6.7. Statistical analysis

Statistical analysis was performed by unpaired t test and one- way/two-way ANOVA or non-parametric t-test (Welch test) using Prism software (GraphPad Software, Inc.; San Diego, CA), as appropriate. All data were expressed as means±SEM. The level of $p<0.05$ was considered significant. The individual p-values are indicated in the figure legends.

7. Results

7.1. Muscle phenotype of *Compact* mice

7.1.1. Body- and muscle weight

We compared 2.5-month-old Mstn mutant *Cmpt* mice with wild-type BALB/c mice in terms of body and muscle weight. *Cmpt* male mice were significantly larger than BALB/c regarding their body weight (Fig. 11A).

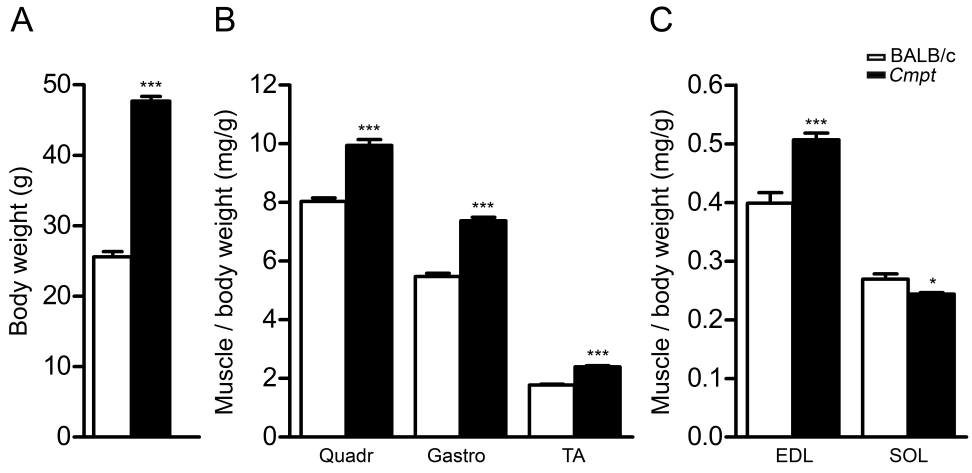

Figure 11. Body weight (A) and normalized muscle masses (B, C) of BALB/c and *Cmpt* male mice. B-C show normalized muscle masses of quadriceps (Quadr), gastrocnemius (Gastro), tibialis anterior (TA), extensor digitorum longus (EDL) and soleus (SOL) muscles. Bars represent mean values±SEM, asterisks show significant differences between BALB/c and *Cmpt* mice (n=5-10, *p<0.05, ***p<0.001).

Absolute weights of the different hindlimb muscles, such as Quadr, Gastro, TA, EDL and SOL muscles, were significantly larger in *Cmpt* mice (data not shown). Similarly, muscle weights normalized to body weights were significantly increased in *Cmpt* animals, with the exception of the oxidative SOL muscle. These results indicated a disproportionate increase in muscle masses in *Cmpt* mice (Fig. 11B-C). To assure that the 2.5-month-old *Cmpt* mice had already finished the intense growing phase, we compared body- and muscle (TA, EDL and SOL) weights in mice of different ages as well (Fig. 12). Body weight was similar in young (2.5-month-old) and adult (4- and 7-month-old) animals, while 12-23-month-old mice had slightly higher weight measurements. However, no significant difference was found in muscle weights amongst any of the age groups, indicating that the 2.5-month-old animals have already reached muscle size typical of adult mice.

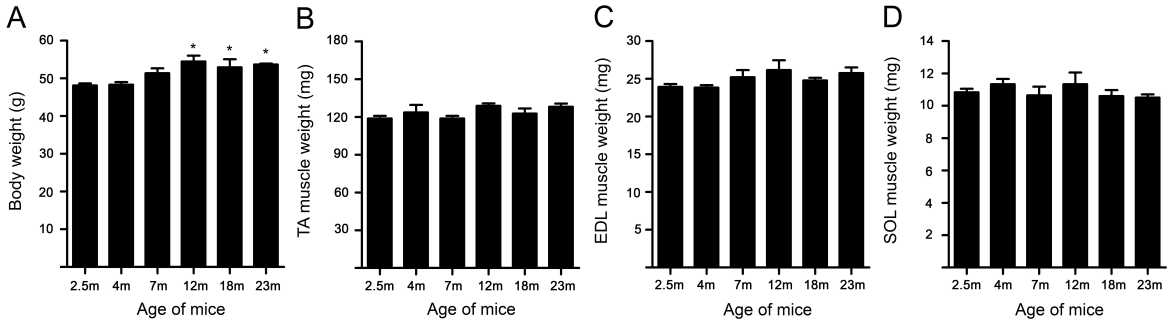

Figure 12. Body weight (A) and muscle masses of TA (B), EDL (C) and SOL (D) muscles of male *Cmpt* mice at different ages. Age of mice is given in months, bars represent mean values±SEM, asterisks show significant differences compared to 2.5-month-old *Cmpt* mice (n=4-10, *p<0.05).

7.1.2. Muscle fiber number and fiber cross sectional area

To define whether the hypermuscularity of *Cmpt* mice is caused by hyperplasia or hypertrophy, we analyzed muscle fibers on HE- or MHC-immunostained serial cross-sections of different muscle types in both mutant and wild-type animals (Fig. 13).

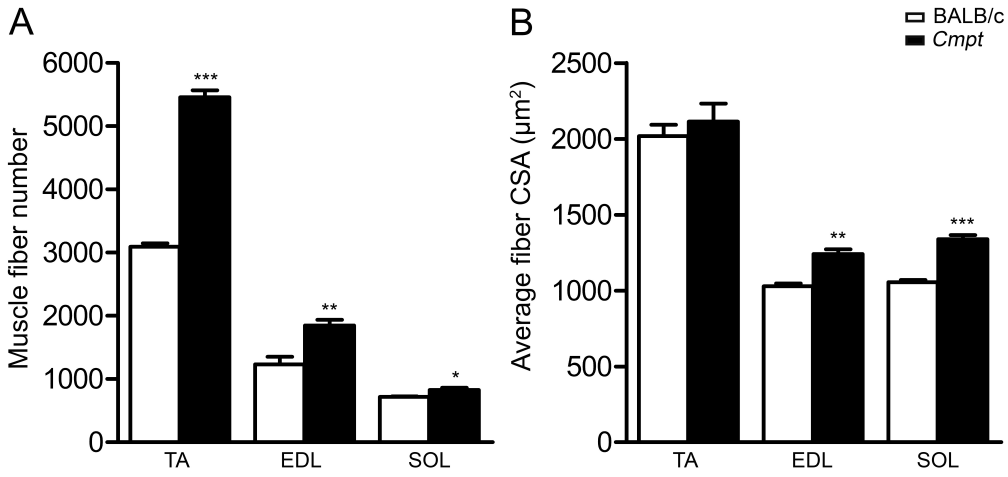

Figure 13. Total muscle fiber number (A) and average fiber cross sectional area (CSA) (B) of TA, EDL and SOL muscles in BALB/c and *Cmpt* male mice. Bars represent mean values±SEM, asterisks show significant differences between BALB/c and *Cmpt* mice (n=3-5, *p<0.05, **p<0.01, ***p<0.001).

Fiber number was significantly higher in all examined muscles of the 2.5-month-old *Cmpt* mice than that observed in wild-type mice. TA muscle revealed the most significant hyperplasia as compared with EDL and SOL muscles (Fig. 13A). However, fiber size did not differ in TA muscles between *Cmpt* and BALB/c mice. EDL and SOL muscles of *Cmpt* mice, on the other hand, showed clear evidence of hypertrophy as well (Fig. 13B). To control fiber

parameter alterations in *Cmpt* mice along with aging, we analyzed TA muscles of 7-month-old *Cmpt* mice and found no differences compared with 2.5-month-old mice (Table 4).

In summary, based on our results, hypermuscularity of *Cmpt* mice is characterized by fiber hyperplasia in TA muscle and by a combination of hyperplasia and different grades of hypertrophy in EDL and SOL muscles.

	Cmpt	Cmpt
Age (in months)	2.5	7
Muscle type	TA	TA
Fiber number (mean ± SEM)	5455 ± 114	5450 ± 136
Fiber size (mean ± SEM)	2114 ± 118	2193 ± 95
Number of values	5	3

Table 4. Muscle cellularity of TA muscles in 2.5-month-old vs. 7-month-old male *Cmpt* mice.

7.1.3. MHC composition and fiber size distribution

To analyze the possible effects of the *Cmpt* mutation on MHC composition, serial cryosections of TA, EDL and SOL muscles were immunostained using sets of monoclonal antibodies in order to differentiate type I, IIA, IIX and IIB fibers, respectively (Fig. 14-17).

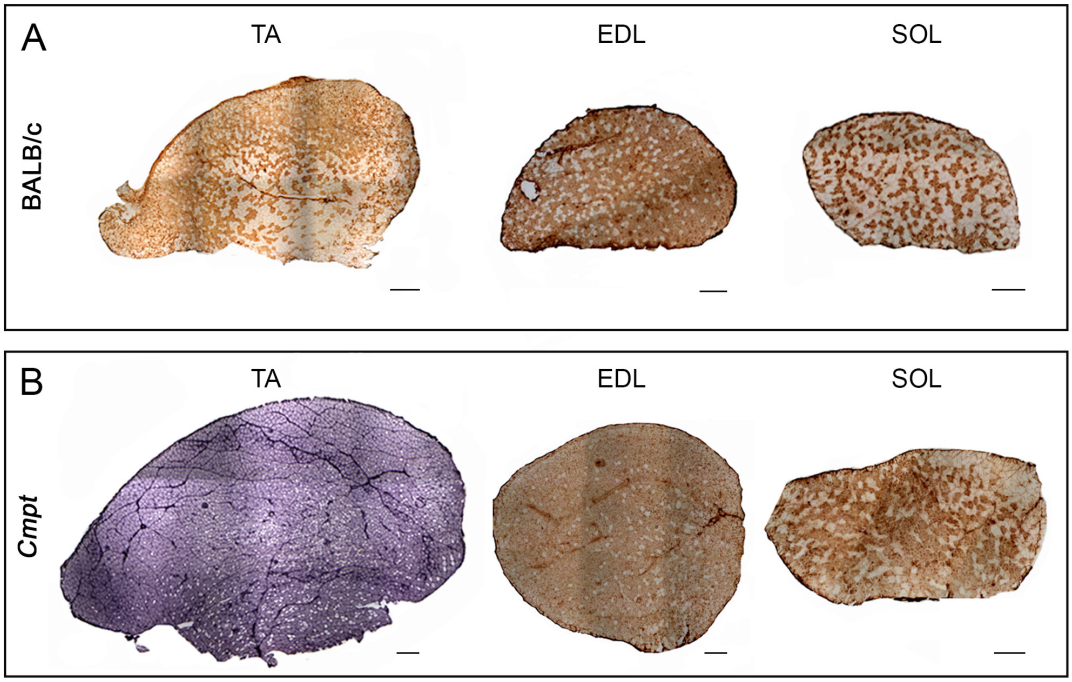

Figure 14. Representative immunohistochemical stainings of tibialis anterior (TA), extensor digitorum longus (EDL), and soleus (SOL) muscles of BALB/c (A) and *Cmpt* (B) male mice. Panel A represents whole cross-sectional areas of TA, EDL, SOL muscles stained either by MHCIIB antibody (in TA and EDL muscles) or by MHCI antibody (in SOL muscle) in BALB/c mice, and Panel B shows the same tissue staining for sections in *Cmpt* male mice. All muscles were stained by diaminobenzidine but *Cmpt* TA muscle was additionally nickel enhanced. Scale bars represent 400 µm for TA, 200 µm for EDL and 200 µm for SOL muscles.

In line with the literature (Bloemberg and Quadrilatero 2012), only MHCII isoforms were detected in TA and EDL muscles of both mouse lines (Fig. 14-17), whereas no MHCIIB fibers were found in SOL muscle. Therefore, we next analyzed the parameters of the slow-type I and the fast-type IIA and IIX fibers in SOL muscle (Fig. 14-17).

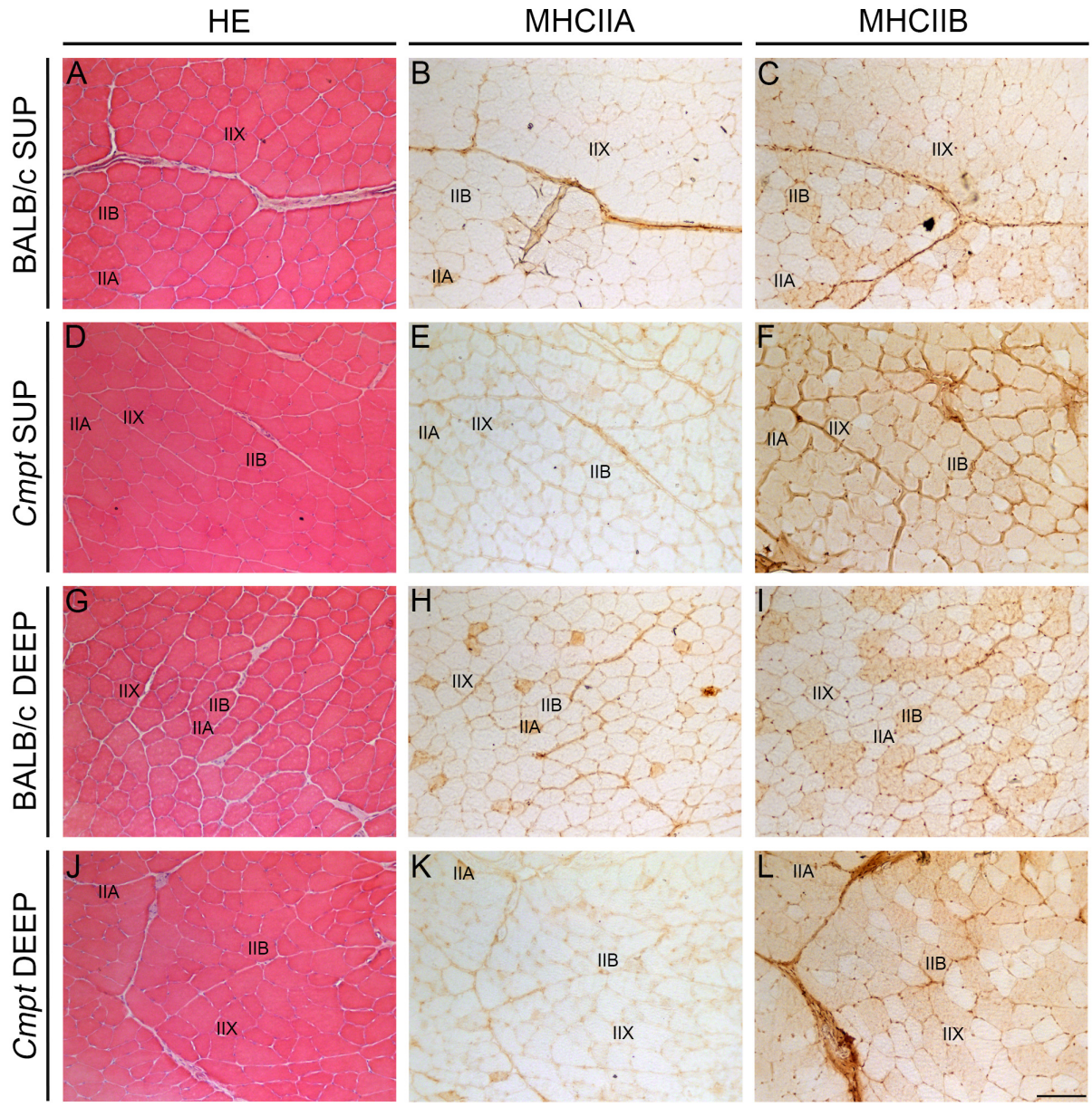

Figure 15. Immunohistochemical analysis of myosin heavy chain (MHC) isoforms in different regions of TA muscles of BALB/c and *Cmpt* male mice. A-C represent the superficial region of BALB/c mice while D-F depict that of *Cmpt* mice; G-I and J-L show BALB/c and *Cmpt* deep regions, respectively. HE staining (A,D,G,J) and antibodies against MHCIIA (B,E,H,K) and MHCIIB (C,F,I,L) were applied. Representative fibers are marked as IIA, IIB and IIX fibers. Scale bars represent 100 µm.

By counting different fiber types on whole cross sectional images, we noted that the fast-type TA muscles of *Cmpt* mice contained significantly more glycolytic IIB fibers while a decreased number of IIX and IIA fibers as compared with that in wild-type mice (Fig. 14, 15, 16A).

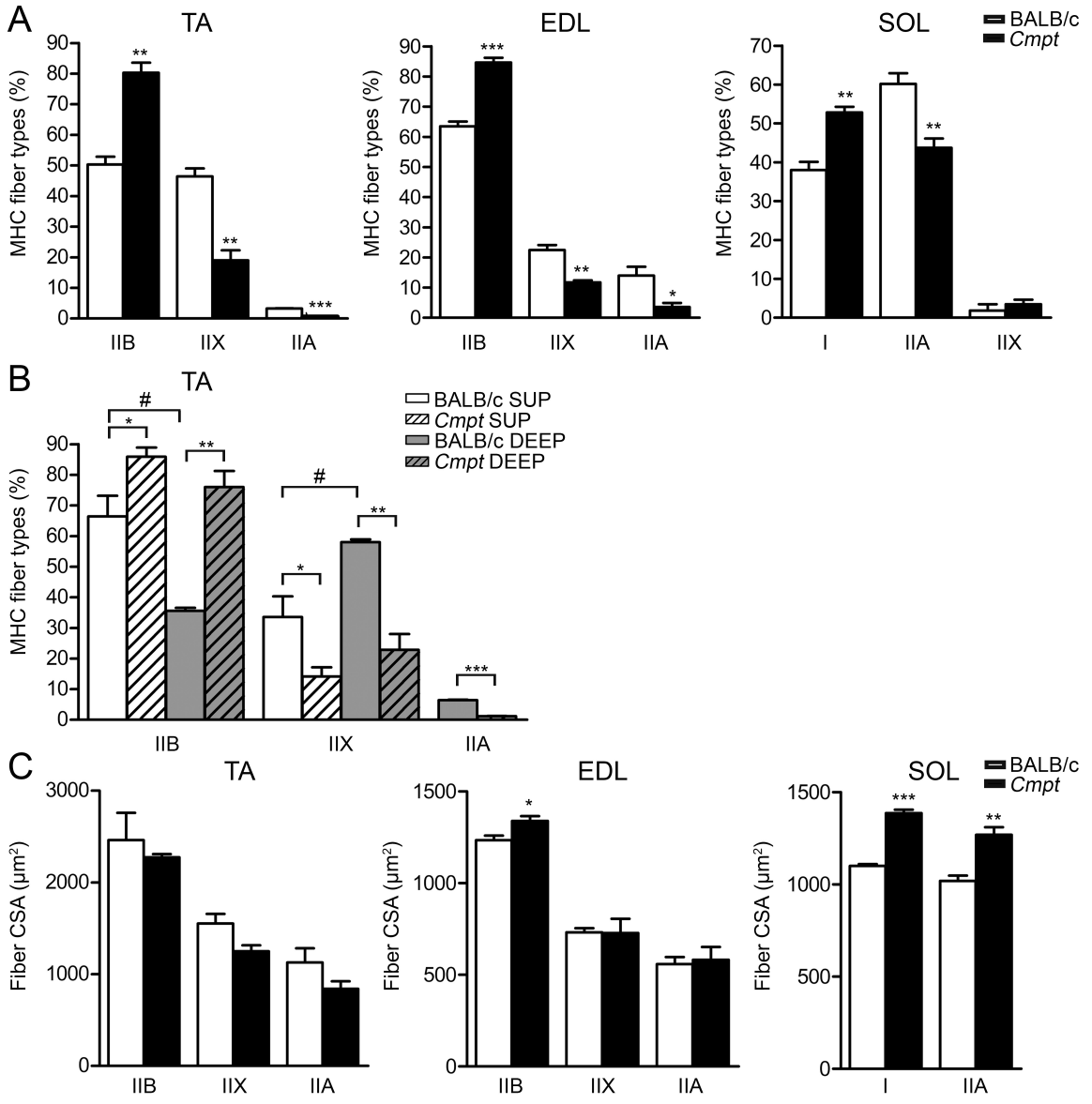

Figure 16. Fiber type composition (A-B) and mean fiber cross sectional area (C) in TA, EDL and SOL muscles of BALB/c and *Cmpt* male mice (mean±SEM). Panel A represents fiber type composition of all fibers in TA, EDL and SOL muscles, while panel B shows regional fiber type distribution of TA muscles subdivided into superficial and deep regions. Panel C represents mean fiber cross sectional area (CSA) of the different (I, IIA, IIX and IIB) fibers in TA, EDL and SOL muscles. Asterisks show significant differences between BALB/c and *Cmpt* mice (n=3-4, *p<0.05, **p<0.01, ***p<0.001) while double cross indicates significant changes between superficial and deep portions of the same TA muscle within a specific mouse line (n=3, $^{\#}$p<0.05).

Fiber composition has been shown to be different in superficial and deep portions of TA muscles in wild-type mice, with more glycolytic IIB fibers at the periphery (Bloemberg and Quadrilatero 2012)). Therefore, we also compared the regional fiber type composition in both mouse lines (Fig. 15, 16B). The number of IIB fibers was significantly higher in both superficial and deep regions of *Cmpt* mice compared with that in wild-type animals (Fig. 15, 16B). Moreover, both muscle regions contained similar number of IIB fibers, whereas in wild-type BALB/c mice, IIB fibers were abundant only in the superficial region, as expected (Fig. 15, 16B). In contrast, the proportion of the glycolytic-oxidative IIX fibers significantly decreased in both TA regions of *Cmpt* mice, without any regional difference in fiber number (Fig. 15, 16B). In wild type mice, however, we found a significantly higher proportion of IIX fibers in the deep region (Fig. 15, 16B). Finally, the low number of the oxidative IIA fibers were almost exclusively confined to the deep region of TA muscles in both mouse strains; however, the number of IIA fibers was further reduced in *Cmpt* mice (Fig. 15, 16B).

Similar to TA muscles, the number of glycolytic IIB fibers was increased in the fast-type EDL muscles of *Cmpt* mice, while the number of IIX and IIA fibers was significantly lower as compared with that of wild-type mice (Fig. 14, 16A).

In contrast, the oxidative SOL muscles in *Cmpt* mice contained more slow-type I fibers and less fast-type IIA fibers than those in wild-type mice, while the number of IIX fibers was very low and not different in the two mouse lines (Fig. 14, 16A).

Together, our findings clearly demonstrate a substantial shift toward a more glycolytic phenotype in the fast-type TA and EDL muscles but not in the mixed-type oxidative SOL muscles of *Cmpt* mice.

In line with our results regarding average fiber size (Fig. 13B), we could not detect specific hypertrophy for any of the IIB, IIX or IIA fiber types in TA muscles (Fig. 16C). Indeed, size distribution of IIB, IIX and IIA fibers in TA muscle revealed only minimal changes in terms of peak position or shape of the histograms in *Cmpt* mice when compared to wild-type muscles (Fig. 17A).

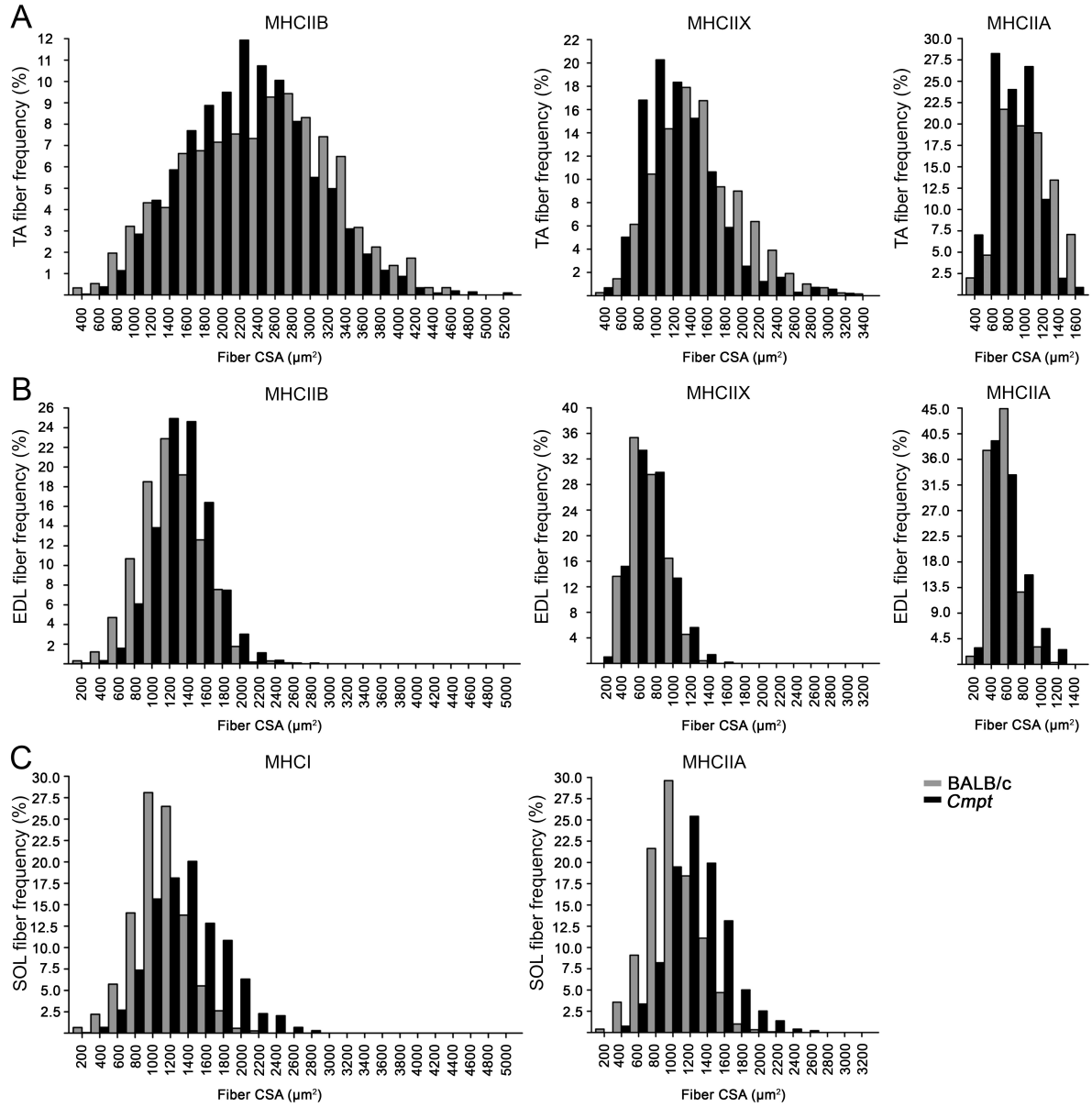

Figure 17. Frequency distribution of MHCIIB, MHCIIX, MHCIIA and MHCI fiber size in TA (A), EDL (B) and SOL (C) muscles of BALB/c and *Cmpt* male mice. CSA: mean fiber cross-sectional area.

In EDL muscles, however, fiber hypertrophy (Fig. 13B) was exclusively detected in IIB fibers, while the size of IIX and IIA fibers were unchanged (Fig. 16C). In line with these findings, IIB fiber distribution in EDL muscles has been shifted toward larger fiber size in *Cmpt* mice, while IIX and IIA histograms were not different between the *Cmpt* and BALB/c lines (Fig. 17B). In contrast to fast muscles, both I and IIA fibers showed evidence of hypertrophy in SOL of *Cmpt* mice (Fig. 16C). Indeed, both fiber frequencies shifted toward a

size increase (Fig. 17C). Due to their low number, IIX fiber size was not analyzed in SOL muscles.

7.1.4. mRNA levels of MHC isoforms

In order to determine the transcript levels of MHC isoforms (*ie*. MHCI, IIA, IIB, IIX) we performed qRT-PCR analysis in TA muscles of both *Cmpt* and BALB/c male mice (Fig. 18).

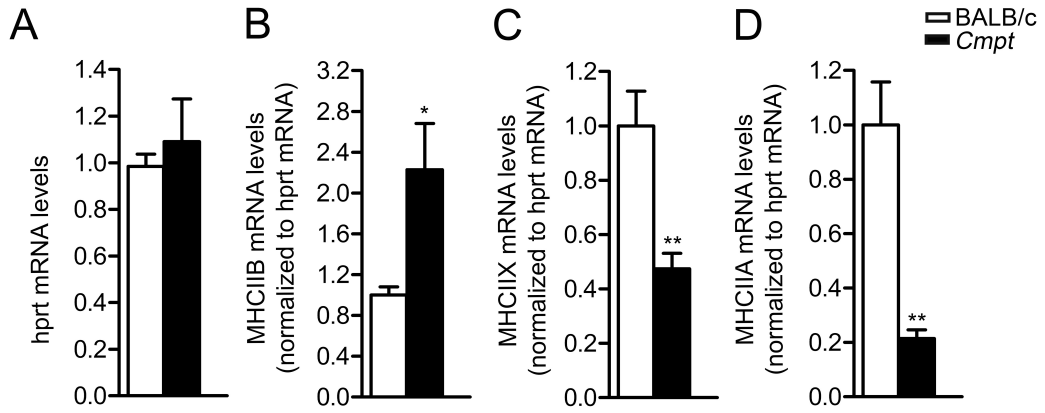

Figure 18. mRNA levels of MHC isoforms and hprt in TA muscles of BALB/c and *Cmpt* male mice. Bars in B-D represent mRNA levels of MHCII isoforms normalized to hprt transcripts (A) (mean±SEM, *p<0.05, **p<0.01, n=5).

Hprt was used as an internal control because Hprt levels were similar in *Cmpt* vs. wild-type TA muscles (Fig. 18A). We found that MHCIIB mRNA levels were significantly increased (Fig. 18B), while MHCIIX (Fig. 18C) and MHCIIA transcript levels (Fig. 18D) both decreased in *Cmpt*. The slow MHCI isoform was almost undetectable (data not shown). These results are in line with those obtained by immunohistochemical analysis, suggesting that the fiber-type shift in the TA muscle is regulated at the level of MHC transcription.

7.2. Myostatin and IGF-I signaling in the human heart

7.2.1. Study patients

A detailed summary of the pre-transplant data and drug therapy of study subjects are shown in Table 5.

	CONT	DCM	ICM
Number of samples	5	5	5
Gender (female/male)	3/2	2/3	4/1
Age (year)	29 ± 9	39 ± 10	57 ± 11$^{*\#}$
NYHA functional class III/IV, *n*	n.a.	0/5	3/2
PAP, mmHg	n.a.	31.6 ± 4.7	30.8 ± 5.6
PWP, mmHg	n.a.	24 ± 4.3	21 ± 3.5
LVED, mm	n.a.	68 ± 4	71 ± 4
LVSD, mm	n.a.	63 ± 5	61 ± 8
PW, mm	n.a.	9.5 ± 0.5	10 ± 1.5
IVS, mm	n.a.	10 ± 0.7	11 ± 1.5
LVEF, %	n.a.	16 ± 3	23 ± 3
Medications			
ACE-inhibitor	-	++	++
β-Blocker	-	++	++
Diuretics	-	++	++
Digitalis	-	+	+
PDE-inhibitor	-	++	++
Dopamine/Noradrenaline	++	++	+
Statin	-	-	++
Aspirin	-	-	++
Desmopressin	++	-	-

Table 5. Clinical, echocardiographic and hemodynamic characteristics of DCM and ICM patients. Values are given in mean±SEM; $^{*}p<0.05$ compared to control; $^{\#}p<0.05$ compared to DCM Abbreviations: CONT: healthy control individuals, DCM: dilated cardiomyopathy, ICM: ischemic cardiomyopathy, NYHA: New York Heart Association, PAP: mean pulmonary artery pressure, PWP: mean pulmonary wedge pressure, LVED: left ventricular end-diastolic diameter, LVSD: left ventricular end-systolic diameter, PW: posterior wall thickness, IVS: interventricular septum thickness, LVEF: left ventricular ejection fraction, ACE: angiotensin converting enzyme, PDE: phosphodiesterase, n.a.: not applicable

Both female and male patients were included in all groups. The age of ICM patients differed as expected significantly from both CONT and DCM, since ICM patients are usually diagnosed with end-stage heart failure later than DCM patients. DCM and ICM patients were in either NYHA class III or IV with no difference in pulmonary artery pressure (PAP, PWP)

left ventricle size parameters (LVED, LVSD, IVS, PW) or left ventricular ejection fraction (LVEF) among groups. Extra care was taken to exclude diabetic (insulin-treated) patients from the study to avoid possible modification of the IGF-I signaling by insulin treatment. All patients were managed with angiotensin-converting enzyme (ACE)-inhibitors, beta-blockers and diuretics, however, aspirin and statins were only used in case of ICM patients. CONT subjects received iv. treatment composed of very low catecholamine infusion (noradrenaline: 01.-0.2 μg/kg/min, dopamine: 1-2 μg/kg/min) whereas adequate fluid balance was maintained with intravenous fluids including colloids (e.g. Voluven - hydroxyethyl starch) and Desmopressin.

7.2.2. Myostatin and IGF-I signaling in healthy human control hearts

So far, no comprehensive study has been carried out to reveal gene expression of the growth regulators Mstn and IGF-I and their receptors in different regions of healthy human hearts. In the present work we detected no significant difference in Mstn (Fig. 19A) and ActRIIB (Fig. 19B) transcript levels nor in Mstn signaling index (Fig. 19C) between septum (S), left ventricle (LV) and right ventricle (RV), however, Mstn levels showed decreasing tendency in the RV (Fig. 19A). In contrast, both IGF-I mRNAs (Fig. 19D) and IGF-I signaling index (Fig. 19F) followed an increasing tendency in RV accompanied with a significantly higher IGF-IR levels compared to those of LV (Fig. 19E).

As a consequence, the ratio of Mstn/IGF-I gene expression (Fig. 20A) as well as those of ActRIIB/IGF-I receptors (Fig. 20B) and finally, the ratio of Mstn to IGF-I signaling (Fig. 20C) all showed significantly higher values in LV/S as compared to RV.

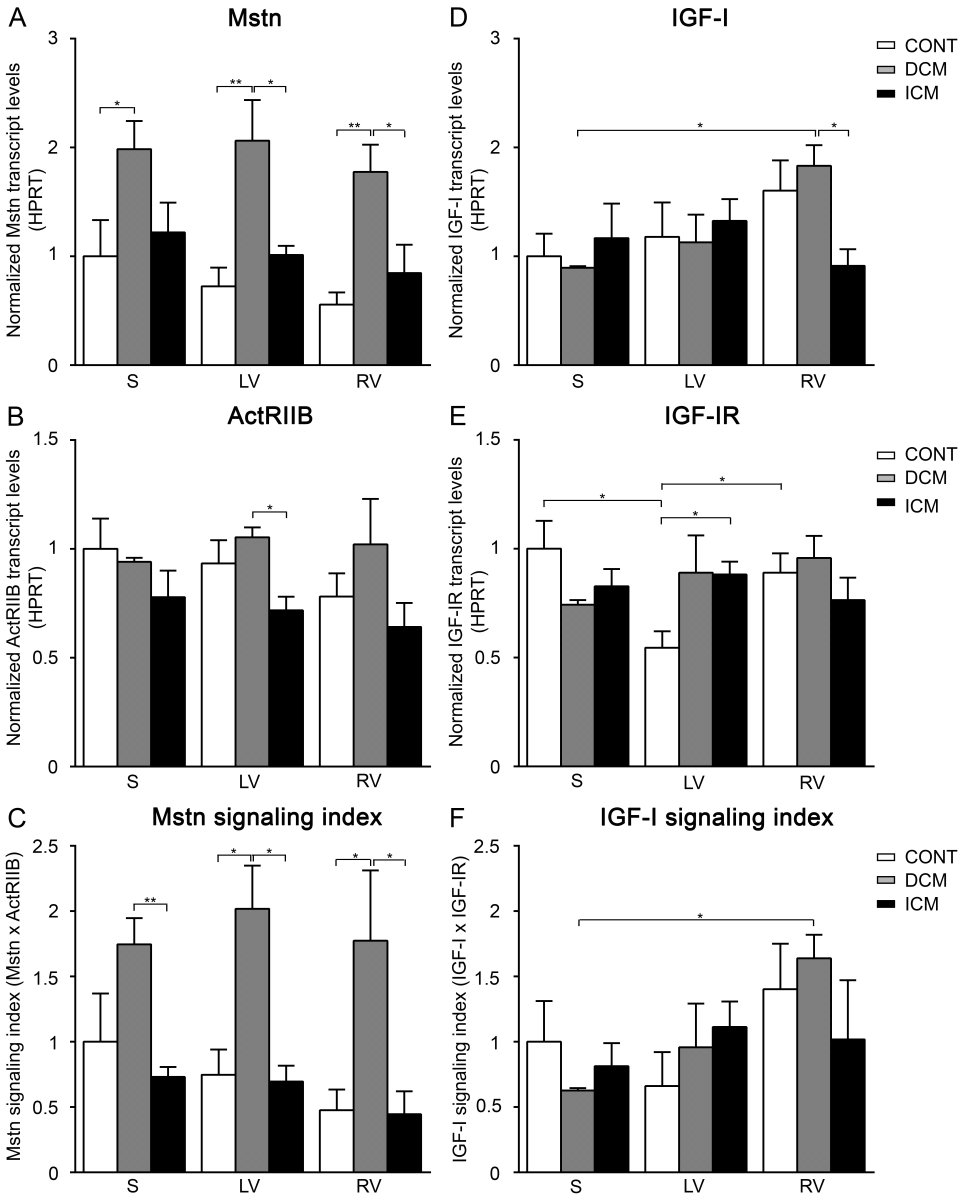

Figure 19. Gene expression levels of Mstn and IGF-I as well as their receptors ActRIIB and IGF-IR normalized to HPRT in the septum (S), left ventricles (LV) and right ventricles (RV) of control (CONT)-, DCM-, and ICM hearts, respectively. Bars represent normalized Mstn- (A), ActRIIB- (B), IGF-I- (D), and IGF-IR- (E) transcript levels. Panel C shows 'Mstn signaling index' (Mstn multiplied by ActRIIB mRNA levels) while panel F represents 'IGF-I signaling index' (IGF-I multiplied by IGF-IR mRNA levels). Data are expressed in mean±SEM, asterisks show significant differences (n=5, *p<0.05, **p<0.01).

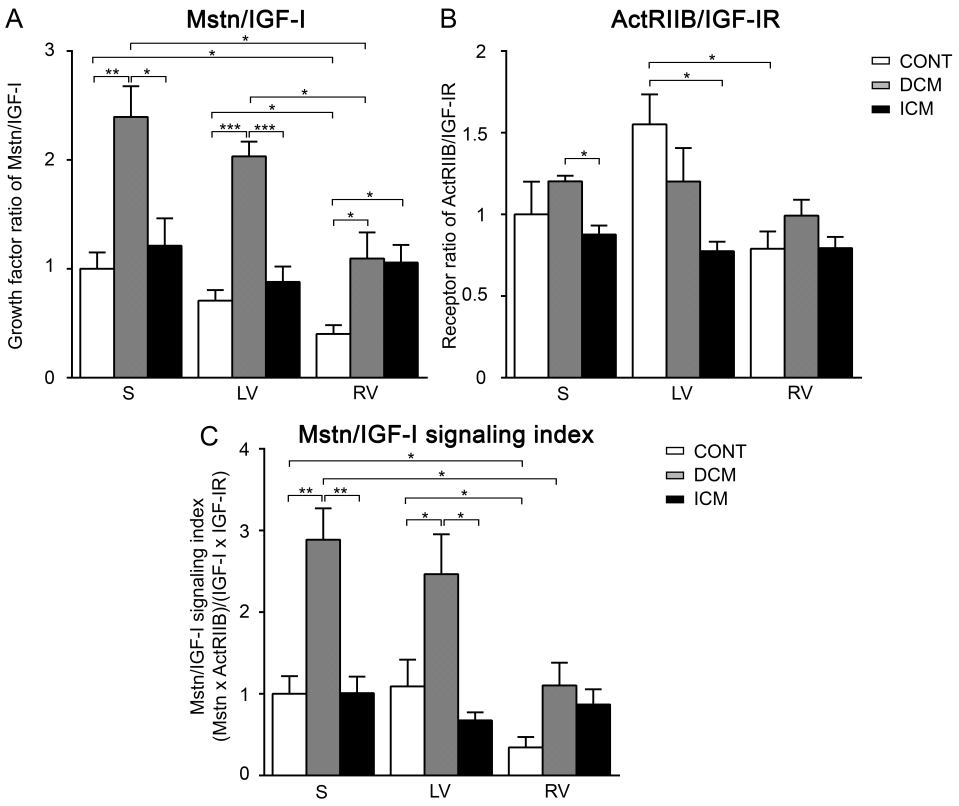

Figure 20. Growth factor ratio of Mstn/IGF-I (A), receptor ratio of ActRIIB/IGF-IR (B) and 'Mstn/IGF-I signaling index' (C) in the septum (S), left ventricles (LV) and right ventricles (RV) of control (CONT)-, DCM-, and ICM hearts, respectively. Panel C represents the ratio of Mstn and IGF-I signaling referred to as 'Mstn/IGF-I signaling index' ('Mstn signaling index' divided by 'IGF-I signaling index' (Mstn x ActRIIB)/(IGF-I x IGF-IR)). Data are expressed in mean±SEM, asterisks show significant differences (n=5, *p<0.05, **p<0.01, ***p<0.001).

These data clearly demonstrate that Mstn signaling dominates over IGF-I in the LV more than in RV of healthy human hearts.

7.2.3. Myostatin and IGF-I signaling in DCM patients compared to healthy controls

In DCM patients we measured massive upregulation of Mstn mRNA (Fig. 1A) associated with an increased Mstn signaling index (Fig. 19C) in all heart regions compared to CONT, although ActRIIB levels remained relatively unchanged (Fig. 19B). Similar to healthy hearts, we found a significant upregulation of IGF-I transcripts (Fig. 19D) as well as of IGF-I signaling index (Fig. 19F) in RV of the failing hearts when compared to those of S, although IGF-IR expression did not show significant difference in either region nor in comparison to CONT hearts (Fig. 19E). Thus, the ratio of Mstn/IGF-I mRNA levels (Fig. 20A) and the Mstn/IGF-I signaling index (Fig. 20C) proved to be significantly higher in the left versus right

side of the DCM hearts and showed much higher levels than those of the CONT regions. Since the ratio of the ActRIIB/IGF-I receptors (Fig. 20B) did not change significantly we can conclude that Mstn was upregulated in all regions of failing hearts in DCM patients as compared to CONT. However, given the higher IGF-I levels in RV, left and right side of failing heart differed significantly from each other in regard to the ratio of Mstn/IGF-I signaling similar to those of healthy ones (Fig. 20C).

7.2.4. Myostatin and IGF-I signaling in ICM patients compared to healthy controls

In contrast to DCM patients, we could not detect any difference in either Mstn (Fig. 19A) or ActRIIB transcript levels (Fig. 19B) or in Mstn signaling index (Fig. 19C) in any heart region of ICM patients compared to those of CONT. Similarly, IGF-I (Fig. 19D) and IGF-IR levels (Fig. 19E) as well as IGF-I signaling index (Fig. 19F) did not differ in ICM heart regions; however, in comparison to CONT, IGF-I showed a decreasing tendency of expression in the RV, while increased expression of IGF-IR in the LV was present. Consequently, both ratios of Mstn/IGF-I (Fig. 20A) and ActRIIB/IGF-IR (Fig. 20B) were similar in all analyzed regions of ICM hearts. However, significantly higher Mstn/IGF-I ratios were revealed in RV due to decreased IGF-I levels as well as significantly lower ActRIIB/IGF-IR ratios in LV when compared to CONT hearts (due to increased IGF-IR levels). In summary, ICM hearts did not show significantly altered modulation of Mstn signaling in either heart region, whereas IGF-I signaling, in contrast to the healthy situation, seemed to be moderately induced in the LV, while inhibited in the RV.

7.2.5. Differences in Myostatin/IGF-I signaling between DCM and ICM patients

Based on our results, all regions of DCM hearts showed significantly higher Mstn levels (Fig. 19A) as well as elevated Mstn signaling index (Fig. 19C) than those of ICM hearts. Moreover, ActRIIB (Fig. 19B) also revealed increased levels in LV of DCM vs. ICM patients. Nevertheless, we found no significant difference in IGF-I signaling on the left side of failing hearts (Fig. 19D-F), although significantly less IGF-I transcripts were evident on the right side of ICM hearts in comparison with that of DCM ones (Fig. 19D). As a consequence, all parameters describing the ratio of Mstn to IGF-I signaling (Fig. 20A-C) showed significantly increased values in the LV of DCM versus ICM hearts. Although in the RV we have revealed similar signaling ratio in both types of failing hearts (Fig. 20A-C) the reason for

that was an upregulation of Mstn signaling in DCM patients while a downregulation of IGF-I signaling in ICM heart samples.

7.2.6. miR-208 in relation to myostatin expression in DCM and ICM patients compared to healthy controls

In parallel with the massive upregulation of Mstn mRNA in the LV of DCM patients we measured a mild upregulation of miR-208b (1.505 fold change) compared to CONT. A similar but less pronounced upregulation was seen in ICM hearts (1.405 fold change) when compared to CONT, however, no significant difference was detected between DCM and ICM patients (Table 6).

Left ventricle	CONT	DCM	ICM
miR-208b (mean ± SEM)	1 ± 0.19	1.505 ± 0.26	1.405 ± 0.24
Number of values	5	3	4

Table 6. miR-208b expression level in left ventricle region of human heart. CONT: control, DCM: dilated cardiomyopathy, ICM: ischemic cardiomyopathy.

8. Discussion

Mstn belongs to the TGF-β family and is a negative regulator of skeletal muscle growth. However, it plays also a crucial role in governing heart growth, metabolism and contraction. Our aim was to describe different aspects of Mstn signaling in skeletal muscle and heart tissue. To this end, two different model systems have been used in our experiments, (i) the Mstn propeptide-mutant *Cmpt* mice as well as (ii) healthy and pathological human hearts (S, LV, RV samples of DCM and ICM patients). Muscle cellularity and fiber type distribution have been analyzed in the fast TA and EDL as well as the mixed-type SOL muscles of *Cmpt* mice and transcript levels of MHC isoforms were quantified by qPCR. On the other hand, gene expression of Mstn and IGF-I, the two major but mostly counter-acting regulators of cardiac tissue have been investigated in different regions of healthy or pathological human hearts by measuring transcript levels of Mstn, ActRIIB, IGF-I, IGF-IR and miR-208, the negative posttranscriptional regulator of Mstn.

8.1. Muscle phenotype of *Cmpt* mice

The *Cmpt* mouse line takes a special place in the group of hypermuscular animals carrying naturally occurring Mstn mutations, as the propeptide region, not the biologically active domain of Mstn is affected. Abnormal propeptide structure might play an important role in misfolding, inefficient secretion, and/ or abnormal processing of Mstn in *Cmpt* mice (Szabó et al. 1998). It has also been shown that the *Cmpt* mutation of Mstn is an indispensable yet not satisfactory requirement for the full expression of the hypermuscular phenotype, pinpointing the potential significance of additional modifier genes (Varga et al. 1997, 2003, 2005).

Since the genetic background of the *Cmpt* mice is very complex and no appropriate genetic control line was available at the time of our experiments, we decided to analyze BALB/c mice as a control for the following reasons: i) This inbred line was used for mapping the Mstn mutation and the modifier genes in *Cmpt* mice (Szabó et al. 1998). ii) BALB/c mice are generally used as wild-type controls and their muscle parameters as well as fiber composition have already been reported (Freitas et al. 2002; Luedeke et al. 2004). iii) Muscle characteristics of BALB/c mice are similar to those of C57BL/6, another wild-type mice used as a genetic background for Mstn KO mice (McPherron et al. 1997), suggesting that these lines might be comparable to some extent (Luedeke et al. 2004; Pellegrino et al. 2005; Bloemberg and Quadrilatero 2012; McKeehen et al. 2013).

In the present study we show, in accordance with others (Bünger et al. 2004; Rehfeldt et al. 2005; Amthor et al. 2007, 2009) that body- and muscle weights of male *Cmpt* mice are higher than those of wild type BALB/c mice. Body mass is even higher in *Cmpt* mice (47,7g) than in male Mstn KO of the same age (38-41g, McPherron et al. 1997). However, muscle weights normalized to body weight are comparable in both Mstn mutant lines, suggesting that *Cmpt* and Mstn KO mice represent a similar grade of muscularity. One exception was the soleus muscle, which seemed to be different in this regard, as its relative muscle-to body weight did not increase in *Cmpt* compared with the wild type mice. Indeed, it has previously been reported that the oxidative soleus muscle contained less Mstn transcript than the glycolytic EDL (Mendler et al. 2000; Wang et al. 2012) and, that the lack of Mstn had stronger effect on glycolytic muscles than on oxidative ones (McPherron et al. 1997; Carlson et al. 1999; Hennebry et al. 2009; Wang et al. 2012). Therefore, we analyzed three different hindlimb muscles: the fast-glycolytic TA and EDL as well as the oxidative SOL muscles in *Cmpt* mice. Based on extensive morphometrical analysis - measuring and counting all fibers on HE stained cross sections or 500-1000 fibers on MHCIIB-stained sections - TA muscles were exclusively characterized by muscle fiber hyperplasia, with no obvious hypertrophy (Fig. 21).

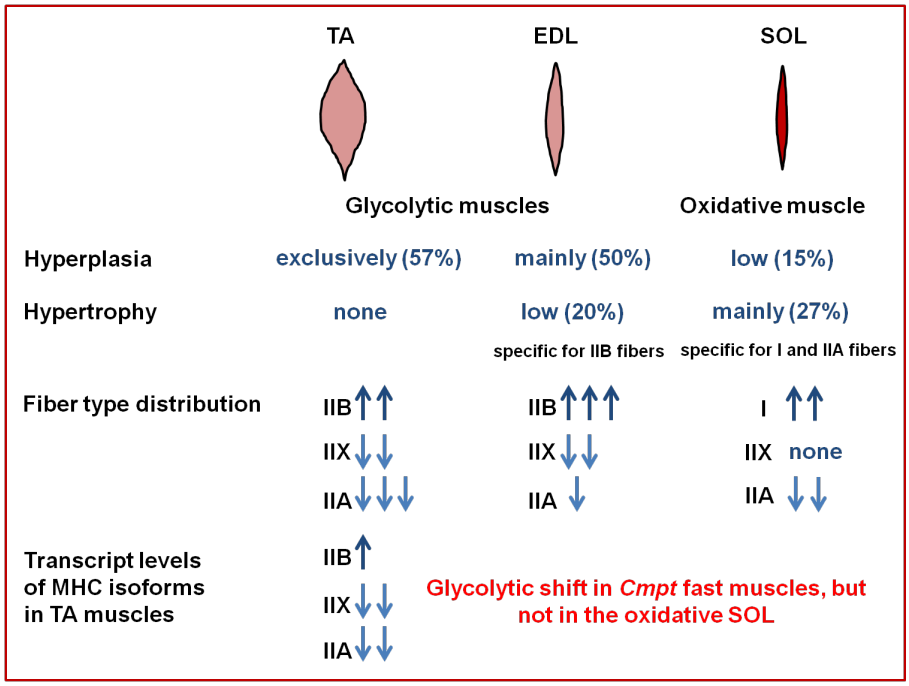

Figure 21. Summary of muscle morphometrical and immunohistochemical results in myostatin mutant *Cmpt* mice. Arrows show increase or decrease in specific fiber types and MHC (myosin heavy chain) transcript levels. TA: m. tibialis anterior, EDL: m. extensor digitorum longus, SOL: m. soleus.

This observation may somewhat be surprising, as previous reports described both hyperplasia and hypertrophy in different Mstn KO animals (McPherron and Lee, 1997; Amthor et al. 2009). However, even in the original Mstn KO mouse study (McPherron et al. 1997), the ratio of hyperplasia to hypertrophy varied in different muscles, *e.g*. the TA muscles of Mstn KO mice were dominated by hyperplasia, while only 14% fiber hypertrophy was documented. To note, Mstn KO vs. $Mstn^{+/+}$ control mice (McPherron et al. 1997) contained similar fiber number in TA muscles (5470 vs. 2936) as the *Cmpt* vs. BALB/c mice in our study (5455 vs. 3093), making KO and *Cmpt* experiments comparable. In contrast to TA, EDL muscles of *Cmpt* mice were characterized by a combination of hyperplasia (50%) and hypertrophy (20%), whereas EDL in the Mstn KO mice showed only a moderate hyperplasia and a stronger hypertrophy (Amthor et al. 2009) (Fig. 21). Amthor and colleagues (2009) compared EDL muscles of the Mstn KO with that of the female 'Berlin' *Cmpt* mice ($BEH^{c/c}$). In line with our findings, they also detected stronger hyperplasia in female $BEH^{c/c}$ EDL muscles (1589) than in the Mstn KO (1200). In addition, fiber number of both $BEH^{+/+}$ and $Mstn^{+/+}$ controls were comparable with ours (1083 and 1160 vs. 1232, respectively). However, our results are somewhat different from those of $BEH^{c/c}$ females, in which fiber hypertrophy was very pronounced and dominated over hyperplasia (Amthor et al. 2009). We found that the moderate fiber hypertrophy in *Cmpt* EDL confined to the most glycolytic IIB fibers and was not present in IIX or IIA fibers (Fig. 21). This is again in accordance with the previous reports on a stronger effect of Mstn on glycolytic muscles (McPherron et al. 1997; Carlson et al. 1999; Hennebry et al. 2009; Wang et al. 2012). We believe that the long separation of the 'Berlin' and Hungarian *Cmpt* lines, gender differences, the use of different controls as well as our detailed sample analysis (counting 3000/1800 fibers in *Cmpt*/BALB/c vs. 150/180 fibers in $BEH^{c/c}$/$BEH^{+/+}$ (Amthor et al. 2009)) may account for these differencies.

In the oxidative SOL muscle of *Cmpt* mice, low-grade hyperplasia (15%) and mainly hypertrophy (27%) accounted for the moderately higher muscle mass (Fig. 21). Moreover, both the oxidative I and IIA fibers showed hypertrophy compared with the wild-type control. The changes in SOL are different from those of fast TA and EDL muscles in the *Cmpt* line. Intriguingly, controversial results have been published regarding SOL in Mstn KO mice, where either 32% hyperplasia (Girgenrath et al. 2005), or 20% fiber hypertrophy has been described (Gentry et al. 2011).

It is not known so far, how cellularity in different muscle types is regulated upon Mstn defect. However, prenatal hyperplasia seems to be the major effect of developmental Mstn deficiency in most muscles of mice and cattle (McPherron et al. 1997; Grobet et al. 1997; Lee and McPherron 1997). Based on the different ratio of hyperplasia to hypertrophy in various Mstn deficient muscles, Mstn might have a strong, but muscle-type dependent effect on proliferation of muscle precursor cells. Consequently, postnatal fiber hypertrophy might be restricted to different grade. Rehfeldt and co-workers (2005) introgressed the Mstn mutant *Cmpt* allele into a special high growth mouse line (DUHi) and detected exclusively hyperplasia, similar to our results, in the predominantly fast rectus femoris and longissimus dorsi muscles. These data suggest that, at least in fast muscles, hyperplasia is even more pronounced in *Cmpt* than in Mstn KO mice. This difference might reside in the allelic variation of Mstn defect and/or in modifier genes influencing *Cmpt* phenotype. To prove that the dominance of hyperplasia (over hypertrophy) in 2.5-month-old *Cmpt* muscles is not the consequence of postnatal delay in fiber growth, we have analyzed TA muscles of 7-month-old *Cmpt* male mice. We found a similar hyperplasia without any substantial fiber hypertrophy in older animals as well, which refutes the idea that fiber growth might reach its peak later in adulthood.

Although TA and EDL muscles contain predominantly type II glycolytic fibers (Bloemberg and Quadrilatero 2012), we observed a significant glycolytic shift within type II fibers in *Cmpt* mice. This result is consistent with that of Rehfeldt et al. (2005) who found more glycolytic fibers in the rectus femoris muscle of the special *Cmpt*-DUHi line by NADH-tetrazolium reductase staining. A substantial glycolytic shift has also been described in EDL muscles of Mstn KO mice as well as in double-muscled cattle by applying different methods (ATPase and SDH staining vs. immunohistochemical analysis), which suggests that both metabolic and structural protein changes occur upon Mstn deficiency (Wegner et al. 2000; Girgenrath et al. 2005; Amthor et al. 2007). However, immunohistochemical staining of MHC isoforms is more appropriate to distinguish between fiber types. We have detected significantly more IIB fibers and less IIX or IIA fibers in TA muscles of *Cmpt* mice than in the wild type. Additionally, we analyzed fiber type distribution in both superficial and deep portions of TA, since regional differences in glycolytic fiber distribution are well-known in wild-type mice (Bloemberg and Quadrilatero 2012). Interestingly, the regional difference

disappeared in *Cmpt* mice, so that both superficial and deep regions of TA muscles were dominated by the glycolytic IIB fibers of a quite uniform fiber size. Transcript levels were in agreement with our immunohistochemical results; MHCIIB mRNA levels were significantly higher, while those of MHCIIX and IIA significantly lower in *Cmpt* TA muscles compared with those genes in wild type muscles. These findings suggest that the glycolytic fiber-type shift in fast muscles is supported by respective changes of MHC transcripts.

Along this line, we measured the same ratio of IIB/IIX/IIA fibers in EDL muscles of *Cmpt* by using immunohistochemical methods. Amthor and colleagues (2007) demonstrated similar consequencies in regard to glycolytic shift in Mstn KO mice. Consistently, decrease in mitochondrial content, reduced expression of cytochrome c oxidase, lower citrate synthase activity and shortening of contraction as well as relaxation time have been described in Mstn KO mice (Amthor et al. 2007; Savage and McPherron 2010). Moreover, Mstn KOs showed impaired tolerance to chronic repetitive contractions (Ploquin et al. 2012) and a decrease in specific force generation, similar to what was measured in $BEH^{c/c}$ female EDL muscles (Amthor et al. 2007). Altogether, these data suggest that the function of the bigger and more glycolytic muscles is impaired upon Mstn defect.

However, the oxidative SOL muscle has not shown any glycolytic shift in *Cmpt* mice (53% slow-oxidative type I fibers, 44% fast-oxidative IIA fibers) as compared with BALB/c line (38% type I fibers, 60% type IIA fibers). In contrast, these fibers were even more oxidative than the controls. Fiber type composition of BALB/c SOL in our experiments were in agreement with previous data (Freitas et al. 2002; Luedeke et al. 2004) and represented a fiber ratio typical of a wild-type SOL, with less than 40% slow-type I fibers (Pellegrino et al. 2005; Bloemberg and Quadrilatero 2012; McKeehen et al. 2013). Therefore, it is unlikely that BALB/c mouse was not an appropriate type of control for our experiments in this regard. Based on literature search, more than 50% slow-type I fibers in *Cmpt* animals is rather unusual for a SOL muscle in any type of mice, and also contradicts previous reports on Mstn KO mice (Girgenrath et al. 2005; Gentry et al. 2011; Wang et al. 2012). To conclude, different mechanisms of Mstn deficiency -with or without the influence of modifier genes- may induce differential and muscle-specific effects.

In summary, *Cmpt* mouse, inspite of its complex genetic background, shows similarities (at least in fast muscles) to Mstn KO mice in terms of muscle cellularity and glycolytic muscle

phenotype, suggesting that the lack of Mstn is responsible for these morphological/functional changes. However, based on the more pronounced hyperplasia in *Cmpt* fast muscles as well as the different cellularity and oxidative phenotype of *Cmpt* SOL, additional studies are needed to elucidate the molecular mechanisms of Mstn inactivity and the possible role of modifier genes in *Cmpt* mice.

8.2. Myostatin and IGF-I signaling in the human heart

Mstn and IGF-I both have been shown to play a crucial role in the pathomechanism of human heart failure with upregulated Mstn protein in the failing myocardium (George et al. 2010). However, the exact mechanism and their possible interplay in the course of heart failure have not been clarified yet. In this study, we have measured Mstn, ActRIIB, IGF-I, IGF-IR transcript levels in different heart regions of normal and pathological human hearts, as well as the miR-208 expression serving as a negative regulator of Mstn expression. In order to characterize Mstn and IGF-I signaling we created complex parameters by combining respective transcript levels.

In the present comprehensive qRT-PCR study we have found that Mstn dominated over IGF-I signaling much more in the LV than in the RV of healthy human hearts, and that DCM hearts upregulated Mstn expression in contrast to ICM hearts. This is the first demonstration that Mstn/IGF-I signaling differs in LV and RV in healthy hearts and shows significant alterations in end-stage heart failure due to DCM and ICM (Fig. 22).

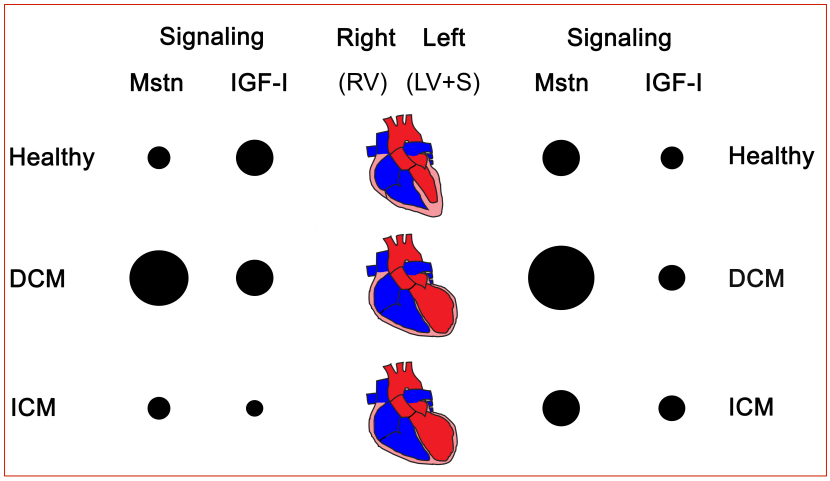

Figure 22. Summary of gene expression alterations regarding myostatin and IGF-I signaling in healthy human hearts as well as in DCM and ICM patients, respectively. Bigger circles represent higher expression of the signaling molecules in healthy vs. dilated cardiomyopathic (DCM) or ischemic cardiomyopathic (ICM) hearts or in left vs. right side of the hearts. Mstn: myostatin, IGF-I: insulin-like growth factor I, LV: left ventricle, S: septum, RV: right ventricle.

Several studies exist in the literature, indicating the presence and/or de-regulation of both Mstn and IGF-I under different conditions in the heart, however, the majority of data were collected from whole hearts or separately, from the LV (Sharma et al. 1999; Serneri et al. 1999, 2001; George et al. 2010). Regarding Mstn expression in healthy hearts, only one study has been published so far on higher transcript levels of Mstn in LV as compared to RV in young piglet hearts (Torrado et al. 2010). In line with these data we have demonstrated here an obvious reciprocal regulation of Mstn and IGF-I in LV compared to RV characterized by elevated ratios of both Mstn/IGF-I and ActRIIB/IGF-IR transcripts in healthy human LV (Fig. 22). Septum (S) samples, as being part of LV from the functional point of view, revealed similar values to those of LV in most cases. We assume that cardiomyocyte growth in LV/S should be balanced more tightly by growth inhibitors (i.e. Mstn) than that of RV since LV is exposed to higher-pressure overload, while RV to a relatively higher-volume overload. In addition to Mstn and IGF-I, several other factors have been reported to be enriched in either LV or RV; their asymmetric expression might reflect a molecular predisposition of myocardium to LV-concentric or RV-eccentric remodeling during postnatal development (Torrado et al. 2010; Modesti et al. 2004). Similarly, higher expression levels in LV versus RV have been demonstrated for cytochrome c oxidases and PGC1α, both of which are known to contribute to maintain mitochondrial function and oxidative metabolism (Zungu et al. 2008). Recently, it has been shown that Mstn plays an important role in the regulation of oxidative metabolism of the myocardium (Biesemann et al. 2014). Therefore our results support the idea that the elevated ratio of Mstn/IGF-I signaling is an important regulatory mechanism under physiological conditions maintaining higher workload and oxidative metabolism in the LV. These results are also in accordance with the glycolytic shift in skeletal muscles upon Mstn defect and suggest that Mstn exert similar metabolic effects in both skeletal muscle and cardiac tissues, at least in the LV.

In human failing hearts (in whole hearts or LV), Mstn protein activation was reported to be accelerated in both DCM and ICM patients (George et al. 2010). In parallel with this observation several groups found increased serum levels of Mstn protein in patients suffering from heart failure, although no correlation was demonstrated with the severity or type of cardiac disease (George et al. 2010; Heineke et al. 2010; Gruson et al. 2011; Breitbart et al. 2013). One should also consider that elevated serum Mstn levels in cardiomyopathic patients

might be a combined effect of increased secretion from both cardiac and skeletal muscles. Nevertheless, exercise training lead to a reduction of Mstn levels only in skeletal muscles but not in serum of patients with chronic heart failure (Lenk et al. 2012). Intriguingly, it has not been clarified, whether protein activation in failing heart is regulated either at the level of gene expression or posttranscriptionally. Here we show that DCM hearts are indeed characterized by upregulated Mstn transcripts in both LV/S and RV supporting the previous reports on protein activation in LV (George et al. 2010). However, we could not detect any significant elevation of Mstn transcript levels in ICM patients (Fig. 22). We also tested the miRNA-dependent posttranscriptional regulation of Mstn. miR-208 have been reported to be a negative regulator of Mstn expression (Callis et al. 2009), and to be upregulated in various forms of cardiomyopathy (Bostjancic et al. 2010; Satoh et al. 2010) and myocardial ischemia (Varga et al. 2014). In line with these, we detected a mild upregulation of miR-208b in the LV of DCM patients characterized by massive increase of Mstn transcripts that might suggest an adaptive counter-regulatory mechanism fine-tuning the expression of Mstn during heart failure. Since we have found no difference in miR-208b expression between DCM and ICM hearts, it is likely that increased Mstn mRNA is mainly regulated at the level of transcription. Although alterations in Mstn gene expression are followed by similar changes at the protein level in most cases (Shyu et al. 2006; McKoy et al. 2007; Lenk et al. 2009), the intra- or extracellular proMstn-pool might be posttranslationally activated by the cleavage of the propeptide (Mendler et al. 2000, 2007; Anderson et al. 2008). Thus, ICM patients might have a Mstn activation at the protein level (George et al. 2010), however, not at the level of transcription, whereas DCM hearts react with significant upregulation of Mstn transcripts. Similar to the results of George et al. (2010) we detected lower level of ActRIIB in ICM than in DCM patients, but this occured only in the LV. On the other hand, IGF-I expression was shown to be dynamically regulated in the course of heart failure as an important compensatory mechanism; however, conflicting data exist in the literature with both down- and upregulated IGF-I levels in end-stage heart failure (Serneri et al. 1999; Barton et al. 2005; Pucci et al. 2009). We could confirm significant decrease of IGF-I signaling in the RV of ICM patients but not in LV or DCM patients. Moreover, DCM patients still maintained the physiological difference in Mstn/IGF-I signaling ratios in LV versus RV, whereas no asymmetric gene expression pattern was detected in ICM patients (Fig. 22). The mechanisms

leading to different regulation of growth factor signaling in DCM and ICM patients remain to be clarified, however, it might relate to the different pathomechanism of heart failure and/or alternative regulation of compensatory mechanisms. Indeed, Mstn upregulation detected in DCM hearts might be part of adaptation reactions since Biesemann et al (2014) have recently reported that acute cardiac-specific deletion of Mstn in adult mouse hearts induces dilated cardiomyopathy followed by a massive compensatory up-regulation of Mstn in non-cardiomyocytes. It is known, however, that various cardiac disease conditions, i.e. hypoxia can result in an imbalance of chamber-associated gene expression in myocardium (Chugh et al. 2003; Modesti et al. 2004; Zungu et al. 2008; Torrado et al. 2010). Therefore, ICM hearts of ischemic origin might not be able to compensate as effective as do DCM patients by upregulating Mstn to maintain oxidative metabolism (Biesemann et al. 2014) and by regulating their IGF-I signaling to counteract decreased contractility (Serneri et al. 1999). However, further research is needed to elucidate the physiological and pathological relevance of the complex Mstn/IGF-I network in human heart.

9. Conclusions

We have described different aspects of Mstn signaling in skeletal muscle and heart tissue by applying two different model systems (i) the Mstn mutant hypermuscular *Cmpt* mice and (ii) healthy and pathological human hearts.

1. We have morphologically analyzed different glycolytic (TA, EDL) versus oxidative (SOL) skeletal muscles of *Cmpt* mice. All of them were significantly larger characterized by fiber hyperplasia of various grade. Fiber hypertrophy was either not present (TA) or confined to a specific type (IIB fibers in EDL) or in contrast, present in all fibers (SOL). These findings imply for muscle-specific morphological effects of Mstn defect in *Cmpt* mice.

2. Fast-type glycolytic muscles (TA, EDL) of *Cmpt* mice contained significantly more glycolytic IIB fibers as well as increased MHCIIB transcript levels. According to previous reports, similar glycolytic shift was observed in Mstn KO mice suggesting that the lack of Mstn might be responsible for these changes in both *Cmpt* and Mstn KO mice. However, the genetic background (modifier genes) might also have an impact, since the oxidative SOL muscle in *Cmpt* mice did not display any glycolytic alteration.

3. According to our human heart study we have found, that Mstn dominated over IGF-I signaling much more in the LV than in the RV of healthy human hearts. The spatial asymmetry in the expression pattern of Mstn/IGF-I is likely to play a role in the different growth regulation of LV versus RV.

4. We identified Mstn as a massively up-regulated gene in DCM but not in ICM as part of potential compensatory mechanisms in the failing heart.

5. Mild upregulation of miR-208b in pathological human hearts might serve as a Mstn counter-regulatory mechanism. Since miR-208b expression was similar in DCM and ICM hearts, higher levels of Mstn mRNAs in DCM might be maintained through accelerated transcription.

10. Acknowledgements

This work was supported by the 3-year doctoral fellowship of the Hungarian Ministry of Education; by Hungarian National Development Agency, the European Union and co-funded by the European Social Fund [project numbers: TÁMOP 4.2.2/B-10/1-2010-0012; TÁMOP 4.2.2.A-11-1-KONV-2012-0035], by "National Excellence Program" [TÁMOP 4.2.4.A/2-11-1-2012-0001], and by Hungarian Scientific Research Fund (OTKA K109739, OTKA ANN 107803).

I greatly acknowledge Professor László Dux for providing me possibility to work at the Department of Biochemistry.

I am especially thankful to my supervisor Luca Mendler who was supporting me without sparing her time and energy over the past few years. Her guidance and encouragement were indispensible all the time.

I am greatful to Przemyslaw Leszek and Mariusz Kuśmierczyk who measured clinical, echocardiographic and hemodynamic characteristics of heart failure patients, and together with Péter Ferdinandy provided me with human cardiac samples.

I am greatful to Zoltán V. Varga and Tamás Baranyai for their cooperation, especially for the performance of the miR-208 qRT-PCR analysis.

Many thanks to Makráné Felhő Zita, Csontos Lászlóné and Balásházy Istvánné for their skillful technical assistances.

I would like to give my special thanks to all of my present and past colleagues and friends. Finally, I take this opportunity to acknowledge my family for their support, especially my mother and my future husband.

11. References

1. Amthor H, Macharia R, Navarrete R, Schuelke M, Brown SC, Otto A, Voit T, Muntoni F, Vrbóva G, Partridge T, Zammit P, Bünger L, Patel K. 2007. Lack of myostatin results in excessive muscle growth but impaired force generation. Proc Natl Acad Sci. 104:1835-1840.
2. Amthor H, Otto A, Vulin A, Rochat A, Dumonceaux J, Garcia L, Mouisel E, Hourdé C, Macharia R, Friedrichs M, Relaix F, Zammit PS, Matsakas A, Patel K, Partridge T. 2009. Muscle hypertrophy driven by myostatin blockade does not require stem/precursor-cell activity. Proc Natl Acad Sci. 106:7479-7484.
3. Anderson SB, Goldberg AL, Whitman M. 2008. Identification of a novel pool of extracellular pro-myostatin in skeletal muscle. J Biol Chem. 283:7027-7035.
4. Arcopinto M, Bobbio E, Bossone E, Perrone-Filardi P, Napoli R, Sacca L, Cittadini A. 2013. The GH/IGF-1 Axis in Chronic Heart Failure. Endocrin Metab Immun Disord Drug Targets. 13:76-91.
5. Artaza JN, Reisz-Porszasz S, Dow JS, Kloner RA, Tsao J, Bhasin S, Gonzalez-Cadavid NF. 2007. Alterations in myostatin expression are associated with changes in cardiac left ventricular mass but not ejection fraction in the mouse. J Endocrinol. 194:63–76.
6. Artaza JN, Singh R, Ferrini MG, Braga M, Tsao J, Gonzales-Cadavid NF. 2008. Myostatin promotes a fibrotic phenotypic switch in multipotent C3H 10T1/2 cells without affecting their differentiation into myofibroblasts. J Endocrinol. 196:235-249.
7. Bailey-Downs LC, Sosnowska D, Toth P, Mitschelen M, Gautam T, Henthorn JC, Ballabh P, Koller A, Farley JA, Sonntag WE, Csiszar A, Ungvari Z. 2012. Growth hormone and IGF-1 deficiency exacerbate high-fat diet-induced endothelial impairment in obese Lewis dwarf rats: implications for vascular aging. J Gerontol A Biol Sci Med Sci. 67:553-64.
8. Barton PJ, Felkin LE, Birks EJ, Culle ME, Banner NR, Grindle S, Hall Jl, Miller LW, Yacoub MH. 2005. Myocardial insulin-like growth factor-I gene expression during recovery from heart failure after combined left ventricular assist device and clenbuterol therapy. Circulation. 112: I46-I50.

9. Biesemann N, Mendler L, Wietelmann A, Hermann S, Schäfers M, Krüger M, Boettger T, Borchardt T, Braun T. 2014. Myostatin Regulates Energy Homeostasis in the Heart and Prevents Heart Failure. Circ Res. 115:296-310.
10. Biesemann N, Mendler L, Kostin S, Wietelmann A, Borchardt T, Braun T. 2015. Myostatin induces interstitial fibrosis in the heart via TAK1 and p38. Cell Tissue Res. doi: 10.1007/s00441-015-2139-2.
11. Bloemberg D, Quadrilatero J. 2012. Rapid determination of myosin heavy chain expression in rat, mouse and human skeletal muscle using multicolor immunofluorescence analysis. Plos One. 7:1-11.
12. Bogdanovich S, Krag TO, Barton ER, Morris LD, Whittemore LA, Ahima RS, Khurana TS. 2002. Functional improvement of dystrophic muscle by myostatin blockade. Nature. 420:418-421.
13. Boman IA, Klemetsdal G, Blichfeldt T, Nafstad O, Vage DI. 2009. A frameshift mutation in the coding region of the myostatin gene (MSTN) affects carcass conformation and fatness in Norwegian white sheep (Ovis aries). Anim Genetics. 40:418-422.
14. Bostjancic E, Zidar N, Stajer D, Glavac D. 2010. MicroRNAs miR-1, miR-133a, miR-133b and miR-208 are dysregulated in human myocardial infarction. Cardiology. 115:163-169.
15. Breitbart A, Auger-Messier M, Molkentin JD, Heineke J. 2011. Myostatin from the heart: local and systemic actions in cardiac failure and muscle wasting. Am J Physiol Heart Circ Physiol. 300:H1973-H1982.
16. Breitbart A, Scharf GM, Duncker D, Widera C, Gottlieb J, Vogel A, Schmidt S, Brandes G, Heuft HG, Lichtinghagen R, Kempf T, Wollert KC, Bauersachs J, Heineke J. 2013. Highly specific detection of myostatin prodomain by an Immunoradiometric sandwich assay in serum of healthy individuals and patients. Plos One. doi: 10:10.1371/journal.pone.0080454.
17. Bullough WS, Laurence EB. 1960. The control of epidermal mitotic activity in the mouse. Proc R Soc Lond B Biol Sci. 151:517-536.
18. Bünger L, Laidlaw AH, Bulfield G, Eisen EJ, Medrano JF, Bradford GE, Prichner F, Renne U, Schlote W, Hill WG. 2001. Inbred lines of mice derived from long-term on

growth selected lines: unique resources for mapping growth genes. Mamm Genome. 12:678-686.

19. Bünger L, Ott G, Varga L, Schlote W, Rehfeldt C, Williams JL, Hill WG. 2004. Marker assisted introgression of the Compact mutant myostatin allele: MstnCmpt-dl1Abc into a mouse line with extreme growth-effects on body composition and muscularity. Genet Res. 84:161-173.
20. Callis TE, Pandya K, Seok HY, Tang RH, Tatsuguchi M, Huang ZP, Chen JF, Deng Z, Gunn B, Shumate J, Willis MS, Selzman CH, Wang DZ. 2009. MicroRNA-208a is a regulator of cardiac hypertrophy and conduction in mice. J Clin Invest. 119:2772-2786.
21. Carlson CJ, Booth FW, Gordon SE. 1999. Skeletal muscle myostatin mRNA expression is fiber-type specific and increases during hindlimb unloading. Am J Physiol. 277:R601-606.
22. Chargé SBP, Rudnicki MA. 2004. Cellular and molecular regulation of muscle regeneration. Physiol Rew. 84: 209-238.
23. Chen Y, Lebrun JJ, Vale W. 1996. Regulation of transforming growth factor beta-and activin-induced transcription by mammalian Mad proteins. Proc. Natl. Acad.Sci. USA. 93: 12992-12997.
24. Chomczynski P, Sacchi N. 1987. Single-step method of RNA isolation by acid guanidinium thiocyanate-phenol-chloroform extraction. Anal Biochem. 162:156-159.
25. Chugh SS, Whitesel S, Turner M, Roberts CT Jr, Nagalla SR. 2003. Genetic basis for chamber-specific ventricular phenotypes in the rat infarct model. Cardiovasc Res. 57:477-485.
26. Clop A, Marcq F, Takeda H, Pirottin D, Tordoir X, Bibé B, Bouix J, Caiment F, Elsen JM, Eychenne F, Larzul C, Laville E, Meish F, Milenkovic D, Tobin J, Charlier C, Georges M. 2006. A mutation creating a potential illegitimate microRNA target site in the myostatin gene affects muscularity in sheep. Nat Genet. 38:813-818.
27. Cohn RD, Liang HY, Shetty R, Abraham T, Wagner KR. 2007. Mstn does not regulate cardiac hypertrophy or fibrosis. Neuromuscul Disord. 17:290–296.
28. Cook SA, Matsui T, Li L, Rosenzweig A. 2002. Transcriptional effects of chronic Akt activation in the heart. J. Biol. Chem. 277 (25): 22528-22533.

29. Elkina Y, von Haehling S, Anker SD, Springer J. 2011. The role of myostatin in muscle wasting: an overview. J. Cachexia Sarcopenia Muscle. 2:143-151.
30. Forbes D, Jackman M, Bishop A, Thomas M, Kambadur R, Sharma M. 2006. Myostatin autoregulates its expression by feedback loop through Smad7 dependent mechanism. J. Cell. Physiol. 206: 264-272.
31. Freitas EM, Dal Pai Silva M, da Cruz-Höfling MA. 2002. Histochemical differences in the responses of predominantly fast-twitch glycolytic muscle and slow-twitch oxidative muscle to veratrine. Toxicon. 40:1471-1481.
32. Gaussin V, Depre C. 2005. Myostatin, the cardiac chalone of insulin-like growth factor-1. Cardiovasc Res. 68:347-349.
33. Gentry BA, Ferreira JA, Phillips CL, Brown M. 2011. Hindlimb skeletal muscle function in myostatin-deficient mice. Muscle Nerve. 43:49-57.
34. George I, Bish LT, Kamalakkannan G, Petrilli CM, Oz MC, Naka Y, Sweeney HL, Maybaum S. 2010. Myostatin activation in patients with advanced heart failure and after mechanical unloading. Eur J Heart Fail.12:444-453.
35. Girgenrath S, Song K, Whittemore LA. 2005. Loss of myostatin expression alters fiber-type distribution and expression of myosin heavy chain isoforms in slow- and fast-type skeletal muscle. Muscle Nerve. 31:34-40.
36. Grobet L, Martin LJ, Poncelet D, Pirottin D, Brouwers B, Riquet J, Schoeberlein A, Dunner S, Ménissier F, Massabanda J, Fries R, Hanset R, Georges M. 1997. A deletion in the bovine myostatin gene causes the double-muscled phenotype in cattle. Nat Genet. 17:71-74.
37. Gruson D, Ahn SA, Ketelslegers JM, Rousseau MF. 2011. Increased plasma myostatin in heart failure. Eur J Heart Fail. 13:734-736.
38. Guo T, Jou W, Chanturiya T, Portas J, Gavrilova O, McPherron AC. 2009. Myostatin inhibition in muscle, but not adipose tissue, decreases fat mass and improves insulin sensitivity. PLoS ONE 4(3): e4937. doi:10.1371/journal.pone.0004937.
39. Heineke J, Auger-Messier M, Xu J, Sargent M, York A, Welle S, Molkentin JD. 2010. Genetic deletion of myostatin from the heart prevents skeletal muscle atrophy in heart failure. Circulation. 121:419-425.

40. Hennebry A, Berry C, Siriett V, O'Callaghan P, Chau L, Watson T, Sharma M, Kambadur R. 2009. Myostatin regulates fiber-type composition of skeletal muscle by regulating MEF2 and MyoD gene expression. Am J Physiol Cell Physiol. 296:C525-534.
41. Hill JJ, Qiu Y, Hewick RM, Wolfman NM. 2003. Regulation of myostatin in vivo by growth and differentiation factor-associated serum protein-1: a novel protein with protease and follistatin domains. Mol. Endocrinol. 17: 1144-1154.
42. Jackson MF, Luong D, Vang DD, Garikipati DK, Stanton JB, Nelson OL, Rodgers BD. 2012. The aging Mstn null phenotype: reduced adiposity, cardiac hypertrophy, enhanced cardiac stress response, and sexual dimorphism. J Endocrinol. 213:263–275.
43. Johnson PL, McEwan JC, Dodds KG, Purchas RW, Blair HT. 2005. Meat quality traits were unaffected by a quantitative trait locus affecting leg composition traits in Texel sheep. J. Anim. Sci. 83: 2729-2735.
44. Ji M, Zhang Q, Ye J, Wang X, Yang W, Zhu D. 2008. Myostatin induces p300 degradation to silence cyclin D1 expression through the PI3K/PTEN/Akt pathway. Cell Signal. 1452-1458.
45. Kambadur R, Sharma M, Smith TP, Bass JJ. 1997. Mutations in myostatin (GDF8) in double-muscled Belgian Blue and Piedmontese cattle. Genome Res. 7: 910-916.
46. Kollias HD, McDermott JC. 2008. Transforming growth factor-beta and myostatin signaling in skeletal muscle. J. Appl. Physiol. 104: 579-587.
47. Langley B, Thomas M, Bishop A, Sharma M, Gilmour S, Kambadur R. 2002. Myostatin inhibits myoblast differentiation by down-regulating MyoD expression. J. Biol. Chem. 277: 49831-49840.
48. Lee SJ, McPherron AC. 2001. Regulation of myostatin activity and muscle growth. Proc. Natl. Acad. Sci. USA. 98: 9306-9311.
49. Lee SJ. 2004. Regulation of muscle mass by myostatin. Annu Rev Cell Dev Biol. 20:61-86.
50. Lenk K, Schur R, Linke A, Erbs S, Matsumoto Y, Adams V, Schuler G 2009. Impact of exercise training on myostatin expression in the myocardium and skeletal muscle in a chronic heart failure model. Eur J Heart Fail. 11:342–348.
51. Lenk K, Erbs S, Höllriegel R, Beck E, Linke A, Gielen S, Winkler SM, Sandri M, Hambrecht R, Schuler G, Adams V. 2012. Exercise training leads to a reduction of

elevated myostatin levels in patients with chronic heart failure. Eur J Prev Cardiol. 19:404-11.

52. Luedeke JD, McCall RD, Dillaman RM, Kinsey ST. 2004. Properties of slow- and fast-twitch skeletal muscle from mice with an inherited capacity for hypoxic exercise. Comp Biochem Physiol A Mol Integr Physiol. 138:373-382.
53. Madonna R, Geng YJ, Bolli R, Rokosh G, Ferdinandy P, Patterson C, De Caterina R. 2014. Co-activation of nuclear factor-κB and myocardin/serum response factor conveys the hypertrophy signal of high insulin levels in cardiac myoblasts. J Biol Chem. 289: 19585-98.
54. Massague J. 1998. TGF-beta signal transduction. Ann. Rev. Biochem. 67:753-791.
55. McKeehen JN, Novotny SA, Baltgalvis KA, Call JA, Nuckley DJ, Lowe DA. 2013. Adaptation of mouse skeletal muscle to low-intensity vibration training. Med Sci Sports Exerc. 45:1051-1059.
56. McKoy G, Bicknell KA, Patel K, Brooks G. 2007. Developmental expression of myostatin in cardiomyocytes and its effect on foetal and neonatal rat cardiomyocyte proliferation. Cardiovasc Res. 74:304–312.
57. McPherron AC, Lawler AM, Lee SJ. 1997. Regulation of skeletal muscle mass in mice by a new TGF-β superfamily member. Nature. 387:83-90.
58. McPherron AC, Lee SJ. 1997. Double muscling in cattle due to mutations in the myostatin gene. Proc Natl Acad Sci. 94:12457-12461.
59. McPherron AC, Lee SJ. 2002. Suppression of body fat accumulation in myostatin-deficient mice. J Cln Invest. 109:595-601.
60. Mendler L, Zádor E, Ver Heyen M, Dux L, Wuytack F. 2000. Myostatin levels in regenerating rat muscles and in myogenic cell cultures. J Muscle Res Cell Motil. 21:551-563.
61. Mendler L, Baka Z, Kovács-Simon A, Dux L. 2007. Androgens negatively regulate myostatin expression in an androgen-dependent skeletal muscle. Biochem Biophys Res Commun. 361:237-242.
62. Modesti PA, Vanni S, Bertolozzi I, Cecioni I, Lumachi C, Perna AM, Boddi M, Gensini GF. 2004. Different growth factor activation in the right and left ventricles in experimental volume overload. Hypertension. 43:101-108.

63. Morissette MR, Cook SA, Foo S, McKoy G, Ashida N, Novikov M, Scherrer-Crosbie M, Li L, Matsui T, Brooks G, Rosenzweig A. 2006. Myostatin regulates cardiomyocyte growth through modulation of Akt signaling. Circ Res. 99:15-24.
64. Morissette MR, Stricker JC, Rosenberg MA, Buranasombati C, Levitan EB, Mittleman MA, Rosenzweig A. 2009. Effects of myostatin deletion in aging mice. Aging Cell. 8:B573-583.
65. Morissette MR, Cook SA, Buranasombati C, Rosenberg MA, Rosenzweig A. 2009. Myostatin inhibits IGF-I-induced myotube hypertrophy through Akt. Am J Physiol Cell Physiol. 297:C1124-1132.
66. Mosher DS, Quignon P, Bustamante CD, Sutter NB, Mellersh CS, Parker HG, Ostrander EA. 2007. A mutation in the myostatin gene increases muscle mass and enhances racing performance in heterozygote dogs. PloS Genetics. 0779-0786.
67. Otto A, Patel K. 2010. Signalling and the control of skeletal muscle size. Experimental Cell Research. 316:3059-3066.
68. Palmieri EA, Benincasa G, Di Rella F, Casaburi C, Monti MG, De Simone G, Chiariotti L, Palombini L, Bruni CB, Sacca L, Cittadini A. 2002. Differential expression of TNF-α, IL-6, and IGF-1 by graded mechanical stress in normal rat myocardium. Am J. Physiol Heart Circ Physiol. 282:H926-H934.
69. Pellegrino MA, Brocca L, Dioguardi FS, Bottinelli R, D'Antona G. 2005. Effects of voluntary wheel running and amino acid supplementation on skeletal muscle of mice. Eur J Appl Physiol. 93:655-664.
70. Philip B, Lu Z, Gao Y. 2005. Regulation of GDF-8 signaling by the p38 MAPK. Cell Signal. 17: 365-375.
71. Ploquin C, Chabi B, Fouret G, Vernus B, Feillet-Coudray C, Coudray C, Bonnieu A, Ramonatxo C. 2012. Lack of myostatin alters intermyofibrillar mitochondria activity, unbalances redox status, and impairs tolerance to chronic repetitive contractions in muscle. Am J Physiol Endocrinol Metab. 302:E1000-1008.
72. Pucci A, Zanini C, Granata R, Ghigone R, Iavarone A, Broglio F, Sorrentino P, Bergamasco L, Rinaldi M, Ghigo E. 2009. Myocardial insulin-like growth factor-1 and insulin-like growth factor binding protein-3 gene expression in failing hearts harvested from patients undergoing cardiac transplantation. J Heart Lung Transplant. 28:402-405.

73. Rehfeldt C, Ott G, Gerrard DE, Varga L, Schlote W, Williams JL, Renne U, Bünger L. 2005. Effects of the Compact mutant myostatin allele MstnCmpt-dl1Abc introgressed into a high growth mouse line on skeletal muscle cellularity. J Muscle Res Cell Mot. 26:103-112.
74. Reisz-Porszasz S, Bhasin S, Artaza JN, Shen R, Sinha-Hikim I, Hogue A, Fielder TJ, Gonzalez-Cadavid NF. 2003. Lower skeletal muscle mass in male transgenic mice with muscle-specific overexpression of Mstn. Am J Physiol Endocrinol Metab. 285:E876–E888.
75. Rodgers BD, Garikipati DK. 2008. Clinical, agricultural, and evolutionary biology of myostatin: A Coperative Review. Endocr. Rev. 29: 513-534.
76. Rodgers BD, Interlichia JP, Garikipati DK, Mamidi R, Chandra M, Nelson OL, Murry CE, Santana LF. 2009. Myostatin represses physiological hypertrophy of the heart and excitation-contration coupling. J Physiol. 587:4873-4886.
77. Satoh M, Minami Y, Takahashi Y, Tabuchi T, Nakamura M. 2010. Expression of microRNA-208 is associated with adverse clinical outcomes in human dilated cardiomyopathy. J Card Fail. 16:404-410.
78. Savage KJ, McPherron AC. 2010. Endurance exercise training in myostatin null mice. Muscle Nerve. 42:355-362.
79. Schiaffino S, Reggiani C. Fiber types in mammalian skeletal muscles. 2011. Physiol Rev. 91:1447-1531.
80. Schuelke M, Wagner KR, Stolz LE, Hübner C, Riebel T, Komen W, Braun T, Tobin JF, Lee SJ. 2004. Myostatin mutation associated with gross muscle hypertrophy in a child. New Engl J Med. 350:2682-2688.
81. Serneri GG, Modesti PA, Boddi M, Cecioni I, Pannicia R, Coppo M, Galanti G, Simonetti I, Vanni S, Papa L, Bandinelli B, Migliorini A, Modesti A, Maccherini M, Sani G, Toscano M. 1999. Cardiac growth factors in human hypertrophy: Relations with myocardial contractility and wall stress. Circ Res. 85:57-67.
82. Serneri GG, Boddi M, Cecioni I, Vanni S, Coppo M, Papa ML, Bandinelli B, Bertolozzi I, Polidori G, Toscano T, Maccherini M, Modesti PA. 2001. Cardiac angiotensin II formation in the clinical course of heart failure and its relationship with left ventricular function. Circ Res. 88:961-968.

83. Sharma M, Kambadur R, Matthews KG, Somers WG, Devlin GP, Conaglen JV, Fowke PJ, Bass JJ. 1999. Myostatin, a transforming growth factor-β superfamily member, is expressed in heart muscle and is upregulated in cardiomyocytes after infarct. J Cell Physiol. 180:1-9.
84. Shyu KG, Ko WH, Yang WS, Wang BW, Kuan P. 2005. Insulin-like growth factor-1 mediates stretch-induced upregulation of myostatin expression in neonatal rat cardiomyocytes. Cardiovasc Res. 68:405-414.
85. Shyu KG, Lu MJ, Wang BW, Sun HY, Chang H. 2006. Myostatin expression in ventricular myocardium in a rat model of volume-overload heart failure. Eur J Clin Invest. 36:713-719.
86. Stinckens A, Luyten T, Bijttebier J, Van den Maagdenberg K, Dieltiens D, Janssens S, De Smet S, Georges M, Buys N. 2008. Characterization of the complete porcine MSTN gene and expression levels in pig breeds differing in muscularity. Anim Genet. 39:586-596.
87. Sun Y, Li Y, Luo D, Liao DJ. 2012. Pseudogenes as weaknesses of ACTB (Actb) and GAPDH (Gapdh) used as reference genes in reverse transcription and polymerase chain reactions. PLoS One. doi: 10.1371/journal.pone.0041659.
88. Szabó G, Dallmann G, Müller G, Patthy L, Soller M, Varga L. 1998. A deletion in the myostatin gene causes the compact (Cmpt) hypermuscular mutation in mice. Mamm Genome. 9:671-672.
89. Torrado M, Iglesias R, Nespereira B, Mikhailov AT. 2010. Identification of candidate genes potentially relevant to chamber-specific remodeling in postnatal ventricular myocardium. J Biomed Biotechnol. doi:10.1155/2010/603159.
90. Toth P, Tucsek Z, Tarantini S, Sosnowska D, Gautam T, Mitschelen M, Koller A, Sonntag WE, Csiszar A, Ungvari Z. 2014. IGF-1 deficiency impairs cerebral myogenic autoregulation in hypertensive mice. J Cereb Blood Flow Metab. doi: 10.1038/jcbfm.2014.156.
91. Ungvari Z, Csiszar A. 2012. The emerging role of IGF-1 deficiency in cardiovascular aging: recent advances. J Gerontol A Biol Sci Med Sci. 67:599-610.
92. Valle Zarate A, Horst P, Weniger JH. 1994. Antagonism Between Growth and Productive Adaptability in Mice. Archiv für Tierzucht-Archives of Animal Breeding. 37:185-198.

93. Varga L, Szabó G, Darvasi A, Müller G, Sass M, Soller M. 1997. Inheritance and mapping of Compact (Cmpt), a new mutation causing hypermuscularity in mice. Genetics. 147:755-764.
94. Varga L, Müller G, Szabó G, Pinke O, Korom E, Kovács B, Patthy L Soller M. 2003. Mapping modifers affecting muscularity of the myostatin mutant (MstnCmpt-dl1Abc) Compact mouse. Genetics. 165:257-267.
95. Varga L, Pinke O, Müller G, Kovács B, Korom E, Szabó G, Soller M. 2005. Mapping a syntenic modifier on mouse chromosome 1 influencing the expressivity of the Compact phenotype in the myostatin mutant (MstnCmpt-dl1Abc) Compact mouse. Genetics. 169:489-493.
96. Varga ZV, Zvara A, Faragó N, Kocsis GF, Pipicz M, Gáspár R, Bencsik P, Görbe A, Csonka C, Puskás LG, Thum T, Csont T, Ferdinandy P. 2014. MicroRNAs associated with ischemia-reperfusion injury and cardioprotection by ischemic pre- and postconditioning: protectomiRs. Am J Physiol Heart Circ Physiol. 307: H216-27.
97. Wang M, Yu H, Kim YS, Bidwell CA, Kuang S. 2012. Myostatin facilitates slow and inhibits fast myosin heavy chain expression during myogenic differentiation. Biochem Biophys Res Commun. 426:83-88.
98. Wegner J, Albrecht E, Fiedler I, Teuscher F, Papstein HJ, Ender K. 2000. Growth and breed-related changes of muscle fiber characteristics in cattle. J Anim Sci. 78:1485-1496.
99. Weniger JH, Horst P, Steinhauf D, Major F, Wolf M, Tawfik ES. 1974. Model experiments on selection for endurance and its relation to growth. Part I. Introduction, methods and preliminary investigations on the basic population. Journal of Animal Breeding and Genetics-Zeitschrift für Tierzüchtung und Züchtungsbiologie. 91:265-270.
100. Yang W, Zhang Y, Li Y, Wu Z, Zhu D. 2007. Myostatin induces cyclin D1 degradation to cause cell cycle arrest through a phosphatidylinositol 3-kinase/AKT/GSK-3 beta pathway and is antagonized by insulin-like growth factor 1. J Biol Chem. 282:3799-3808.
101. Zungu M, Young ME, Stanley WC, Essop MF. 2008. Expression of mitochondrial regulatory genes parallels respiratory capacity and contractile function in a rat model of hypoxia-induced right ventricular hypertrophy. Mol Cell Biochem. 318:175-181.

12. Annex

I.

Journal of Histochemistry & Cytochemistry 61(12) 889–900

DOI: 10.1369/0022155413503661
jhc.sagepub.com
SAGE

The *Compact* Mutation of Myostatin Causes a Glycolytic Shift in the Phenotype of Fast Skeletal Muscles

Júlia Aliz Baán, Tamás Kocsis, Anikó Keller-Pintér, Géza Müller, Ernő Zádor, László Dux, and Luca Mendler

Institute of Biochemistry, Faculty of General Medicine, University of Szeged, Dóm tér 9., 6720 Szeged, Hungary (JAB, TK, AKP, EZ, LD, LM); and Egis Pharmaceuticals, H-1475 Budapest, Hungary (GM).

Summary

Myostatin is an important negative regulator of skeletal muscle growth. The hypermuscular *Compact* (*Cmpt*) mice carry a 12-bp natural mutation in the myostatin propeptide, with additional modifier genes being responsible for the phenotype. Muscle cellularity of the fast-type tibialis anterior (TA) and extensor digitorum longus (EDL) as well as the mixed-type soleus (SOL) muscles of *Cmpt* and wild-type mice was examined by immunohistochemical staining of the myosin heavy chain (MHC) proteins. In addition, transcript levels of MHC isoforms were quantified by qPCR. Based on our results, all investigated muscles of *Cmpt* mice were significantly larger compared with that of wild-type mice, as characterized by fiber hyperplasia of different grades. Fiber hypertrophy was not present in TA; however, EDL muscles showed specific IIB fiber hypertrophy while the (I and IIA) fibers of SOL muscles were generally hypertrophied. Both the fast TA and EDL muscles of *Cmpt* mice contained significantly more glycolytic IIB fibers accompanied by a decreased number of IIX and IIA fibers; however, this was not the case for SOL muscles. In summary, despite the variances found in muscle cellularity between the different myostatin mutant mice, similar glycolytic shifts were observed in *Cmpt* fast muscles as in muscles from myostatin knockout mice. (J Histochem Cytochem 61:889–900, 2013)

Keywords

myostatin, *Compact* mice, muscle, tibialis anterior, extensor digitorum longus, soleus, hyperplasia, hypertrophy, myosin heavy chain, fiber type transition

1. Introduction

Myostatin, also known as growth/differentiation factor 8 (GDF-8) is a member of the transforming growth factor (TGF)-β superfamily and has been shown to be a negative regulator of skeletal muscle growth. The myostatin knockout (KO) mouse (McPherron et al. 1997) shows a hypermuscular phenotype similar to that of several different organisms (cattle, dog, pig, sheep, human) carrying naturally occurring mutations of myostatin (McPherron and Lee, 1997; Schuelke et al. 2004; Clop et al. 2006; Mosher et al. 2007; Stinckens et al. 2008). Most of the natural mutations result in an inactive protein caused by either an early STOP codon or a frameshift mutation in the bioactive domain of myostatin (McPherron and Lee, 1997; Mosher et al. 2007, Boman et al. 2009). One report details that missplicing of the myostatin pre-mRNA was responsible for hypermuscularity observed in a human infant (Schuelke et al. 2004). In contrast, another mechanism of myostatin inactivation induces the hypermuscular phenotype of the *Compact (Cmpt)* mice, which was originally selected for high protein content and body weight in the Technical

Received for publication March 22, 2013; accepted August 1, 2013.

Supplementary material for this article is available on the *Journal of Histochemistry & Cytochemistry* Web site at http://jhc.sagepub.com/supplemental.

Corresponding Author:
Luca Mendler MD PhD, Institute of Biochemistry, Faculty of General Medicine, University of Szeged, Dóm tér 9., 6720 Szeged, Hungary.
E-mail: mendler.luca@med.u-szeged.hu

University of Berlin (Bünger et al. 2001). Analysis of the Hungarian inbred subpopulation of the *Cmpt* line identified myostatin as the major gene containing a 12-bp non-frameshift deletion in the propeptide region, although the biologically active part of the molecule was unaffected (Varga et al. 1997). Additional modifiers seem to be essentially involved in determining the full expressivity of the *Cmpt* phenotype; however these genes have not been identified yet (Szabó et al. 1998; Varga et al. 2003, 2005). To date, few studies describe the phenotypical or molecular analysis of the *Cmpt* mice (Bünger et al. 2004; Rehfeldt et al. 2005; Amthor et al. 2007, 2009), even though this line represents, in contrast to myostatin KO, a complex and mainly unknown mechanism of myostatin-dependent hypermuscularity.

Various contradictory results exist in the literature regarding muscle cellularity in myostatin-deficient mice. Thus, in the present study, we aimed to describe the muscle phenotype of young male *Cmpt* mice using morphological assessments. By analyzing the fast-type tibialis anterior (TA) and extensor digitorum longus (EDL) as well as the mixed-type soleus (SOL) muscles, we show here that hypermuscularity is characterized by either muscle fiber hyperplasia or combined hyperplasia and hypertrophy of different grades depending on muscle type, and that a significant glycolytic shift occurs in the fiber type composition of the fast-type muscles of *Cmpt* mice.

2. Materials and Methods

2.1 Animals

The genetic background of BEHi (Berlin High inbred) line is not well defined because it was derived from an out-bred line founded from mice bought from pet shops more than 40 years ago (Bünger et al. 2001). It was initially selected on protein mass (Weniger et al. 1974), then on high body weight/low fat content (Valle Zarate et al. 1994) and finally on body weight (Bünger et al. 2004). The '*Compact'* line in Berlin was derived from the first mice seen in early generations of the BEH line showing this phenotype, and were separated to form a new line that was selected on a muscularity score by visual inspection (Szabó et al. 1998; Varga et al. 2003, 2005). Animals of the Berlin *Cmpt* line were used as the founders for the Hungarian *Cmpt* line, and there was no further exchange of genetic material between the laboratories in Berlin and Hungary. The Hungarian subpopulation of the *Cmpt* mice was inbred and kept by Géza Müller until 2010 in the Institute for Animal Biology, Agricultural Animal Center, H-2101 Gödöllő, Hungary, and in EGIS Pharmaceuticals, Budapest, Hungary. Since 2010, these mice have been kept in the Institute of Biochemistry, Faculty of General Medicine, University of Szeged, Hungary.

BALB/c mice, serving as wild-type control for the experiments, were purchased from Biological Research Centre of Szeged, Hungary.

2.2. Experimental Design

Male, 2.5-month (10–12-week)-old *Cmpt* (44-50.7 g) and BALB/c (24-28g) wild-type mice were used for the experiments (n=5–10). Typical hindlimb muscles (quadriceps (Quadr), tibialis anterior (TA), extensor digitorum longus (EDL), soleus (SOL) and gastrocnemius (Gastro)) of both strains were removed under intraperitoneal anesthesia (3% chloral hydrate, 0.15 ml/10 g body weight). Older male *Cmpt* mice (4-, 7-, 12-, 18-, and 23-month-old) were also used for comparison of body and muscle weight, as well as for some fiber analyses of TA muscles. All muscles were weighed and frozen in isopenthane/liquid nitrogen and kept at -80C until further use. TA, EDL and SOL muscles from the right leg were used for morphological and immunohistochemical analysis while RNA isolation and quantitative RT-PCR was carried out on the contralateral TA counterparts. Animal experiments were approved by the Institutional Animal Care and Use Committee at the University of Szeged in accordance with the U.S. National Institutes of Health guidelines for animal care.

2.3. Morphological Analysis

For morphological analysis, 10-μm serial cryostat sections were taken from the mid-belly region of different muscles of both *Cmpt* and BALB/c mice followed by standard hematoxylin-eosin (HE) staining. Using images from all microscopic fields, we reconstructed the whole cross-sectional area (CSA) of each muscle using the Cell B program (Olympus DP Soft software, Version 3.2., Soft Imaging System GmbH; Münster, Germany) and fiber number was determined by counting all fibers in TA, EDL and SOL muscles using Digimizer software (MedCalc Software, Mariakerke, Belgium).

2.4. Myosin Heavy Chain (MHC) Immunohistochemistry

Fiber type analysis was carried out on 10-μm thick serial cryosections of TA, EDL and SOL muscles from both *Cmpt* and BALB/c wild-type male mice. Sections were first blocked in 5% non-fat milk powder in PBS, then incubated with mouse monoclonal primary antibodies BA-D5 (1:25), sc-71 (1:25) and BF-F3 (1:5), which are specific for myosin heavy chain (MHC) I (slow oxidative) MHCIIA (fast oxidative) and MHCIIB (fast glycolytic), respectively (Deutsche Sammlung von Mikroorganismen und Zellkulturen [DSMZ], Braunschweig, Germany). After incubation with the peroxidase-conjugated secondary antibody (rabbit anti-mouse; Dako, Denmark) immunocomplexes were visualized by diaminobenzidine (DAB) staining with or without nickel enhancement. IIX fibers were considered as those not stained by any of the above antibodies. The size and distribution of muscle fibers in SOL were determined by analyzing all

Table 1. Primer sequences of different MHC isoforms and Hprt used in qRT-PCR.

Target	Accession number	Forward primer	Reverse primer	Product size (bp)
MHCIIB	NM_010855.2	GTGATTTCTCCTGTCACCTCTC	GGAGGACCGCAAGAACGTGCTGA	280
MHCIIX	NM_030679.1	ACGGTCGAAGTTGCATCCC	CAGTAGTTCCGCCTTCGGTC	272
MHCIIA	NM_001039545.2	TGCACCTTCTCGTTTGCCAG	GGCCATGTCCTCGATCTTGT	320
MHCI	NM_003689292.1	CTACAGGCCTGGGCTTACCT	TCTCCTTCTCAGACTTCCGC	126
Hprt	NM_013556.2	TCAGTCAACGGGGGACATAAA	GGGGCTGTACTGCTTAACCAG	142

bp: base pair; MHC: myosin heavy chain; Hprt: Hypoxanthine guanine phosphorybosyltransferase.

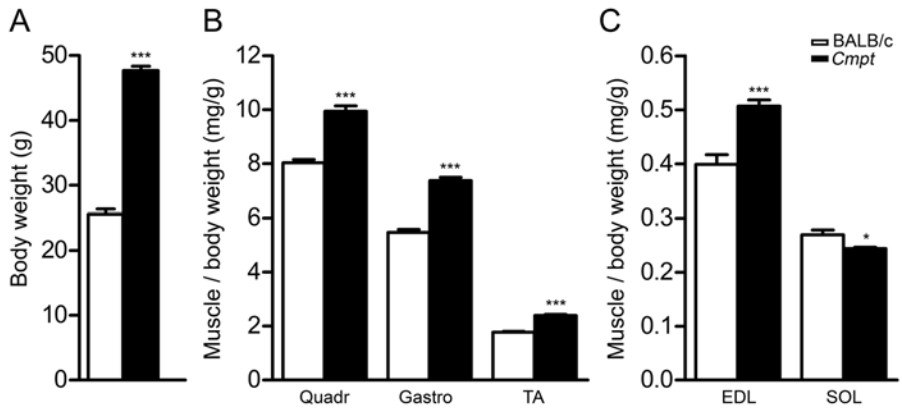

Figure 1. Body weight (A) and normalized muscle mass (B, C) of BALB/c and *Cmpt* male mice. B-C show normalized muscle masses of quadriceps (Quadr), gastrocnemius (Gastro), tibialis anterior (TA), extensor digitorum longus (EDL) and soleus (SOL) muscles. Bars represent mean ± SEM; asterisks show significant differences between BALB/c and *Cmpt* mice (n=5-10, *p<0.05, ***p<0.001).

(700-800) fibers in each muscle using Cell B and Digimizer software; in EDL muscles, about 50% of the fibers (600 to 1100 fibers in BALB/c and *Cmpt* mice, respectively) were measured. In TA muscles, an analysis of fiber size as well as fiber type distribution was done by examining 2-3 representative microscopic fields (with 10x objective) of both superficial and deep portions of TA muscles. Regional results were then summarized for the whole cross-sectional area of each TA muscle (500 to 1000 fibers/muscle in 4-7 microscopic fields in BALB/c and *Cmpt* mice, respectively).

2.5. Quantitative RT-PCR Analysis

Total RNA was isolated from TA muscles of *Cmpt* and BALB/c male mice (n=5) with TRI reagent according to the manufacturer's instructions (Molecular Research Center, Inc. Cincinnati, OH), followed by reverse transcription (MMLV-Moloney Murine Leukemia Virus Reverse Transcriptase, 28025-013, Sigma-Aldrich, St. Louis, MO). For the detection of transcript levels of MHCI, MHCIIA, MHCIIX and MHCIIB, quantitative PCR was carried out with SYBR GREEN master mix (Fermentas, Thermo Fischer Scientific, Pittsburgh, PA) on a Light Cycler 1.5 (Roche Applied Science, Indianapolis, IN). As an internal control, *Hprt* (hypoxanthine guanine phosphorybosyltransferase) was amplified using the same TA muscle probes. Cycle conditions were set as an initial denaturation step for 10 min at 95C, followed by 45 cycles of 10 sec at 95C for template denaturation, 10 sec at 58C for annealing phase and 10 sec at 72C for extension. Specificity of the PCR products was confirmed by melting curve analysis followed by verification of the amplicon length on 1.5% agarose gels stained with ethidium bromide. Primer pairs for *Hprt*, MHCI, MHCIIA, MHCIIX and MHCIIB were designed against sequences of intron-spanning exons by Primer 3 Input software (version 0.4.0; http://frodo.wi.mit.edu/primer3/input.htm) and tested to avoid primer dimers, non-specific amplification and self-priming (Table 1).

2.6. Statistical Analysis

Statistical analysis was performed by unpaired t test using Prism software (GraphPad Software, Inc.; San Diego, CA). Age-dependent body and muscle weights of *Cmpt* mice (Fig. S1) were tested using a one-way ANOVA and Newman-Keuls multiple comparison tests. All data are expressed as the mean ± SEM. The level of p<0.05 was considered significant. The individual p-values are indicated in the legends to each figure.

3. Results

3.1. Body and Muscle Weight of Cmpt *Mice*

We phenotypically compared 2.5-month-old myostatin mutant *Cmpt* mice (Varga et al. 1997) with wild-type BALB/c mouse using scores of body and muscle weight. *Cmpt* male mice were significantly larger than BALB/c mice in terms of body weight (Fig. 1A). Absolute weights

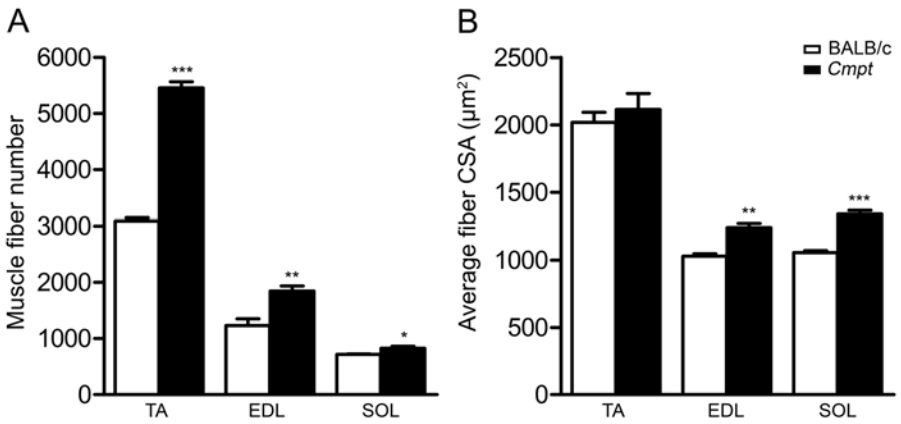

Figure 2. Total muscle fiber number (A) and average fiber cross-sectional area (CSA) (B) of tibialis anterior (TA), extensor digitorum longus (EDL) and soleus (SOL) muscles in BALB/c and *Cmpt* male mice. Bars represent the mean ± SEM; asterisks show significant differences between BALB/c and *Cmpt* mice (n=3-5, *p<0.05, **p<0.01, ***p<0.001).

of the different hindlimb muscles, such as Quadr, Gastro, TA, EDL and SOL muscles, were significantly larger in *Cmpt* mice (data not shown). Similarly, muscle weights, normalized to body weights, were significantly larger in *Cmpt* animals, with the exception of the oxidative SOL muscle. These results indicated a disproportionate increase in mass for most muscles of *Cmpt* mice (Fig. 1B-C). To assure that the 2.5-month-old *Cmpt* mice had already finished the intense growing phase, we compared body and muscle (TA, EDL and SOL) weights in mice of different ages (Fig. S1). Body weight was similar in young (2.5-month-old) and adult (4- and 7-month-old) animals, while 12–23-month-old mice had slightly higher weight measurements. However, no significant difference was found in muscle weights amongst any of the age groups, indicating that the 2.5-month-old animals we used for the experiments have already reached muscle sizes typical of adult mice.

3.2. Muscle Fiber Number and Fiber Cross-sectional Area

To define whether the hypermuscularity of *Cmpt* mice is caused by hyperplasia or hypertrophy within the muscle, we analyzed muscle fibers on HE- or MHC-immunostained serial cross-sections of different muscle types—glycolytic TA and EDL muscles and oxidative SOL muscles—in both mutant and wild-type groups (Fig. 2). Fiber number in all examined muscles of the 2.5-month-old *Cmpt* mice was significantly higher than that observed in wild-type mice. The TA muscle demonstrated the most significant hyperplasia as compared with the EDL and SOL muscles (Fig. 2A). However, fiber size did not differ in TA muscles between *Cmpt* and BALB/c mice. EDL and SOL muscles of *Cmpt* mice, on the other hand, showed evidence of hypertrophy (Fig. 2B). To check whether older *Cmpt* mice also show changes in fiber parameters, we analyzed TA muscles of 7-month-old *Cmpt* mice and found no differences in mean fiber number or size compared with the 2.5-month-old *Cmpt* mice (fiber number: 5450 ± 135 vs. 5455 ± 114; fiber size: 2193 ± 95 vs. 2114 ± 118, respectively) (Table S1). In summary, based on our results, hypermuscularity of *Cmpt* mice is characterized by fiber hyperplasia in TA muscles and by a combination of hyperplasia and different grades of hypertrophy in EDL and SOL muscles.

3.3. MHC Composition and Fiber Size Distribution

To analyze the possible effects of the *Cmpt* mutation on MHC composition, serial cryosections of TA, EDL and SOL muscles were immunostained using sets of monoclonal antibodies in order to differentiate type I, IIA, IIX and IIB fibers (Figs. 3-6). In line with the literature (Bloemberg et al. 2012), only MHCII isoforms were detected in TA and EDL muscles of both mouse lines (Figs. 3-6). Whereas, no MHCIIB fibers were found in SOL muscles. Therefore, we next analyzed the parameters of the slow-type I and the fast-type IIA and IIX fibers in SOL muscles (Figs. 3-6).

By counting different fiber types on whole cross-sectional images, we noted that the fast-type TA muscles of *Cmpt* mice contained significantly more glycolytic IIB fibers and a decreased number of IIX and IIA fibers as compared with that in wild-type mice (Fig. 3, 4, 5A). Fiber composition has been shown to be different in superficial and deep portions of TA muscles in wild-type mice, with more glycolytic IIB fibers at the periphery (Bloemberg et al. 2012). Therefore, we also compared the regional fiber type composition in both mouse lines (Fig. 4, 5B). The number of IIB fibers was significantly higher in both superficial and deep regions of *Cmpt* mice compared with that in wild-type animals (Fig. 4, 5B). Moreover, in *Cmpt* mice, both muscle regions contained a similar number of IIB fibers, whereas, in wild-type BALB/c mice, the IIB fibers were abundant only in the superficial region, as expected (Fig. 4, 5B). In contrast, the proportion of the glycolytic-oxidative IIX fibers significantly decreased in both TA regions of *Cmpt* mice, without any regional difference in fiber number

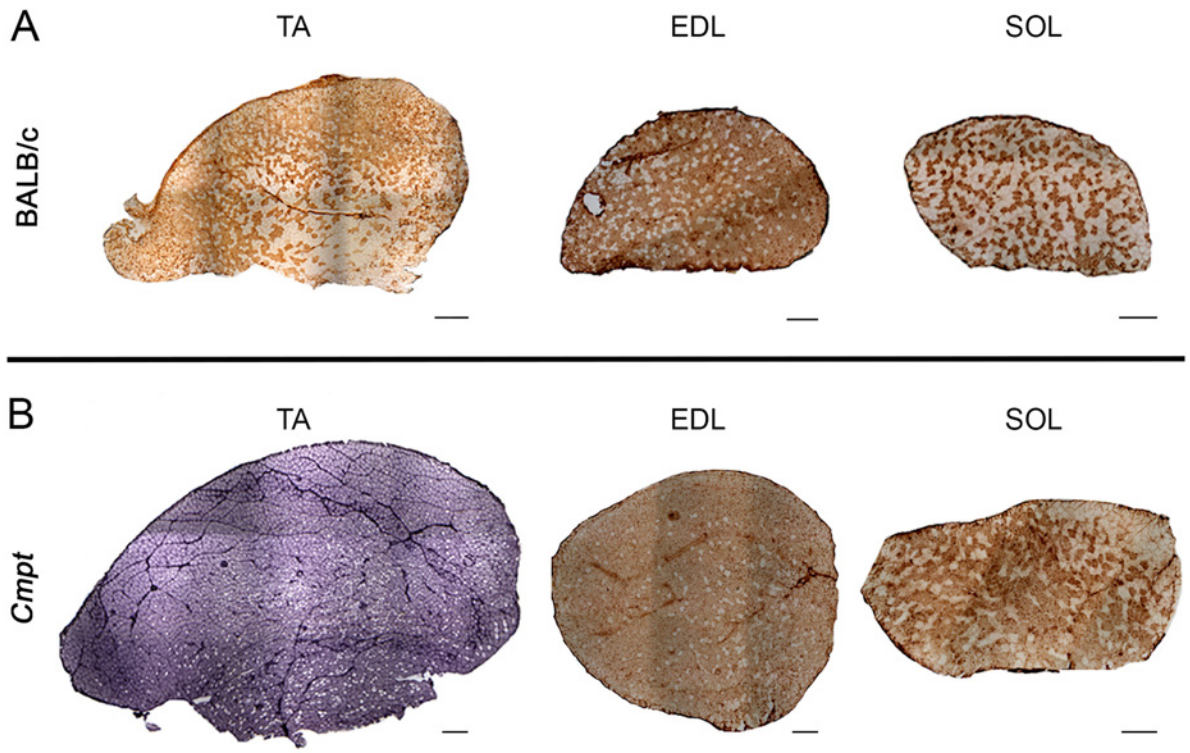

Figure 3. Representative immunohistochemical stainings of tibialis anterior (TA), extensor digitorum longus (EDL) and soleus (SOL) muscles of BALB/c (A) and *Cmpt* (B) male mice. Panel A represents whole cross-sectional areas of TA, EDL and SOL muscles stained either by MHCIIB antibody (in TA and EDL muscles) or by MHCI antibody (in SOL muscle) in BALB/c mice, and panel B shows the same tissue staining for sections from *Cmpt* male mice. All muscles were stained by diaminobenzidine but *Cmpt* TA muscle was additionally nickel enhanced. Scale bars represent 400 µm for TA, 200 µm for EDL and 200 µm for SOL muscles.

(Fig. 4, 5B). In wild-type mice, however, we found a significantly higher proportion of IIX fibers in the deep region (Fig. 4, 5B). Finally, the number of the oxidative IIA fibers was very low, and these were almost exclusively confined to the deep region of TA muscles in both mouse strains; however, the number of IIA fibers was even reduced in *Cmpt* mutant mice compared with wild-type animals (Fig. 4, 5B).

Similar to TA muscles, the number of glycolytic IIB fibers was higher in the fast-type EDL muscles of *Cmpt* mice, while the number of IIX and IIA fibers was significantly lower as compared with that of wild-type mice (Fig. 3, 5A). In contrast, the oxidative SOL muscles in *Cmpt* mice contained more slow-type I fibers and less fast-type IIA fibers than those in wild-type mice, while the number of IIX fibers was very low and not different in the two mouse lines (Fig. 3, 5A).

Together, our findings clearly demonstrate a substantial shift toward a more glycolytic phenotype in the fast-type TA and EDL muscles but not in the mixed-type oxidative SOL muscles of *Cmpt* mice.

In line with our results regarding average fiber size (Fig. 2B), we could not detect any specific hypertrophy for any of the IIB, IIX or IIA fiber types in TA muscles (Fig. 5C). Indeed, the size distribution of the IIB, IIX and IIA fibers in TA muscles revealed only minimal changes in terms of peak position or shape of the histograms in *Cmpt* mice when compared with the results seen for wild-type mice (Fig. 6A). In EDL muscles, however, fiber hypertrophy (Fig. 2B) was exclusively caused by the increased size of IIB fibers, while the sizes of IIX and IIA fibers were unchanged (Fig. 5C). In line with these findings, IIB fiber distribution in EDL muscles was shifted toward larger fiber size in *Cmpt* mice, while IIX and IIA histograms were not different between the *Cmpt* and BALB/c lines (Fig. 6B). In contrast to fast muscles, both I and IIA fibers showed evidence of hypertrophy for *Cmpt* mice (Fig. 5C), such that both fiber frequencies shifted toward an increase in size in *Cmpt* SOL muscles as compared with BALB/c SOL muscles (Fig. 6C). Because of their low number, IIX fiber size was not analyzed in SOL muscles.

3.4. mRNA Levels of MHC Isoforms Detected by Quantitative RT-PCR

In order to determine the transcript levels of MHC isoforms (MHCI, IIA, IIB, IIX), we performed qRT-PCR analysis in TA muscles of both *Cmpt* and BALB/c male mice (Fig. 7).

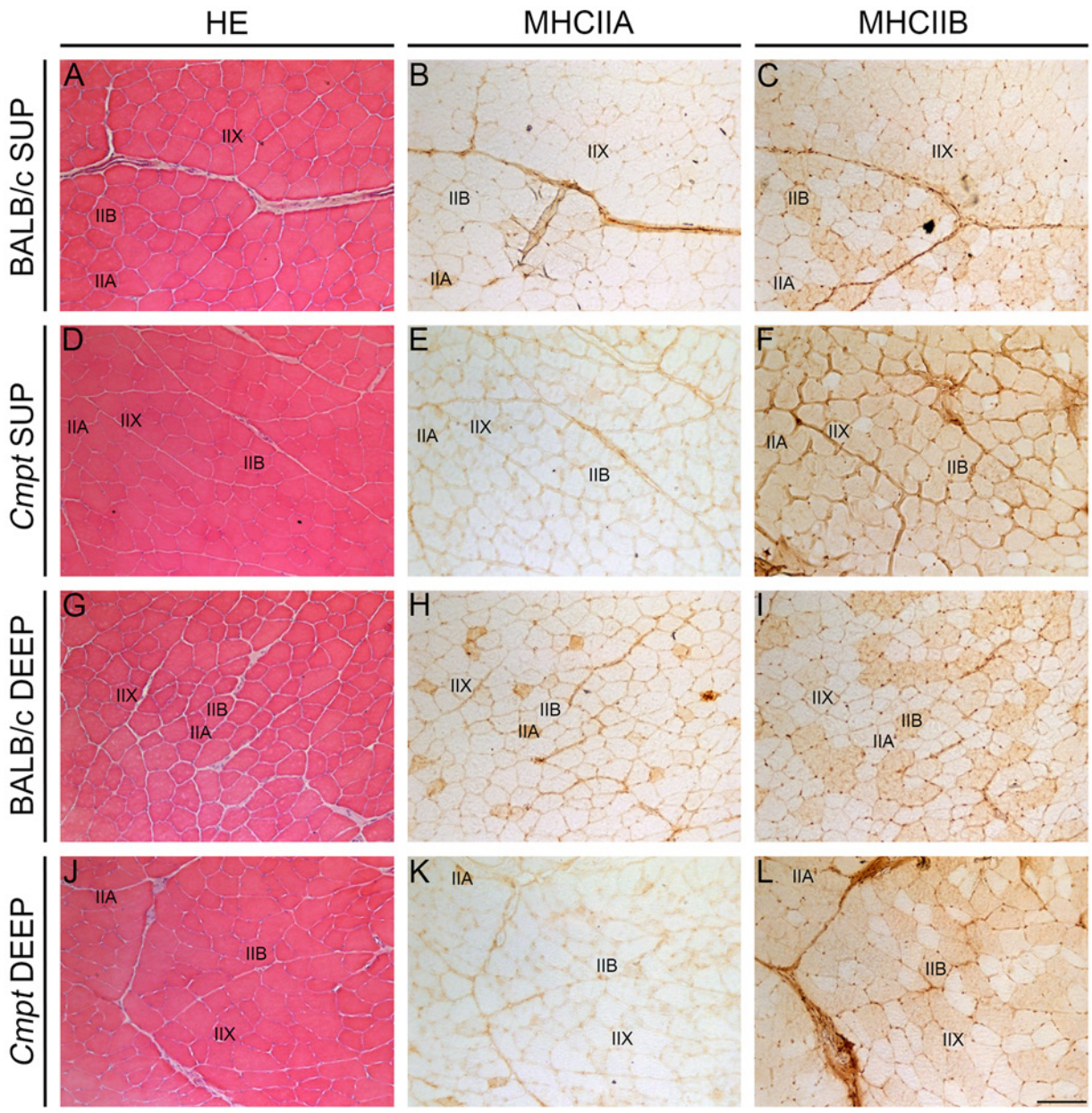

Figure 4. Immunohistochemical analysis of myosin heavy chain (MHC) isoforms in different regions of tibialis anterior (TA) muscles of BALB/c and *Cmpt* male mice. A-C represent the superficial region of BALB/c mice and D-F depict that of *Cmpt* mice; G-I and J-L show BALB/c and *Cmpt* deep regions, respectively. HE staining (A, D, G, J) and antibodies against MHCIIA (B, E, H, K) and MHCIIB (C, F, I, L) were used. Representative fibers are marked as IIA, IIB and IIX fibers. Scale bars represent 100 μm.

Hprt was used as an internal control because *Hprt* levels were similar in *Cmpt* vs. wild-type TA muscles (Fig. 7A). We found that MHCIIB mRNA levels were significantly increased (Fig. 7B), while MHCIIX (Fig. 7C) and MHCIIA transcript levels (Fig. 7D) decreased in *Cmpt* mice compared with those values in wild-type mice. The slow MHCI isoform was almost undetectable (data not shown). These results are in line with those obtained from the immunohistochemical analysis, suggesting that the fiber-type shift in the TA muscle is regulated at the level of MHC transcription.

4. Discussion

The *Cmpt* mouse line takes a special place in the group of hypermuscular animals carrying naturally occurring myostatin mutations, as the propeptide region, not the biologically active domain, of myostatin is affected. Abnormal propeptide structure might play an important role in misfolding, inefficient secretion, and/or abnormal processing of myostatin in *Cmpt* mice (Szabó et al. 1998). It has also been shown that the *Cmpt* mutation of myostatin is an

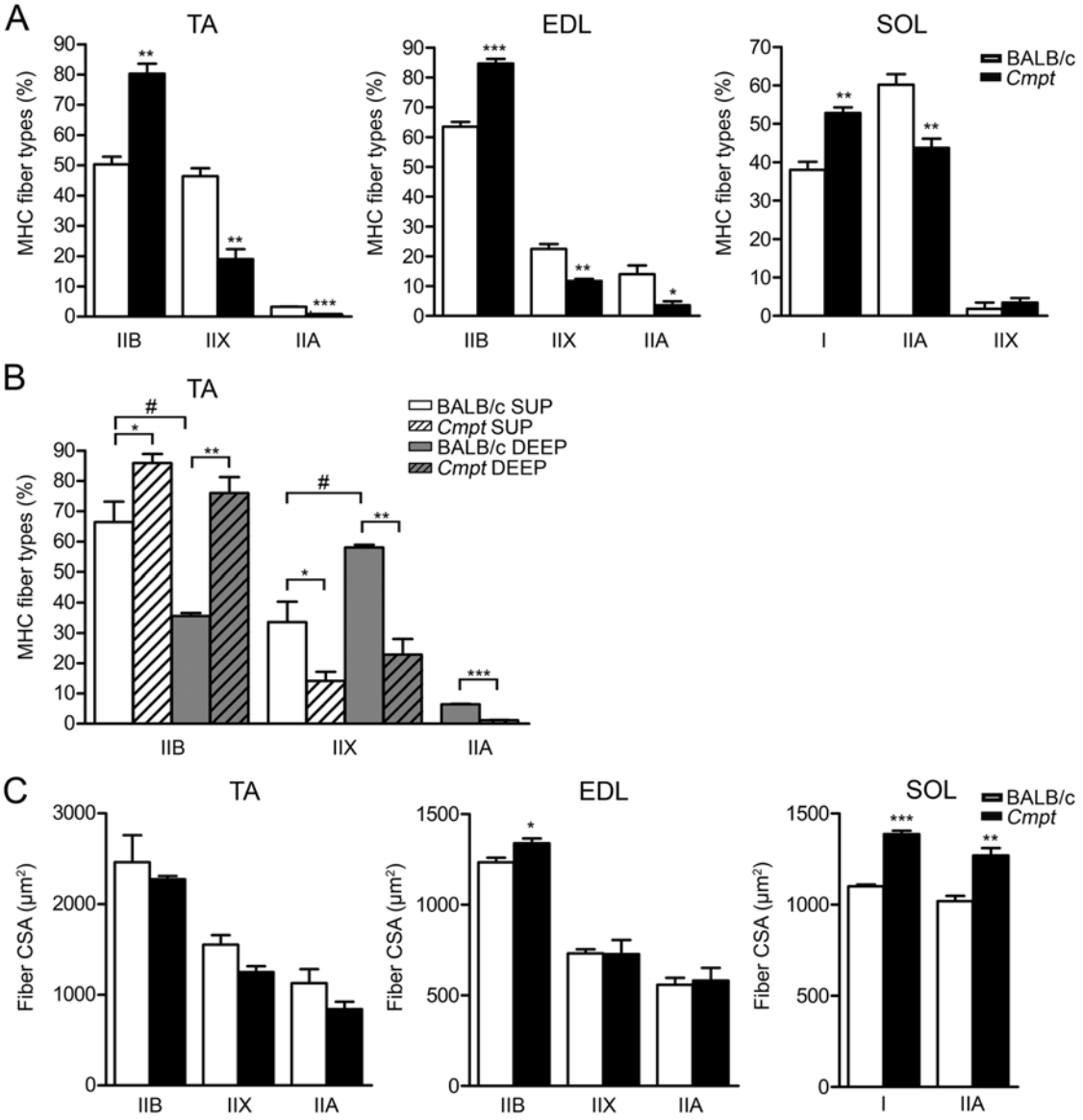

Figure 5. Fiber type composition (A-B) and mean fiber cross-sectional area (C) in tibialis anterior (TA), extensor digitorum longus (EDL) and soleus (SOL) muscles of BALB/c and *Cmpt* male mice. Panel A represents fiber type composition of all fibers in TA, EDL and SOL muscles, while panel B shows regional fiber type distribution of TA muscles subdivided into superficial and deep regions. Panel C represents mean fiber cross sectional area (CSA) of the different (I, IIA, IIX and IIB) fibers in TA, EDL and SOL muscles. Data are presented as the mean ± SEM. Asterisks show significant differences between BALB/c and *Cmpt* mice (n=3–4, *p<0.05, **p<0.01, ***p<0.001) while a crosshatch indicates significant changes between superficial and deep portions of the same TA muscle within a specific mouse line (n=3, $^{\#}p$<0.05).

indispensable yet not satisfactory requirement for the full expression of the hypermuscular phenotype, pinpointing the significance of additional modifier gene or genes (Varga et al. 1997, 2003, 2005).

Since the genetic background of the *Cmpt* mice is very complex and no appropriate genetic control line has been available so far, we decided to use BALB/c mice as a control for the following reasons: 1) This inbred line was used for mapping the myostatin mutation and the modifier genes in *Cmpt* mice (Szabó et al. 1998); 2) These mice are generally used as wild-type controls and their muscle parameters as well as fiber composition have already been reported (Freitas et al. 2002; Luedecke et al. 2004); and 3) Muscle characteristics of BALB/c mice are similar to those of C57BL/6, another wild-type mice used as a genetic background of myostatin KO mice (McPherron et al. 1997), suggesting that these lines are comparable to some extent (Luedecke et al. 2004; Pellegrino et al. 2005; Bloemberg et al. 2012; McKeehen et al. 2013).

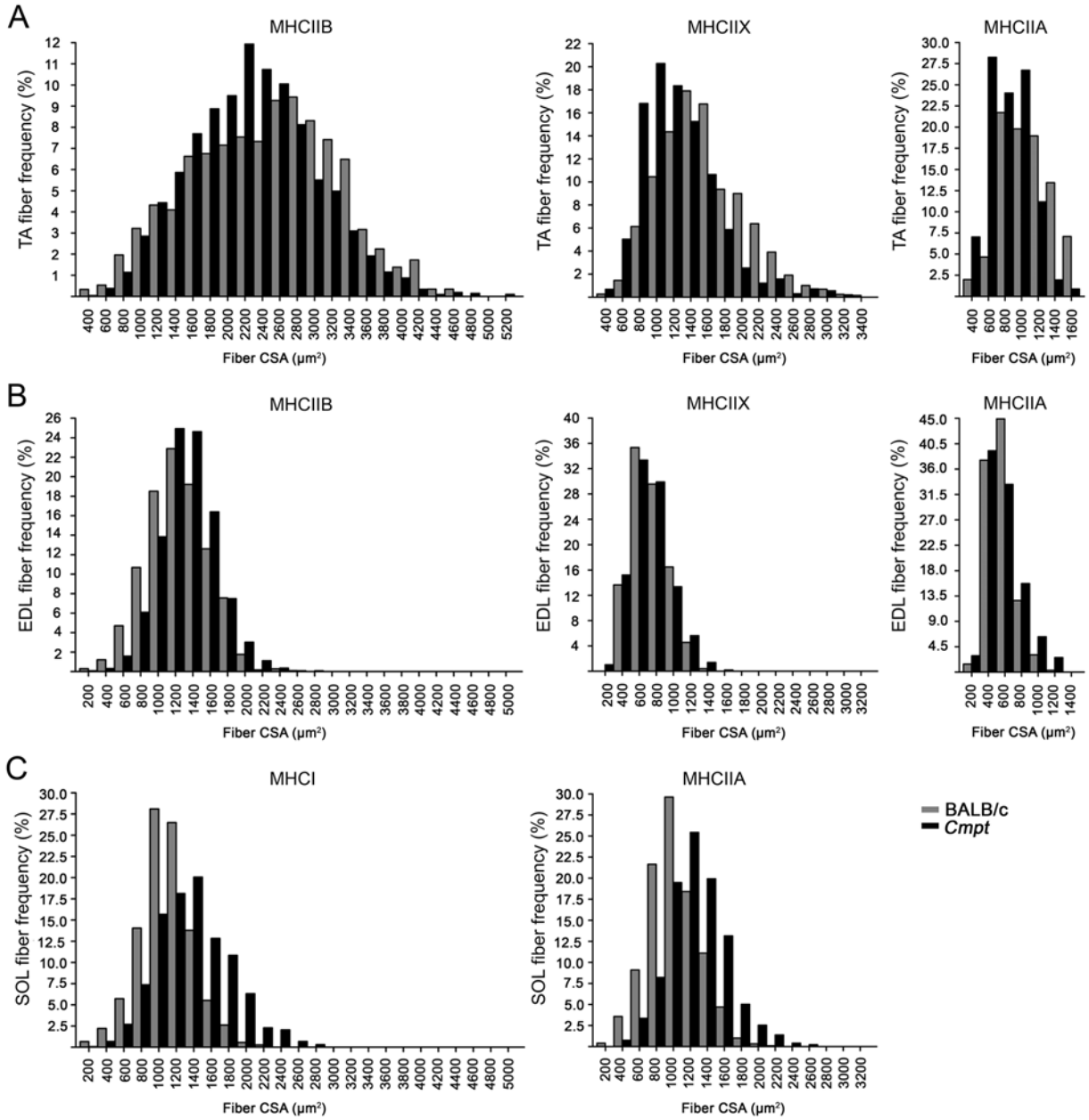

Figure 6. Frequency distribution of fiber size in tibialis anterior (TA) (A), extensor digitorum longus (EDL) (B) and soleus (SOL) (C) muscles of BALB/c and *Cmpt* male mice specific to each myosin heavy chain (MHC) isoform: MHCIIB, MHCIIX, MHCIIA and MHCI. CSA, fiber cross-sectional area.

In the present study we show, in accordance with others (Bünger et al. 2004; Rehfeldt et al. 2005; Amthor et al. 2007, 2009), that body and muscle weights of male *Cmpt* mice are higher than those of wild-type BALB/c mice. Body mass is even higher in *Cmpt* mice (47.7g) than it is described for male myostatin KO of the same age (38–41g) (McPherron et al. 1997). However, muscle weights normalized to body weight are comparable in both myostatin mutant lines, suggesting that *Cmpt* and myostatin KO mice represent a similar grade of muscularity. One exception was the SOL muscle, which seemed to be different in this regard, as its relative muscle-to-body weight did not increase in *Cmpt* compared with the wild-type mice. Indeed, it has been reported earlier that the oxidative SOL muscle contained less myostatin transcripts than the glycolytic EDL muscle (Mendler et al. 2000; Wang et al. 2012) and that the lack of myostatin had a stronger effect on glycolytic muscles than on oxidative ones (McPherron et al. 1997; Carlson et al. 1999; Hennebry et al. 2009; Wang et al. 2012). Therefore, we analyzed three different hindlimb

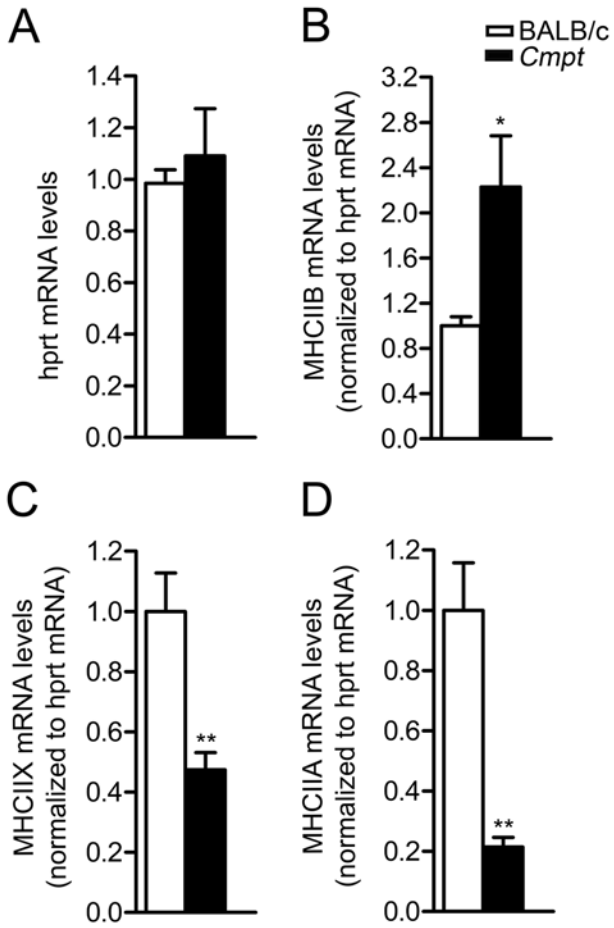

Figure 7. mRNA levels of myosin heavy chain (MHC) isoforms and *Hprt* in TA muscles of BALB/c and *Cmpt* male mice. Bars in B-D represent mRNA levels of MHCII isoforms normalized to *Hprt* transcripts (A). Data are expressed as the mean ± SEM. (n=5, *p<0.05, **p<0.01,).

muscles: the fast-glycolytic TA and EDL as well as the oxidative SOL muscles in *Cmpt* mice.

Based on extensive morphological analyses, measuring and counting all fibers on HE-stained cross sections and 500–1000 fibers on MHCIIB-stained sections, the TA muscles were exclusively characterized by muscle fiber hyperplasia, with an absence of hypertrophy. This observation may be somewhat surprising, as earlier reports described both hyperplasia and hypertrophy in different myostatin KO animals (McPherron and Lee, 1997; Amthor et al. 2009). However, even in the original myostatin KO mouse report (McPherron et al. 1997), the ratio of hyperplasia to hypertrophy varied in the different muscles; *e.g.*, the TA muscles of myostatin KO mice were dominated by hyperplasia, while only 14% fiber hypertrophy was documented. It is worth mentioning that the myostatin KO vs. myostatin$^{+/+}$ control mice (McPherron et al. 1997) contained similar fiber number in TA muscles (5470 vs. 2936) as observed with the *Cmpt* vs. BALB/c mice in our study (5455 vs. 3093), which makes the KO and *Cmpt* experiments somewhat comparable. In contrast to TA, the EDL muscles of *Cmpt* mice were characterized by a combination of hyperplasia (50%) and hypertrophy (20%), whereas, in the myostatin KO, the same type of muscles showed only a moderate hyperplasia and a stronger hypertrophy (Amthor et al. 2009). Amthor and colleagues (2009) compared EDL muscles of KO mice with that of the female 'Berlin' *Cmpt* mice (BEH$^{c/c}$). In line with our findings, they also detected stronger hyperplasia in female BEH$^{c/c}$ EDL muscles (1589) than in the KO (1200). Interestingly, the fiber number of both BEH$^{+/+}$ and myostatin$^{+/+}$ controls were also comparable with ours (1083 and 1160 vs. 1232, respectively). However, our results are somewhat different from those described for the BEH$^{c/c}$ females, for which fiber hypertrophy was very pronounced and still dominated over hyperplasia (Amthor et al. 2009). We found that the moderate fiber hypertrophy in *Cmpt* EDL was confined to the most glycolytic IIB fibers and not to the IIX or IIA fibers. This is again in accordance with the earlier reports that showed a stronger effect of myostatin on glycolytic muscles (McPherron et al. 1997; Carlson et al. 1999; Hennebry et al. 2009; Wang et al. 2012). We believe that the long separation of the 'Berlin' and Hungarian *Cmpt* lines, gender differences, the use of different controls as well as the higher number of fibers analyzed in our experiments (3000/1800 fibers in *Cmpt*/BALB/c vs. 150/180 fibers in BEH$^{c/c}$ /BEH$^{+/+}$ (Amthor et al. 2009) may account for these differences.

In the oxidative SOL muscle of *Cmpt* mice, low-grade hyperplasia (15%) and mainly hypertrophy (27%) accounted for the moderately higher mass of the mice as compared with wild-type mice. Moreover, both the oxidative I and IIA fibers showed evidence of hypertrophy compared with the wild-type mice. The changes in SOL are quite different from those of fast TA and EDL muscles in the *Cmpt* line and it is also difficult to compare them to myostatin KO mice where either 32% hyperplasia (Girgenrath et al. 2005) or 20% fiber hypertrophy has previously been described (Gentry et al. 2011).

It is not known so far, how cellularity in different muscle types is regulated upon myostatin defect. However, prenatal hyperplasia seems to be the major effect of developmental myostatin deficiency in most muscles of mice and cattle (McPherron et al. 1997; Grobet et al. 1997; Lee and McPherron 1997). Based on the different ratio of hyperplasia to hypertrophy in various myostatin-deficient muscles, myostatin might have a strong, but muscle type-dependent, effect on the proliferation of muscle precursor cells. Consequently, postnatal fiber hypertrophy might be restricted to different grades. Rehfeldt and co-workers (2005) introgressed the myostatin mutant *Cmpt* allele into a special high-growth mouse line (DUHi) and detected,

similar to our results, muscle hyperplasia in the predominantly fast rectus femoris and longissimus dorsi muscles, without any muscle hypertrophy. These data suggest that, at least in fast muscles, hyperplasia is even more pronounced in *Cmpt* mice than in myostatin KO mice. The difference might reside in the allelic variation of the myostatin defect and/or in modifier genes influencing *Cmpt* phenotype. To show that the dominance of hyperplasia (over hypertrophy) found in 2.5-month-old *Cmpt* muscles is not the result of delay in postnatal fiber growth, we analyzed TA muscles of 7-month-old *Cmpt* male mice. We found a similar hyperplasia without any substantial fiber hypertrophy in these older animals, which refutes that the increase of fiber size might reach its peak later in adulthood in *Cmpt* mice.

Although TA and EDL muscles contain predominantly type II glycolytic fibers (Bloemberg et al. 2012), we observed a significant glycolytic shift within type II fibers in *Cmpt* compared with wild-type mice. This result again is consistent with that of Rehfeldt et al. (2005) who found more glycolytic fibers in the rectus femoris muscle of the special *Cmpt*-DUHi line by NADH-tetrazolium reductase staining. A substantial glycolytic shift was also described in EDL muscles of myostatin KO mice as well as in double-muscled cattle using different methods (ATPase and SDH staining vs. immunohistochemical analysis), showing that both metabolic and structural protein changes occur with a myostatin deficiency (Wegner et al. 2000; Girgenrath et al. 2005; Amthor et al. 2007). However, immunohistochemical staining of MHC isoforms used in our study is more appropriate to distinguish between fiber types. By this method, significantly more IIB fibers and less IIX or IIA fibers were detected in TA muscles of *Cmpt* mice than in wild-type mice. Moreover, we analyzed fiber type distribution in superficial and deep portions of TA, as there are regional differences in glycolytic fibers distribution in wild-type mice (Bloemberg et al. 2012). Interestingly, the regional difference disappeared in *Cmpt* mice in contrast to wild-type, so that both superficial and deep regions of TA muscles were dominated by the glycolytic IIB fibers of a quite uniform fiber size. Transcript levels were in agreement with our immunohistochemical results: MHCIIB mRNA levels were significantly higher, while those of MHCIIX and IIA significantly lower in *Cmpt* TA muscles compared with those genes in wild-type muscles. These findings suggest that the fiber–type shift in fast muscles detected in our study is supported at the level of both MHC transcripts and proteins.

Likewise, we measured the same ratio of IIB/IIX/IIA fibers in EDL muscles of *Cmpt* mice using immunohistochemical methods, as performed by Amthor and colleagues (2007) for myostatin KO mice. The results shows that, in fast skeletal muscles, the *Cmpt* mutation results in similar glycolytic changes as the complete lack of myostatin protein in the KO mice. The glycolytic shift was consistent with the decrease in mitochondrial content, a reduced expression of cytochrome c oxidase, a lower citrate synthase activity and a shortening of contraction as well as relaxation time in myostatin KO mice (Amthor et al. 2007; Savage and McPherron 2010). Moreover, KOs showed impaired tolerance to chronic repetitive contractions (Ploquin et al. 2012) and a decrease in specific force generation, similar to that which was measured in $BEH^{c/c}$ female EDL muscles (Amthor et al. 2007). These data suggest that the function of the bigger and more glycolytic muscles is impaired upon myostatin defect.

However, the oxidative SOL muscles did not show any glycolytic shift in *Cmpt* mice in our experiments (53% slow-oxidative type I fibers, 44% fast-oxidative IIA fibers) as compared with that in the BALB/c line (38% type I fibers, 60% type IIA fibers). In contrast, these fibers had even slower oxidative phenotype than the control fibers. The fiber type composition we detected in BALB/c SOL is in agreement with the literature (Freitas et al. 2002; Luedecke et al. 2004) and represents a fiber ratio typical of a wild-type SOL, with less than 40% slow-type I fibers (Pellegrino et al. 2005; Bloemberg et al. 2012; McKeehen et al. 2013). Therefore, it is unlikely that the BALB/c mouse was not an appropriate type of control for our experiments in this regard. Based on the literature, the more than 50% slow-type I fibers in *Cmpt* animals is rather unusual for a SOL muscle in any type of mice, and is different from earlier reports on myostatin KO mice (Girgenrath et al. 2005; Gentry et al. 2011; Wang et al. 2012). This suggests that the different mechanisms of myostatin deficiency—with or without the influence of modifier genes—may induce differential and muscle-specific effects.

In summary, *Cmpt* mouse, in spite of its complex genetic background, shows similarities (at least in fast muscles) to myostatin KO mice in terms of muscle cellularity and glycolytic muscle phenotype, suggesting that the lack of myostatin is responsible for these morphological/functional changes. However, based on the more pronounced hyperplasia in *Cmpt* fast muscles as well as the different cellularity and oxidative phenotype of *Cmpt* SOL, additional studies are needed to elucidate the molecular mechanisms of myostatin inactivity and the possible role of modifier genes in *Cmpt* mice.

Acknowledgments

We thank to Makráné Felhő Zita and Balásházi Istvánné for technical assistance.

Declaration of Conflicting Interests

The author(s) declared no potential conflicts of interest with respect to the research, authorship, and/or publication of this article.

Funding

The author(s) disclosed receipt of the following financial support for the research, authorship, and/or publication of this article: This work was supported by the Hungarian National Development Agency, the European Union and co-funded by the European Social Fund [project numbers: TÁMOP 4.2.2/B-10/1-2010-0012; TÁMOP 4.2.2.A-11-1-KONV-2012-0035] and by "National Excellence Program" [TÁMOP 4.2.4.A/2-11-1-2012-0001].

References

1. Amthor H, Macharia R, Navarrete R, Schuelke M, Brown SC, Otto A, Voit T, Muntoni F, Vrbóva G, Partridge T, Zammit P, Bünger L, Patel K. 2007. Lack of myostatin results in excessive muscle growth but impaired force generation. Proc Natl Acad Sci. 104:1835–1840.
2. Amthor H, Otto A, Vulin A, Rochat A, Dumonceaux J, Garcia L, Mouisel E, Hourdé C, Macharia R, Friedrichs M, Relaix F, Zammit PS, Matsakas A, Patel K, Partridge T. 2009. Muscle hypertrophy driven by myostatin blockade does not require stem/precursor-cell activity. Proc Natl Acad Sci. 106:7479–7484.
3. Bloemberg D, Quadrilatero J. 2012. Rapid determination of myosin heavy chain expression in rat, mouse and human skeletal muscle using multicolor immunofluorescence analysis. Plos One. 7:1–11.
4. Boman IA, Klemetsdal G, Blichfeldt T, Nafstad O, Vage DI. 2009. A frameshift mutation in the coding region of the myostatin gene (MSTN) affects carcass conformation and fatness in Norwegian white sheep (Ovis aries). Anim Genetics. 40:418–422.
5. Bünger L, Laidlaw AH, Bulfield G, Eisen EJ, Medrano JF, Bradford GE, Prichner F, Renne U, Schlote W, Hill WG. 2001. Inbred lines of mice derived from long-term on growth selected lines: unique resources for mapping growth genes. Mamm Genome. 12:678–686.
6. Bünger L, Ott G, Varga L, Schlote W, Rehfeldt C, Williams JL, Hill WG. 2004. Marker assisted introgression of the Compact mutant myostatin allele: $Mstn^{Cmpt\text{-}dl1Abc}$ into a mouse line with extreme growth-effects on body composition and muscularity. Genet Res. 84:161–173.
7. Carlson CJ, Booth FW, Gordon SE. 1999. Skeletal muscle myostatin mRNA expression is fiber-type specific and increases during hindlimb unloading. Am J Physiol. 277:R601–606.
8. Clop A, Marcq F, Takeda H, Pirottin D, Tordoir X, Bibé B, Bouix J, Caiment F, Elsen JM, Eychenne F, Larzul C, Laville E, Meish F, Milenkovic D, Tobin J, Charlier C, Georges M. 2006. A mutation creating a potential illegitimate microRNA target site in the myostatin gene affects muscularity in sheep. Nat Genet. 38:813–818.
9. Freitas EM, Dal Pai Silva M, da Cruz-Höfling MA. 2002. Histochemical differences in the responses of predominantly fast-twitch glycolytic muscle and slow-twitch oxidative muscle to veratrine. Toxicon. 40:1471–1481.
10. Gentry BA, Ferreira JA, Phillips CL, Brown M. 2011. Hindlimb skeletal muscle function in myostatin-deficient mice. Muscle Nerve. 43:49–57.
11. Girgenrath S, Song K, Whittemore LA. 2005. Loss of myostatin expression alters fiber-type distribution and expression of myosin heavy chain isoforms in slow- and fast-type skeletal muscle. Muscle Nerve. 31:34–40.
12. Grobet L, Martin LJ, Poncelet D, Pirottin D, Brouwers B, Riquet J, Schoeberlein A, Dunner S, Ménissier F, Massabanda J, Fries R, Hanset R, Georges M. 1997. A deletion in the bovine myostatin gene causes the double-muscled phenotype in cattle. Nat Genet. 17:71–74.
13. Hennebry A, Berry C, Siriett V, O'Callaghan P, Chau L, Watson T, Sharma M, Kambadur R. 2009. Myostatin regulates fiber-type composition of skeletal muscle by regulating MEF2 and MyoD gene expression. Am J Physiol Cell Physiol. 296:C525–534.
14. McKeehen JN, Novotny SA, Baltgalvis KA, Call JA, Nuckley DJ, Lowe DA. Adaptation of mouse skeletal muscle to low-intensity vibration training. 2013. Med Sci Sports Exerc. 45:1051–1059.
15. McPherron AC, Lawler AM, Lee SJ. 1997. Regulation of skeletal muscle mass in mice by a new TGF-β superfamily member. Nature. 387:83–90.
16. McPherron AC, Lee SJ. 1997. Double muscling in cattle due to mutations in the myostatin gene. Proc Natl Acad Sci. 94:12457–12461.
17. Mendler L, Zádor E, Ver Heyen M, Dux L, Wuytack F. 2000. Myostatin levels in regenerating rat muscles and in myogenic cell cultures. J Muscle Res Cell Motil. 21:551–563.
18. Mosher DS, Quignon P, Bustamante CD, Sutter NB, Mellersh CS, Parker HG, Ostrander EA. 2007. A mutation in the myostatin gene increases muscle mass and enhances racing performance in heterozygote dogs. PloS Genetics. 0779–0786.
19. Pellegrino MA, Brocca L, Dioguardi FS, Bottinelli R, D'Antona G. 2005. Effects of voluntary wheel running and amino acid supplementation on skeletal muscle of mice. Eur J Appl Physiol. 93:655–664.
20. Ploquin C, Chabi B, Fouret G, Vernus B, Feillet-Coudray C, Coudray C, Bonnieu A, Ramonatxo C. 2012. Lack of myostatin alters intermyofibrillar mitochondria activity, unbalances redox status, and impairs tolerance to chronic repetitive contractions in muscle. Am J Physiol Endocrinol Metab. 302:E1000–1008.
21. Rehfeldt C, Ott G, Gerrard DE, Varga L, Schlote W, Williams JL, Renne U, Bünger L. 2005. Effects of the Compact mutant myostatin allele $Mstn^{Cmpt\text{-}dl1Abc}$ introgressed into a high growth mouse line on skeletal muscle cellularity. J Muscle Res Cell Mot. 26:103–112.
22. Savage KJ, McPherron AC. 2010. Endurance exercise training in myostatin null mice. Muscle Nerve. 42:355–362.
23. Schuelke M, Wagner KR, Stolz LE, Hübner C, Riebel T, Komen W, Braun T, Tobin JF, Lee SJ. 2004. Myostatin mutation associated with gross muscle hypertrophy in a child. New Engl J Med. 350:2682–2688.
24. Stinckens A, Luyten T, Bijttebier J, Van den Maagdenberg K, Dieltiens D, Janssens S, De Smet S, Georges M, Buys N. 2008. Characterization of the complete porcine MSTN gene and expression levels in pig breeds differing in muscularity. Anim Genet. 39:586–596.
25. Szabó G, Dallmann G, Müller G, Patthy L, Soller M, Varga L. 1998. A deletion in the myostatin gene causes the compact

(Cmpt) hypermuscular mutation in mice. Mamm Genome. 9:671–672.
26. Valle Zarate A, Horst P, Weniger JH. 1994. Antagonism Between Growth and Productive Adaptability in Mice. Archiv für Tierzucht-Archives of Animal Breeding. 37:185–198.
27. Varga L, Szabó G, Darvasi A, Müller G, Sass M, Soller M. 1997. Inheritance and mapping of Compact (Cmpt), a new mutation causing hypermuscularity in mice. Genetics. 147:755–764.
28. Varga L, Müller G, Szabó G, Pinke O, Korom E, Kovács B, Patthy L Soller M. 2003. Mapping modifers affecting muscularity of the myostatin mutant ($Mstn^{Cmpt\text{-}dl1Abc}$) Compact mouse. Genetics. 165:257–267.
29. Varga L, Pinke O, Müller G, Kovács B, Korom E, Szabó G, Soller M. 2005. Mapping a syntenic modifier on mouse chromosome 1 influencing the expressivity of the Compact phenotype in the myostatin mutant ($Mstn^{Cmpt\text{-}dl1Abc}$) Compact mouse. Genetics. 169:489–493.
30. Wang M, Yu H, Kim YS, Bidwell CA, Kuang S. 2012. Myostatin facilitates slow and inhibits fast myosin heavy chain expression during myogenic differentiation. Biochem Biophys Res Commun. 426:83–88.
31. Wegner J, Albrecht E, Fiedler I, Teuscher F, Papstein HJ, Ender K. 2000. Growth and breed-related changes of muscle fiber characteristics in cattle. J Anim Sci. 78:1485–1496.
32. Weniger JH, Horst P, Steinhauf D, Major F, Wolf M, Tawfik ES. 1974. Model experiments on selection for endurance and its relation to growth. Part I. Introduction, methods and preliminary investigations on the basic population. Journal of Animal Breeding and Genetics-Zeitschrift für Tierzüchtung und Züchtungsbiologie. 91:265–270.

II.

Baán et al. Journal of Translational Medicine (2015) 13:1
DOI 10.1186/s12967-014-0365-0

JOURNAL OF TRANSLATIONAL MEDICINE

RESEARCH Open Access

Myostatin and IGF-I signaling in end-stage human heart failure: a qRT-PCR study

Júlia Aliz Baán[1†], Zoltán V Varga[2†], Przemyslaw Leszek[3], Mariusz Kuśmierczyk[3], Tamás Baranyai[2], László Dux[1], Péter Ferdinandy[2,4], Thomas Braun[5] and Luca Mendler[1,6*]

Abstract

Background: Myostatin (Mstn) is a key regulator of heart metabolism and cardiomyocyte growth interacting tightly with insulin-like growth factor I (IGF-I) under physiological conditions. The pathological role of Mstn has also been suggested since Mstn protein was shown to be upregulated in the myocardium of end-stage heart failure. However, no data are available about the regulation of gene expression of Mstn and IGF-I in different regions of healthy or pathologic human hearts, although they both might play a crucial role in the pathomechanism of heart failure.

Methods: In the present study, heart samples were collected from left ventricles, septum and right ventricles of control healthy individuals as well as from failing hearts of dilated (DCM) or ischemic cardiomyopathic (ICM) patients. A comprehensive qRT-PCR analysis of Mstn and IGF-I signaling was carried out by measuring expression of Mstn, its receptor Activin receptor IIB (ActRIIB), IGF-I, IGF-I receptor (IGF-IR), and the negative regulator of Mstn miR-208, respectively. Moreover, we combined the measured transcript levels and created complex parameters characterizing either Mstn- or IGF-I signaling in the different regions of healthy or failing hearts.

Results: We have found that in healthy control hearts, the ratio of Mstn/IGF-I signaling was significantly higher in the left ventricle/septum than in the right ventricle. Moreover, Mstn transcript levels were significantly upregulated in all heart regions of DCM but not ICM patients. However, the ratio of Mstn/IGF-I signaling remained increased in the left ventricle/septum compared to the right ventricle of DCM patients (similarly to the healthy hearts). In contrast, in ICM hearts significant transcript changes were detected mainly in IGF-I signaling. In paralell with these results miR-208 showed mild upregulation in the left ventricle of both DCM and ICM hearts.

Conclusions: This is the first demonstration of a spatial asymmetry in the expression pattern of Mstn/IGF-I in healthy hearts, which is likely to play a role in the different growth regulation of left vs. right ventricle. Moreover, we identified Mstn as a massively regulated gene in DCM but not in ICM as part of possible compensatory mechanisms in the failing heart.

Keywords: Heart failure, Myostatin, IGF-I, Activin receptor IIB, IGF-I receptor, qRT-PCR, microRNA-208, miRNA

Background

Myostatin (Mstn), the growth inhibitor of skeletal muscle [1], was shown to be expressed in the heart tissue [2] with controversial data about its role in myocardial physiology and pathophysiology. Based on the analysis of constitutive Mstn knockout mice, numerous studies have demonstrated that Mstn inhibits cardiac growth and contractility and induces fibrosis [3-6]. Nevertheless, by analyzing adult cardiac-specific Mstn mutants we have revealed recently a beneficial role of Mstn in maintaining cardiac energy homeostasis and preventing pathological cardiac hypertrophy [7].

Insulin-like growth factor I (IGF-I), on the other hand was shown to play a pivotal role in cardiovascular physiology and aging [8-10]. In concert with insulin itself, IGF-I proved to be a positive regulator of cardiac growth and contractility under both physiological and pathological conditions [11-17]. Previous *in vitro* studies described a

* Correspondence: mendler.luca@med.u-szeged.hu
†Equal contributors
[1]Department of Biochemistry, Faculty of General Medicine, University of Szeged, Dóm tér 9, H-6720 Szeged, Hungary
[6]Institute of Biochemistry II, Goethe University, Faculty of Medicine, Theodor-Stern-Kai 7, 60590 Frankfurt, Germany
Full list of author information is available at the end of the article

tight interplay between Mstn and IGF-I [3,18-20] and proposed that Mstn might be a cardiac chalone of IGF-I since cardiac growth induced by IGF-I was feed-backed by the overexpression of the negative growth regulator Mstn [21]. However, no studies have systematically analyzed the relevance of their possible reciprocal regulation at the gene expression level in healthy or failing human hearts. Previous investigations focused only on Mstn protein activation that has been shown to be accelerated in hearts of dilated or ischemic cardiomyopathic patients (DCM or ICM, respectively) [22]. Moreover, no data exist in the literature about the expression pattern of Mstn in comparison with IGF-I and their receptors in various regions (i. e. left ventricles (LV) versus right ventricles (RV)) of the human heart. Given the different functional requirements LV and RV should cope with, and the markedly different development of these regions, one could assume that the gene expression pattern of Mstn and IGF-I signaling might show remarkable spatial differences under both physiological and pathological conditions. In the present qRT-PCR study we report that Mstn/IGF-I signaling differs in LV versus RV even in healthy hearts and shows significant differences in DCM versus ICM patients.

Methods

Study design

All procedures followed were in accordance with the ethical standards of the responsible committee on human experimentation (institutional and national) and with the Helsinki Declaration of 1975. Informed consent was obtained from all patients for being included in the study according to the protocol approved by the Local Ethics Committee (IK-NP-0021-24/1426/14). Healthy human hearts were obtained from organ donor patients (CONT, n = 5) whose hearts were explanted but due to technical reasons (CMV infection, extensive damage during harvest and size donor/recipient mismatch), not used for transplantation. The donors did not present any important previous medical history or any abnormalities in ECG and echocardiography (LV dimensions/contractility within normal ranges); these organ donors had died from head trauma, cerebral or subarachnoid hemorrhage. Explanted end-stage failing hearts were obtained from patients with advanced heart failure of non-ischaemic (DCM) (n = 5) or ischaemic aethiology (ICM) (n = 5). Before transplantation the clinical state of all patients was determined according to the New York Heart Association (NYHA) classification; patients of NYHA class III–IV underwent a clinical assessment that included resting electrocardiogram, echocardiography and hemodynamic measurements.

Preparation of cardiac tissue

Tissue samples of the right and left ventricular free walls and the inter-ventricular septum were taken at the time of explantation (avoiding scarred, fibrotic, or adipose tissue, endocardium, epicardium or coronary vessels). The samples were rinsed immediately, blotted dry, frozen in liquid nitrogen and kept at – 80°C until further processing.

qRT-PCR analysis of mRNA transcripts

Total RNA was isolated from the LV and RV as well as from inter-ventricular septum (S) of the CONT, DCM or ICM patients with the guanidinium thiocyanate-phenol-chloroform method [23], followed by reverse transcription (Sigma MMLV- Moloney Murine Leukemia Virus Reverse Transcriptase, 28025-013). For the detection of the transcript levels of myostatin (Mstn), activin receptor IIB (ActRIIB), insulin-like growth factor I (IGF-I) and insulin-like growth factor I receptor (IGF-IR) quantitative PCR was carried out with SYBR GREEN master mix (Fermentas) on a Light Cycler 1.5 (Roche Applied Science). Since some of the genes generally used for internal normalization in qRT-PCR contain several pseudogenes (e.g. GAPDH, beta-actin) of which co-amplification may compromise their reliability as reference genes [24], hipoxanthine-guanine phosphorybosyltransferase (HPRT) has been used as a single internal control gene in our experiments. Indeed, HPRT expression did not significantly change between different groups or heart regions (data not shown). Cycle conditions were set as an initial denaturation step for 10 min at 95°C, followed by 45 cycles of 10 sec at 95°C for template denaturation, 10 sec for annealing phase at 58°C and 10 sec at 72°C for extension. Specificity of the PCR products was confirmed by melting curve analysis followed by the verification of the amplicon length on 1.5% agarose gels stained by ethidium bromide. Primer pairs for Mstn, ActRIIB, IGF-I, IGF-IR and HPRT were designed to intron spanning exons by Primer 3 Input (version 0.4.0) software and tested to avoid primer dimers, unspecific amplification and self-priming formation (Table 1).

qRT-PCR analysis of miRNA transcripts

From the above detailed total RNA isolates, cDNA was synthetized and quantitative real-time PCR was performed with miRCURY LNA™ Universal RT microRNA PCR kit (Exiqon, Denmark) on LightCycler®480 (Roche, Switzerland) according to the manufacturer's instructions. Briefly, total RNA was diluted to a final concentration of 5 ng/μL, and mixed with Reaction buffer and Enzyme mix provided with the kit in a final volume of 10 μL. Reaction mixture was incubated for 60 min at 42°C, and reverse transcriptase was heat-inactivated for 5 min at 95°C. Then, cDNA was diluted to 80x and 4 μL of diluted cDNA were mixed with 6 μL of the PCR Master mix and PCR primer mix supplied by the manufacturer. The primers for both microRNA-208b and microRNA-103a-3p was designed and prepared by using Exiqon's LNA™ technology. Polymerase was activated for 10 min at 95°C, and microRNA-

Table 1 Primer properties used in qRT-PCR

Target	Accession number	Forward primer	Reverse primer	Efficiency	Product size (bp)
Mstn	NM_005259.2	TTCGTCTGGAAACAGCTCCT	CATTTGGGTTTTCCATCCAC	1.783	220
ActRIIB	NM_001106.3	TGACTTTGGCTTGGCTGTTC	ATGTACTCATCCACGGGTCC	1.834	219
IGF-I	XM_005268835.1	ATGCTCTTCAGTTCGTGTGTG	GGGTCTTGGGCATGTCGGTG	1.758	219
IGFI-R	NM_000875.3	GACAACCAGAACTTGCAGCA	GATTCTTCGACGTGGTGGTG	1.714	241
HPRT	NM_000194.2	TGCTCGAGATGTGATGAAGG	TCCCCTGTTGACTGGTCATT	2.044	192

bp: base pair, Mstn: myostatin, ActRIIB: activin receptor IIB, IGF-I: insulin-like growth factor I, IGFI-R: insulin-like growth factor I receptor, HPRT: hypoxanthine-guanine phosphorybosyltransferase.

208b and microRNA-103a-3p were amplified and quantified (denaturation: 10 sec at 95°C; annealing/synthesis: 1 min at 60°C). The specificity of amplifications was assessed by melting curve analysis (42°C to 80°C) and by agarose gel electrophoresis (1%). At last, crossing point values (Cp) were calculated. MicroRNA-208b Cp values were normalized to the corresponding housekeeping microRNA-103a-3p Cp values. Then, all pairwise ΔCp value normalization was carried out to control ΔCp values, and expressed as mean of the three replicated of 2-ΔΔCp values (fold change).

Definition of parameters characterizing Mstn and IGF-I signaling in the heart

In order to describe the additive effect of Mstn and its receptor ActRIIB transcript levels we combined these data and defined a multiplied value of Mstn x ActRIIB as 'Mstn signaling index' for each analyzed sample. Similarly, we created a multiplied value of IGF-I x IGF-IR transcript levels referred to as 'IGF-I signaling index'. To show the ratio of Mstn and IGF-I signaling in the different regions of healthy or failing hearts we divided the measured transcript levels by each other to produce either growth factor ratio of Mstn/IGF-I or receptor ratio of ActRIIB/IGF-IR. Finally, we created a complex parameter characterizing the combined ratio of Mstn/IGF-I signaling by dividing 'Mstn signaling index' (Mstn x ActRIIB) by 'IGF-I signaling index' (IGF-I x IGF-IR) referred to as 'Mstn/IGF-I signaling index' ((Mstn x ActRIIB)/(IGF-I x IGF-IR)).

Statistical analysis

Statistical analysis was performed by one-way/two-way ANOVA or non-parametric *t*-test (Welch test) using Prism software (GraphPad Software, Inc.; San Diego, CA), as appropriate. All data were expressed as means ± SEM. For all analyses, a P value <0.05 was considered statistically significant. The individual P-values are indicated in the figure legends.

Results

Study patients

A detailed summary of the pre-transplant data and drug therapy of study subjects are shown in Table 2. Both female and male patients were included in all groups. The age of ICM patients differed as expected significantly from both CONT and DCM, since ICM patients are usually diagnosed with end-stage heart failure later than DCM patients. DCM and ICM patients were in either NYHA class III or IV with no difference in pulmonary artery pressure (PAP, PWP) left ventricle size parameters (LVED, LVSD, IVS, PW) or left ventricular ejection fraction (LVEF) among

Table 2 Clinical, echocardiographic and hemodynamic characteristics of DCM and ICM patients

	CONT	DCM	ICM
Number of samples	5	5	5
Gender (female/male)	3/2	2/3	4/1
Age (year)	29 ± 9	39 ± 10	57 ± 11*#
NYHA functional class III/IV, *n*	n.a.	0/5	3/2
PAP, mmHg	n.a.	31.6 ± 4.7	30.8 ± 5.6
PWP, mmHg	n.a.	24 ± 4.3	21 ± 3.5
LVED, mm	n.a.	68 ± 4	71 ± 4
LVSD, mm	n.a.	63 ± 5	61 ± 8
PW, mm	n.a.	9.5 ± 0.5	10 ± 1.5
IVS, mm	n.a.	10 ± 0.7	11 ± 1.5
LVEF, %	n.a.	16 ± 3	23 ± 3
Medications			
ACE-inhibitor	-	++	++
β-Blocker	-	++	++
Diuretics	-	++	++
Digitalis	-	+	+
PDE-inhibitor	-	++	++
Dopamine/Noradrenaline	++	++	+
Statin	-	-	++
Aspirin	-	-	++
Desmopressin	++	-	-

Values are given in mean ± SEM; *p < 0.05 compared to control; #p < 0.05 compared to DCM Abbreviations: CONT: healthy control individuals, DCM: dilated cardiomyopathy, ICM: ischemic cardiomyopathy, NYHA: New York Heart Association, PAP: mean pulmonary artery pressure, PWP: mean pulmonary wedge pressure, LVED: left ventricular end-diastolic diameter, LVSD: left ventricular end-systolic diameter, PW: posterior wall thickness, IVS: interventricular septum thickness, LVEF: left ventricular ejection fraction, ACE: angiotensin converting enzyme, PDE: phosphodiesterase, n.a.: not applicable.

groups. Extra care was taken to exclude diabetic (insulin-treated) patients from the study to avoid possible modification of the IGF-I signaling by insulin treatment. All patients were managed with angiotensin-converting enzyme (ACE)-inhibitors, beta-blockers and diuretics, however, aspirin and statins were only used in case of ICM patients. CONT subjects received iv. treatment composed of very low catecholamine infusion (noradrenaline: 01.-0.2 μg/kg/min, dopamine: 1-2 μg/kg/min) whereas adequate fluid balance was maintained with intravenous fluids including colloids (e.g. Voluven - hydroxyethyl starch) and Desmopressin.

Mstn and IGF-I signaling in healthy control hearts

So far, no comprehensive study has been carried out to reveal gene expression of the growth regulators Mstn and IGF-I and their receptors in different regions of healthy human hearts. In the present work we detected no significant difference in Mstn (Figure 1A) and ActRIIB (Figure 1B) transcript levels nor in Mstn signaling index (Figure 1C) between septum (S), left ventricle (LV) and right ventricle (RV), however, Mstn levels showed decreasing tendency in the RV (Figure 1A). In contrast, both IGF-I mRNAs (Figure 1D) and IGF-I signaling index

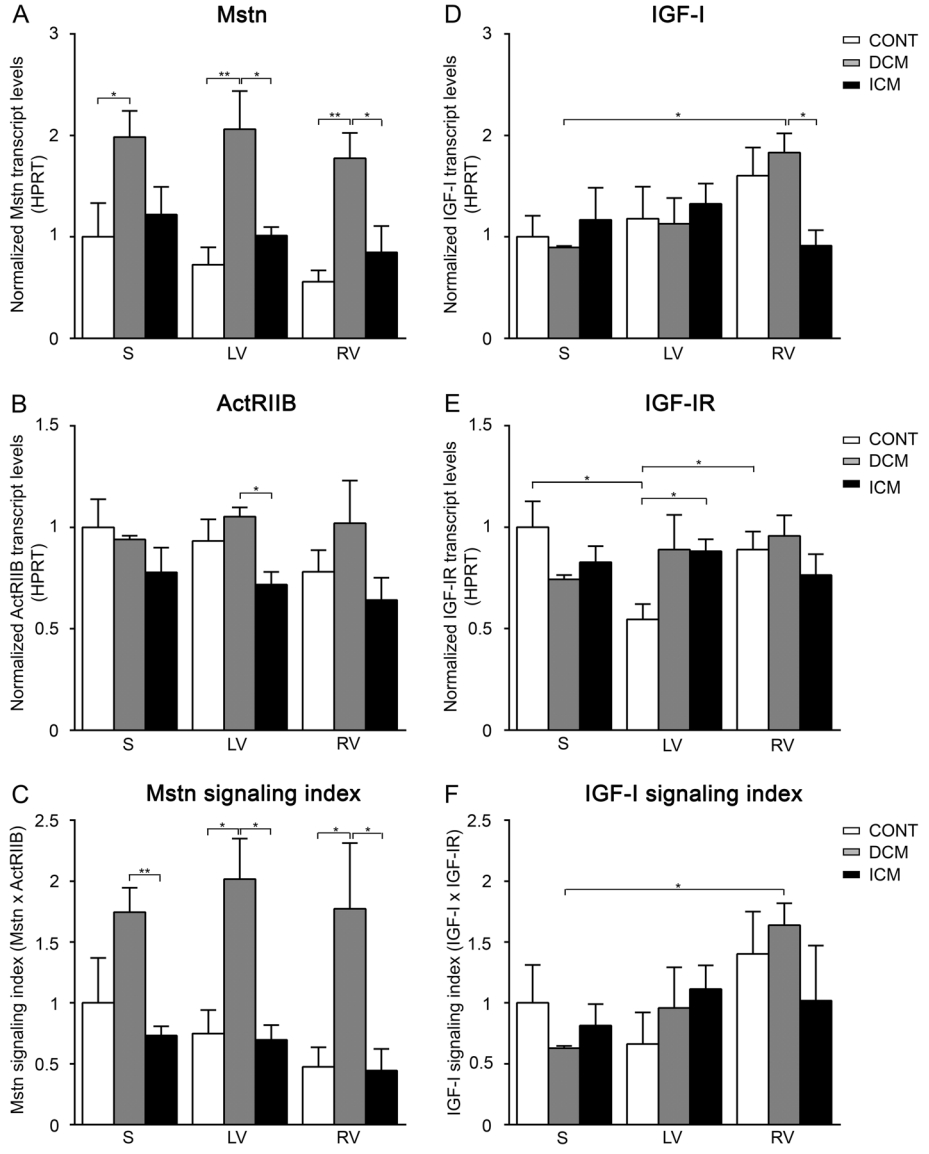

Figure 1 Gene expression levels of Mstn and IGF-I as well as their receptors ActRIIB and IGF-IR normalized to HPRT in the septum (S), left ventricles (LV) and right ventricles (RV) of control (CONT)-, DCM-, and ICM hearts, respectively. Bars represent normalized Mstn- **(A)**, ActRIIB- **(B)**, IGF-I- **(D)**, and IGF-IR- **(E)** transcript levels. Panel **C** shows 'Mstn signaling index' (Mstn multiplied by ActRIIB mRNA levels) while panel **F** represents 'IGF-I signaling index' (IGF-I multiplied by IGF-IR mRNA levels). Data are expressed in mean ± SEM, asterisks show significant differences (n = 5, *p < 0.05, **p < 0.01).

(Figure 1F) followed an increasing tendency in RV accompanied with a significantly higher IGF-IR levels compared to those of LV (Figure 1E). As a consequence, the ratio of Mstn/IGF-I gene expression (Figure 2A) as well as those of ActRIIB/IGF-I receptors (Figure 2B) and finally the ratio of Mstn to IGF-I signaling (Figure 2C) all showed significantly higher values in LV/S as compared to RV. These data clearly demonstrate that Mstn signaling dominates over IGF-I in the LV more than in RV of healthy human hearts.

Mstn and IGF-I signaling in DCM patients compared to healthy controls

In DCM patients we measured massive upregulation of Mstn mRNA (Figure 1A) associated with an increased Mstn signaling index (Figure 1C) in all heart regions compared to CONT, although ActRIIB levels remained relatively unchanged (Figure 1B). Similar to healthy hearts, we found a significant upregulation of IGF-I transcripts (Figure 1D) as well as of IGF-I signaling index (Figure 1F) in RV of the failing hearts when compared to those of S, although IGF-IR expression did not show significant difference in either region nor in comparison to CONT hearts (Figure 1E). Thus, the ratio of Mstn/IGF-I mRNA levels (Figure 2A) and the Mstn/IGF-I signaling index (Figure 2C) proved to be significantly higher in the left versus right side of the DCM hearts and showed much higher levels than those of the CONT regions. Since the ratio of the ActRIIB/IGF-I receptors (Figure 2B) did not change significantly we can conclude that Mstn was upregulated in all regions of failing hearts in DCM patients as compared to CONT. However, given the higher IGF-I levels in RV, left and right side of failing heart differed significantly from each other in regard to the ratio of Mstn/IGF-I signaling similar to those of healthy ones (Figure 2C).

Mstn and IGF-I signaling in ICM patients compared to healthy controls

In contrast to DCM patients, we could not detect any difference in either Mstn (Figure 1A) or ActRIIB transcript levels (Figure 1B) or in Mstn signaling index (Figure 1C) in any heart region of ICM patients compared to those of CONT. Similarly, IGF-I (Figure 1D) and IGF-IR levels (Figure 1E) as well as IGF-I signaling index (Figure 1F) did not differ in ICM heart regions; however, in comparison to CONT IGF-I showed a decreasing tendency of expression in the RV, while increased expression of IGF-IR in the LV was present. Consequently, both ratios of Mstn/

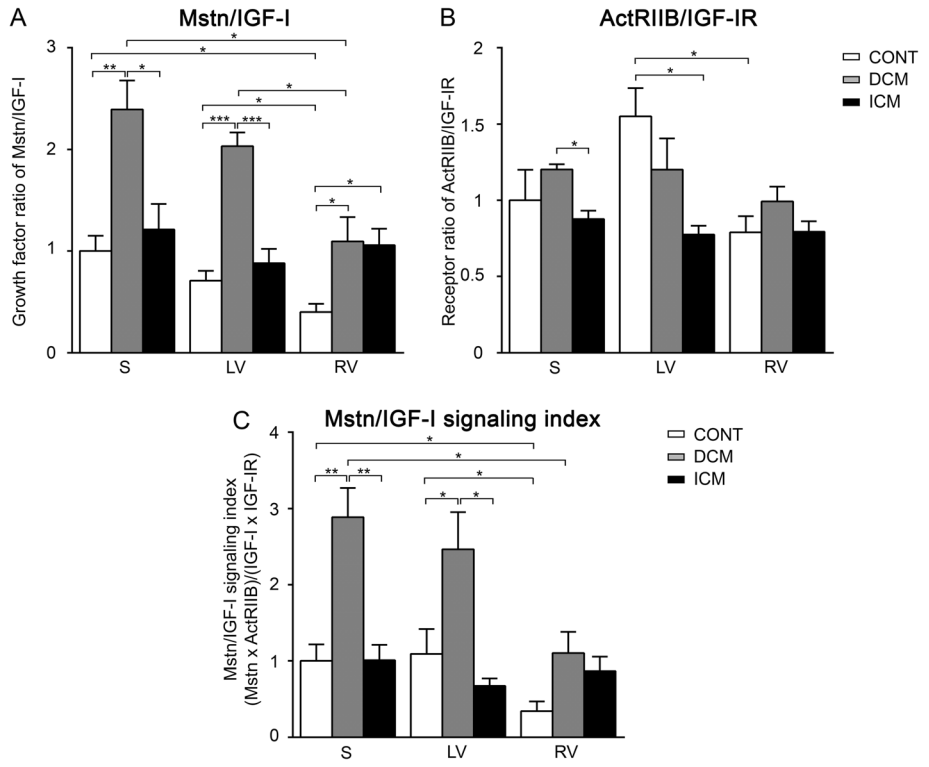

Figure 2 Growth factor ratio of Mstn/IGF-I (A), receptor ratio of ActRIIB/IGF-IR (B) and 'Mstn/IGF-I signaling index' (C) in the septum (S), left ventricles (LV) and right ventricles (RV) of control (CONT)-, DCM-, and ICM hearts, respectively. Panel **C** represents the ratio of Mstn and IGF-I signaling referred to as 'Mstn/IGF-I signaling index' ('Mstn signaling index' divided by 'IGF-I signaling index' (Mstn x ActRIIB)/(IGF-I x IGF-IR)). Data are expressed in mean ± SEM, asterisks show significant differences (n = 5, *p < 0.05, **p < 0.01, ***p < 0.001).

IGF-I (Figure 2A) and ActRIIB/IGF-IR (Figure 2B) were similar in all analyzed regions of ICM hearts. However, significantly higher Mstn/IGF-I ratios were revealed in RV due to decreased IGF-I levels as well as significantly lower ActRIIB/IGF-IR ratios in LV when compared to CONT hearts (due to increased IGF-IR levels). In summary, ICM hearts did not show significantly altered modulation of Mstn signaling in either heart region, whereas IGF-I signaling, in contrast to the healthy situation, seemed to be moderately induced in the LV, while inhibited in the RV.

Differences in Mstn/IGF-I signaling between DCM and ICM patients

Based on our results, all regions of DCM hearts showed significantly higher Mstn levels (Figure 1A) as well as elevated Mstn signaling index (Figure 1C) than those of ICM hearts. Moreover, ActRIIB (Figure 1B) also revealed increased levels in LV of DCM vs. ICM patients. Nevertheless, we found no significant difference in IGF-I signaling on the left side of failing hearts (Figure 1D-F), although significantly less IGF-I transcripts were evident on the right side of ICM hearts in comparison with that of DCM ones (Figure 1D). As a consequence, all parameters describing the ratio of Mstn to IGF-I signaling (Figure 2A-C) showed significantly increased values in the LV of DCM versus ICM hearts. Although in the RV we have revealed similar signaling ratio in both types of failing hearts (Figure 2A-C) the reason for that was an upregulation of Mstn signaling in DCM patients while a downregulation of IGF-I signaling in ICM heart samples.

miR-208 expression in relation to Mstn expression in DCM and ICM patients compared to healthy controls

In parallel with the massive upregulation of Mstn mRNA in the left ventricle of DCM patients we measured a mild upregulation of miR-208b (1.505 fold change) compared to CONT. A similar but less pronounced upregulation was seen in ICM hearts (1.405 fold change) when compared to CONT, however, no significant difference was detected between DCM and ICM patients.

Discussion

In the present comprehensive qRT-PCR study we have found that Mstn dominated over IGF-I signaling much more in the LV than in the RV of healthy human hearts, and that DCM hearts upregulated Mstn expression in contrast to ICM hearts. This is the first demonstration that Mstn/IGF-I signaling differs in LV and RV in healthy hearts and shows significant alterations in end-stage heart failure due to DCM and ICM (Figure 3).

Several studies exist in the literature, indicating the presence and/or de-regulation of both Mstn and IGF-I under different conditions in the heart tissue, however, the majority of data were collected from whole hearts or separately from the LV [2,11,12,22]. Regarding Mstn expression in healthy hearts, only one study has been published so far on higher transcript levels of Mstn in LV as compared to RV in young piglet hearts [25]. In line with these data we have demonstrated here an obvious reciprocal regulation of Mstn and IGF-I in LV compared to RV characterized by elevated ratios of both Mstn/IGF-I and ActRIIB/IGF-IR transcripts in healthy human LV (Figure 3). Septum (S) samples, as being part of LV from the functional point of view, revealed similar values to those of LV in most cases. We assume that cardiomyocyte growth in LV/S should be balanced more tightly by growth inhibitors (i.e. Mstn) than that of RV since LV is exposed to higher-pressure overload, while RV to a relatively higher-volume overload. In addition to Mstn and IGF-I, several other factors have been reported to be enriched in either LV or RV; their asymmetric expression might reflect a molecular predisposition of myocardium to LV-concentric and RV-eccentric remodeling during postnatal development [25,26]. Similarly, higher expression levels in LV vs. RV have been demonstrated for cytochrome c oxidases and PGC1α, both of which are known to contribute to maintain oxidative metabolism [27]. Recently, we have also shown that Mstn plays an important role in the regulation of oxidative metabolism of the myocardium [7]. Therefore our results support the idea that the elevated ratio of Mstn/IGF-I signaling is an important regulatory mechanism under physiological conditions maintaining higher workload and oxidative metabolism in the LV.

In human failing hearts (in whole hearts or LV), Mstn protein activation was reported to be accelerated in both DCM and ICM patients [22]. In parallel with this observation several groups found increased serum levels of Mstn protein in patients suffering from heart failure, although no correlation was demonstrated with the

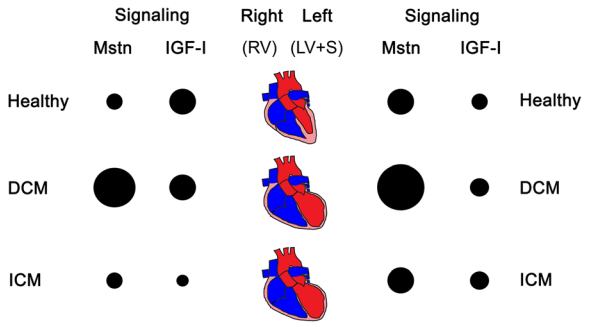

Figure 3 Summary of gene expression alterations regarding myostatin (Mstn) and IGF-I signaling in healthy human hearts as well as in DCM and ICM patients, respectively. Bigger circles represent higher expression of the signaling molecules in control vs. DCM or ICM hearts or in left (left ventricle (LV) + septum (S)) vs. right (right ventricle (RV)) side of the hearts.

severity or type of cardiac disease [22,28-30]. One should also consider that elevated serum myostatin levels in cardiomyopathic patients might be a combined effect of increased secretion from both cardiac and skeletal muscles, although exercise training lead to a reduction of myostatin levels only in skeletal muscles but not in serum of patients with chronic heart failure [31]. Nevertheless, it has been not clarified, whether protein activation in failing heart is regulated either at the level of gene expression or post-transcriptionally. Here we show that DCM hearts are indeed characterized by upregulated Mstn transcripts in both LV/S and RV supporting the previous reports on protein activation in LV [22]. However, we could not detect any significant elevation of Mstn transcript levels in ICM patients (Figure 3). We also tested the miRNA-dependent posttranscriptional regulation of Mstn. MiR-208 have been reported to be a negative regulator of Mstn expression [32], and to be upregulated in various forms of cardiomyopathy [33,34] and myocardial ischemia [35]. In line with these we detected a mild upregulation of miR-208b in the LV of DCM patients characterized by massive increase of myostatin transcripts that might suggest an adaptive counter regulatory mechanism fine-tuning the expression of Mstn during heart failure. Since we have found no difference in miR-208b expression between DCM and ICM hearts, it is likely that higher levels of myostatin mRNAs are mainly regulated at the level of transcription.

Although alterations in Mstn gene expression are followed by similar changes at the protein level in most cases [36-38], the (extracellular) promyostatin-pool might be posttranslationally activated by the cleavage of the propeptide [39-41]. Thus, ICM patients might have a Mstn activation at the protein level [22], however, not at the level of gene expression, whereas DCM hearts react with significant upregulation of Mstn transcripts. Similar to the results of George et al. [22] we detected lower level of ActRIIB in ICM than in DCM patients, but this occured only in the LV. On the other hand, IGF-I expression was shown to be dynamically regulated in the course of heart failure as an important compensatory mechanism; however, conflicting data exist in the literature with both down- and upregulated IGF-I levels in end-stage heart failure [11,14,15]. We could confirm significant decrease of IGF-I signaling in the RV of ICM patients but not in LV or in DCM patients. Moreover, DCM patients still maintained the physiological difference in Mstn/IGF-I signaling ratios in LV vs. RV, whereas no asymmetric gene expression pattern was detected in ICM patients (Figure 3). The mechanisms leading to different regulation of growth factor signaling in DCM and ICM patients remain to be clarified, however, it might relate to the different pathomechanism of heart failure and/or alternative regulation of compensatory mechanisms. Indeed, Mstn upregulation detected in DCM hearts might be part of the compensation reactions since we have reported recently that acute cardiac-specific deletion of Mstn in adult mouse hearts induces dilated cardiomyopathy followed by a massive compensatory up-regulation of Mstn in non-cardiomyocytes [7]. It is known, however, that various cardiac disease conditions, i.e. hypoxia can result in an imbalance of chamber-associated gene expression in myocardium [25-27,42]. Therefore, ICM hearts of ischemic origin might not be able to compensate as effective as do DCM patients by upregulating Mstn to maintain oxidative metabolism [7] and by regulating their IGF-I signaling to counter-act the decreased contractility [11]. However, further research is needed to elucidate the physiological and pathological relevance of the complex Mstn/IGF-I network in human heart.

Conclusions

Altogether, our results uncovered a spatial asymmetry in the expression pattern of Mstn/IGF-I in healthy hearts, which is likely to play a role in the different growth regulation of LV vs. RV. Moreover, we identified Mstn as a massively regulated gene in DCM but not in ICM as part of possible compensatory mechanisms in the failing heart.

Limitations

A clear limitation of the study is that our conclusions are only based on transcript data. However, our goal was to clarify transcriptional and posttranscriptional regulation of myostatin/IGF-1 signaling which is missing from the literature and not the recapitulation of other studies mainly concentrating on protein changes in heart failure patients [22,28-30].

Abbreviations

Mstn: Myostatin; ActRIIB: Activin receptor IIB; IGF-I: Insulin-like growth factor I; IGF-IR: Insulin-like growth factor I receptor; HPRT: Hypoxanthine guanine phosphorybosyl-transferase; DCM: Dilated cardiomyopathy; ICM: Ischemic cardiomyopathy; CONT: Control; CMV: Cytomegalovirus; miR: microRNA; NYHA: New York Heart Association; PAP: Mean pulmonary artery pressure; PWP: Mean pulmonary wedge pressure; LVED: Left ventricular end-diastolic diameter; LVSD: Left ventricular end-systolic diameter; PW: Posterior wall thickness; IVS: Interventricular septum thickness; LVEF: Left ventricular ejection fraction; ACE: Angiotensin converting enzyme; PDE: Phosphodiesterase; PGC1α: Peroxisome proliferator-activated receptor-γ coactivator 1-α.

Competing interests

The authors declare that they have no competing interests.

Authors' contributions

JAB, ZVV and TaB carried out the qRT-PCR experiments. JAB and ZVV analyzed and interpreted the data, made the statistical analysis and prepared the figures. PL and MK collected cardiac samples and measured clinical, echocardiographic and hemodynamic characteristics of patients. LD, PF and TB participated in the study design and coordination, and critically revised the manuscript. LM conceived of the study, coordinated and supervised it. JAB, ZVV and LM drafted the manuscript. All authors read and approved the final manuscript.

Acknowledgements
The authors would like to acknowledge Mrs. Zita Felhő Makráné and Mrs. Lászlóné Csontos for their technical assistance.
This work was supported by the following grants: the Hungarian National Development Agency, the European Union and co-funded by the European Social Fund (4.2.2.A-11-1-KONV-2012-0035) (to JAB, LD and LM), the New Horizons Grant of the European Foundation for the Study of Diabetes, and Hungarian Scientific Research Fund (OTKA K109737, OTKA ANN 107803) (to PF and ZVV). PF is a Szentágothai Fellow of the National Program of Excellence (TAMOP 4.2.4.A/2-11-1-2012-0001).

Author details
[1]Department of Biochemistry, Faculty of General Medicine, University of Szeged, Dóm tér 9, H-6720 Szeged, Hungary. [2]Cardiometabolic Research Group, Department of Pharmacology and Pharmacotherapy, Semmelweis University, Nagyvárad tér 4, H-1089 Budapest, Hungary. [3]Institute of Cardiology, ul. Alpejska 42, 04-628 Warszawa, Poland. [4]Pharmahungary Group, Szeged, Hungary. [5]Department I - Cardiac Development and Remodelling, Max Planck Institute for Heart and Lung Research, Ludwigstrasse 43, D-61231 Bad Nauheim, Germany. [6]Institute of Biochemistry II, Goethe University, Faculty of Medicine, Theodor-Stern-Kai 7, 60590 Frankfurt, Germany.

Received: 22 September 2014 Accepted: 16 December 2014
Published online: 16 January 2015

References

1. McPherron AC, Lawler AM, Lee SJ. Regulation of skeletal muscle mass in mice by a new TGF-beta superfamily member. Nature. 1997;387:83–90.
2. Sharma M, Kambadur R, Matthews KG, Somers WG, Devlin GP, Conaglen JV, et al. Myostatin, a transforming growth factor-ß superfamily member, is expressed in heart muscle and is upregulated in cardiomyocytes after infarct. J Cell Physiol. 1999;180:1–9.
3. Morissette MR, Cook SA, Foo S, McKoy G, Ashida N, Novikov M, et al. Myostatin regulates cardiomyocyte growth through modulation of Akt signaling. Circ Res. 2006;99:15–24.
4. Morissette MR, Stricker JC, Rosenberg MA, Buranasombati C, Levitan EB, Mittleman MA, et al. Effects of myostatin deletion in aging mice. Aging Cell. 2009;8:B573–83.
5. Artaza JN, Singh R, Ferrini MG, Braga M, Tsao J, Gonzales-Cadavid NF. Myostatin promotes a fibrotic phenotypic switch in multipotent C3H 10T1/2 cells without affecting their differentiation into myofibroblasts. J Endocrinol. 2008;196:235–49.
6. Rodgers BD, Interlichia JP, Garikipati DK, Mamidi R, Chandra M, Nelson OL, et al. Myostatin represses physiological hypertrophy of the heart and excitation-contration coupling. J Physiol. 2009;587:4873–86.
7. Biesemann N, Mendler L, Wietelmann A, Hermann S, Schäfers M, Krüger M, et al. Myostatin regulates energy homeostasis in the heart and prevents heart failure. Circ Res. 2014;115:296–310.
8. Ungvari Z, Csiszar A. The emerging role of IGF-1 deficiency in cardiovascular aging: recent advances. J Gerontol A Biol Sci Med Sci. 2012;67:599–610.
9. Bailey-Downs LC, Sosnowska D, Toth P, Mitschelen M, Gautam T, Henthorn JC, et al. Growth hormone and IGF-1 deficiency exacerbate high-fat diet-induced endothelial impairment in obese Lewis dwarf rats: implications for vascular aging. J Gerontol A Biol Sci Med Sci. 2012;67:553–64.
10. Toth P, Tucsek Z, Tarantini S, Sosnowska D, Gautam T, Mitschelen M, Koller A, Sonntag WE, Csiszar A, Ungvari Z. IGF-1 deficiency impairs cerebral myogenic autoregulation in hypertensive mice. J Cereb Blood Flow Metab 2014, doi:10.1038/jcbfm.2014.156.
11. Serneri GG, Modesti PA, Boddi M, Cecioni I, Pannicia R, Coppo M, et al. Cardiac growth factors in human hypertrophy: relations with myocardial contractility and wall stress. Circ Res. 1999;85:57–67.
12. Serneri GG, Boddi M, Cecioni I, Vanni S, Coppo M, Papa ML, et al. Cardiac angiotensin II formation in the clinical course of heart failure and its relationship with left ventricular function. Circ Res. 2001;88:961–8.
13. Palmieri EA, Benincasa G, Di Rella F, Casaburi C, Monti MG, De Simone G, et al. Differential expression of TNF-alpha, IL-6, and IGF-1 by graded mechanical stress in normal rat myocardium. Am J Physiol Heart Circ Physiol. 2002;282:H926–34.
14. Barton PJ, Felkin LE, Birks EJ, Culle ME, Banner NR, Grindle S, et al. Myocardial insulin-like growth factor-I gene expression during recovery from heart failure after combined left ventricular assist device and clenbuterol therapy. Circulation. 2005;112:I46–50.
15. Pucci A, Zanini C, Granata R, Ghigone R, Iavarone A, Broglio F, et al. Myocardial insulin-like growth factor-1 and insulin-like growth factor binding protein-3 gene expression in failing hearts harvested from patients undergoing cardiac transplantation. J Heart Lung Transplant. 2009;28:402–5.
16. Arcopinto M, Bobbio E, Bossone E, Perrone-Filardi P, Napoli R, Sacca L, et al. The GH/IGF-1 axis in chronic heart failure. Endocrin Metab Immun Disord Drug Targets. 2013;13:76–91.
17. Madonna R, Geng YJ, Bolli R, Rokosh G, Ferdinandy P, Patterson C, et al. Co-activation of nuclear factor-?B and myocardin/serum response factor conveys the hypertrophy signal of high insulin levels in cardiac myoblasts. J Biol Chem. 2014;289:19585–98.
18. Shyu KG, Ko WH, Yang WS, Wang BW, Kuan P. Insulin-like growth factor-1 mediates stretch-induced upregulation of myostatin expression in neonatal rat cardiomyocytes. Cardiovasc Res. 2005;68:405–14.
19. Yang W, Zhang Y, Li Y, Wu Z, Zhu D. Myostatin induces cyclin D1 degradation to cause cell cycle arrest through a phosphatidylinositol 3-kinase/AKT/GSK-3 beta pathway and is antagonized by insulin-like growth factor 1. J Biol Chem. 2007;282:3799–808.
20. Morissette MR, Cook SA, Buranasombati C, Rosenberg MA, Rosenzweig A. Myostatin inhibits IGF-I-induced myotube hypertrophy through Akt. Am J Physiol Cell Physiol. 2009;297:C1124–32.
21. Gaussin V, Depre C. Myostatin, the cardiac chalone of insulin-like growth factor-1. Cardiovasc Res. 2005;68:347–9.
22. George I, Bish LT, Kamalakkannan G, Petrilli CM, Oz MC, Naka Y, et al. Myostatin activation in patients with advanced heart failure and after mechanical unloading. Eur J Heart Fail. 2010;12:444–53.
23. Chomczynski P, Sacchi N. Single-step method of RNA isolation by acid guanidinium thiocyanate-phenol-chloroform extraction. Anal Biochem. 1987;162:156–9.
24. Sun Y, Li Y, Luo D, Liao DJ: Pseudogenes as weaknesses of ACTB (Actb) and GAPDH (Gapdh) used as reference genes in reverse transcription and polymerase chain reactions. PLoS One 2012, doi:10.1371/journal.pone.0041659.
25. Torrado M, Iglesias R, Nespereira B, Mikhailov AT. Identification of candidate genes potentially relevant to chamber-specific remodeling in postnatal ventricular myocardium. J Biomed Biotechnol 2010, doi:10.1155/2010/603159.
26. Modesti PA, Vanni S, Bertolozzi I, Cecioni I, Lumachi C, Perna AM, et al. Different growth factor activation in the right and left ventricles in experimental volume overload. Hypertension. 2004;43:101–8.
27. Zungu M, Young ME, Stanley WC, Essop MF. Expression of mitochondrial regulatory genes parallels respiratory capacity and contractile function in a rat model of hypoxia-induced right ventricular hypertrophy. Mol Cell Biochem. 2008;318:175–81.
28. Heineke J, Auger-Messier M, Xu J, Sargent M, York A, Welle S, et al. Genetic deletion of myostatin from the heart prevents skeletal muscle atrophy in heart failure. Circulation. 2010;121:419–25.
29. Gruson D, Ahn SA, Ketelslegers JM, Rousseau MF. Increased plasma myostatin in heart failure. Eur J Heart Fail. 2011;13:734–6.
30. Breitbart A, Scharf GM, Duncker D, Widera C, Gottlieb J, Vogel A, Schmidt S, Brandes G, Heuft HG, Lichtinghagen R, Kempf T, Wollert KC, Bauersachs J, Heineke J. Highly specific detection of myostatin prodomain by an immunoradiometric sandwich assay in serum of healthy individuals and patients. Plos One 2013, doi:10.1371/journal.pone.0080454.
31. Lenk K, Erbs S, Höllriegel R, Beck E, Linke A, Gielen S, et al. Exercise training leads to a reduction of elevated myostatin levels in patients with chronic heart failure. Eur J Prev Cardiol. 2012;19:404–11.
32. Callis TE, Pandya K, Seok HY, Tang RH, Tatsuguchi M, Huang ZP, et al. MicroRNA-208a is a regulator of cardiac hypertrophy and conduction in mice. J Clin Invest. 2009;119:2772–86.
33. Satoh M, Minami Y, Takahashi Y, Tabuchi T, Nakamura M. Expression of microRNA-208 is associated with adverse clinical outcomes in human dilated cardiomyopathy. J Card Fail. 2010;16:404–10.
34. Bostjancic E, Zidar N, Stajer D, Glavac D. MicroRNAs miR-1, miR-133a, miR-133b and miR-208 are dysregulated in human myocardial infarction. Cardiology. 2010;115:163–9.
35. Varga ZV, Zvara A, Faragó N, Kocsis GF, Pipicz M, Gáspár R, et al. MicroRNAs associated with ischemia-reperfusion injury and cardioprotection by ischemic pre- and postconditioning: protectomiRs. Am J Physiol Heart Circ Physiol. 2014;307:H216–27.

36. Shyu KG, Lu MJ, Wang BW, Sun HY, Chang H. Myostatin expression in ventricular myocardium in a rat model of volume-overload heart failure. Eur J Clin Invest. 2006;36:713–9.
37. McKoy G, Bicknell KA, Patel K, Brooks G. Developmental expression of myostatin in cardiomyocytes and its effect on foetal and neonatal rat cardiomyocyte proliferation. Cardiovasc Res. 2007;74:304–12.
38. Lenk K, Schur R, Linke A, Erbs S, Matsumoto Y, Adams V, et al. Impact of exercise training on myostatin expression in the myocardium and skeletal muscle in a chronic heart failure model. Eur J Heart Fail. 2009;11:342–8.
39. Anderson SB, Goldberg AL, Whitman M. Identification of a novel pool of extracellular pro-myostatin in skeletal muscle. J Biol Chem. 2008;283:7027–35.
40. Mendler L, Baka Z, Kovács-Simon A, Dux L. Androgens negatively regulate myostatin expression in an androgen-dependent skeletal muscle. Biochem Biophys Res Commun. 2007;361:237–42.
41. Mendler L, Zádor E, Ver Heyen M, Dux L, Wuytack F. Myostatin levels in regenerating rat muscles and in myogenic cell cultures. J Muscle Res Cell Motil. 2000;21:551–63.
42. Chugh SS, Whitesel S, Turner M, Roberts Jr CT, Nagalla SR. Genetic basis for chamber-specific ventricular phenotypes in the rat infarct model. Cardiovasc Res. 2003;57:477–85.